Mechanisms of liver-induced CD4 T cell tolerance

Dissertationsschrift zur Erlangung des akademischen Grades

Doktor der Naturwissenschaften (Dr. rer. nat.)

im Fachbereich Biologie

der Fakultät für Mathematik, Informatik und Naturwissenschaften

der Universität Hamburg

Vorgelegt von Daria Krzikalla

Hamburg, Dezember 2019

1. Gutachter: Prof. Dr. Johannes Herkel

I. Medizinische Klinik und Poliklinik des Universitätsklinikums Hamburg-Eppendorf

2. Gutachter: Prof. Dr. Jörg Ganzhorn

Institut für Zoologie der Universität Hamburg

Tag der Disputation: 13.03.2020

Table of contents

Abbreviations

ACK	Ammoniumchlorid-Kalium (Ammonium-chloride-potassium)
AIH	Autoimmune hepatitis
ALT	Alanine amino transferase
Aoc3	Amine oxidase, copper containing 3
APC	Antigen-presenting cell
CCR	C-C chemokine receptor
CD	Cluster of differentiation
cDNA	Complementary DNA
CIA	Collagen-induced arthritis
CNS	Central nervous system
CRP	C-reactive protein
CTLA-4	Cytotoxic T-lymphocyte-associated protein 4
CXCL	CXC chemokine ligand
CXCR	CXC chemokine receptor
DC	Dendritic cell
DNA	Deoxyribonucleic acid
EAE	Experimental autoimmune encephalomyelitis
FACS	Fluorescence-activated cell sorting
FCS	Fetal calf serum
Foxp3	Forkhead box P3
GFP	Green fluorescent protein
Havcr2	Hepatitis A virus cellular receptor 2
HBV	Hepatitis B virus
HE	Hematoxylin and eosin stain
HLA	Human leukocyte antigen
Hprt	Hypoxanthine-guanine phosphoribosyltransferase
Icam1	Intercellular adhesion molecule 1
IDO	Indoleamine-pyrrole 2,3-dioxygenase
IFNγ	Interferon-γ
IgG	Immunoglobulin G
IL	Interleukin
i.p.	Intraperitoneal
IPEX	Immunodysregulation polyendocrinopathy enteropathy X-linked
ISG	Interferon-stimulated gene
ITIM	Immunoreceptor tyrosine-based inhibitory motif
KC	Kupffer cell
KO	Knockout
Lag-3	Lymphocyte-activation gene 3
LPS	Lipopolysaccharide
LSEC	Liver sinusoidal endothelial cell
LSECtin	Liver and lymph node sinusoidal endothelial cell C-type lectin

MACS	Magnetic-activated cell sorting
MadCAM-1	Mucosal vascular addressin cell adhesion molecule 1
MBP	Myelin basic protein
MBP-NP	MBP-peptide loaded NP
mHAI	Modified hepatic activity index
MHC	Major histocompatibility complex
MS	Multiple sclerosis
NK	Natural killer
NP	Nanoparticle
NPC	Non-parenchymal cell
ns	Not significant
PacO	Pacific Orange
PBMC	Peripheral blood mononuclear cell
PBS	Phosphate-buffered saline
PD-1	Programmed cell death protein 1
PD-L1	Programmed cell death 1 ligand 1
PMA	Phorbol-12-myristat-13-acetat
pTreg	Peripheral Treg
qPCR	Quantitative polymerase chain reaction
RA	Rheumatoid arthritis
RFP	Red fluorescent protein
RORγt	Retinoic acid receptor-related orphan receptor gamma t
RNA	Ribonucleic acid
RT	Room temperature
RTE	Recent thymic emigrant
SEM	Standard error of mean
SLE	Systemic lupus erythematosus
Stat	Signal transducer and activator of transcription
T1D	Type 1 diabetes
TCR	T cell receptor
Tfh	T follicular helper cell
TGF	Transforming growth factor
Th	T helper cell
TIGIT	T cell immunoreceptor with Ig and ITIM domains
Tim-3	T-cell immunoglobulin and mucin-domain containing-3
TNF	Tumor necrosis factor
Tr1	Type 1 regulatory T cell
Treg	Regulatory T cell
t-SNE	T-distributed stochastic neighbor embedding
tTreg	Thymic-derived Treg
TUNEL	Terminal deoxynucleotidyl transferase dUTP nick end labeling
VAP-1	Vascular adhesion protein 1
VCAM-1	Vascular cell adhesion molecule 1
wt	Wildtype

Figures and tables

1. Introduction

1.1 The liver between immunity and tolerance

The liver is the main metabolic organ in the human body and fulfills various functions including the production of bile and glycogen, iron storage, and clearing the blood of drugs and other harmful substances. However, the liver is also an important organ in immune homeostasis. This is highlighted by the fact that bacterial infections are a leading cause of death in patients suffering from liver failure [1]. The role in frontline immune defense is enabled via the special localization of the liver that is supplied by both oxygenated blood from the hepatic artery and venous blood from the portal vein. 75-80% of the blood supply is derived from the portal vein [2] and – as directly coming from the gastrointestinal tract – contains bacteria and bacterial products as well as harmless dietary antigens. This poses a dual challenge to the liver: first, bacteria and bacterial products must be eradicated from the blood flow as to not generate a systemic immune response and second, the immune response against foreign but innocuous dietary antigens as well as bacterial components must be controlled.

1.1.1 The special architecture of the liver

The liver's special architecture enables eradication of bacteria as well as supply of energy to hepatocytes (described in [3]). The liver lobes consist of smaller hepatic lobules, which have the transversal shape of a hexagon and are mainly populated by hepatocytes with a central vein in the middle (Fig. 1). At the edges of the lobules, the portal fields are located that are made up of a hepatic artery that supplies oxygen, a portal vein rich in nutrients, small bile ducts, lymphatic vessels, and a branch of the vagus nerve. The liver is characterized by a special type of capillary, the so-called sinusoids. Sinusoids receive blood from both the hepatic artery and the portal vein and transport it to the central vein. They are lined with liver sinusoidal endothelial cells (LSECs) and are highly fenestrated. Part of the sinusoids are the Kupffer cells (KCs), the liver-resident macrophages. Both LSECs and KCs play an important role in the removal of blood-borne antigens and waste products. Indeed, previously thought to be second in line after KCs, LSECs were shown to eliminate 75% of bacterial lipopolysaccharide (LPS), whereas KCs were

responsible for the clearance of the remaining 25% [4]. A slow blood flow within the sinusoids increases the likelihood for KCs and LSECs to catch gut-derived antigens and thus maintain immune tolerance.

The space between the endothelium and the hepatocytes is called the space of Disse. The fenestrated endothelium allows direct delivery of blood plasma into the 10-15 µm large space where it can provide nutrients to hepatocytes. The space of Disse also harbors hepatic stellate cells, which are pericytes that are in a quiescent state in the healthy liver and might play a role as a liver-resident antigen-presenting cell (APC) population [5]. They are the main storage for vitamin A in the body and when activated produce high amounts of extracellular matrix and collagen favoring the development of liver cirrhosis [6]. The unique liver architecture thus allows delivery of nutrients to hepatocytes, increases the visibility for blood-derived antigens, and enables their clearance via liver APCs.

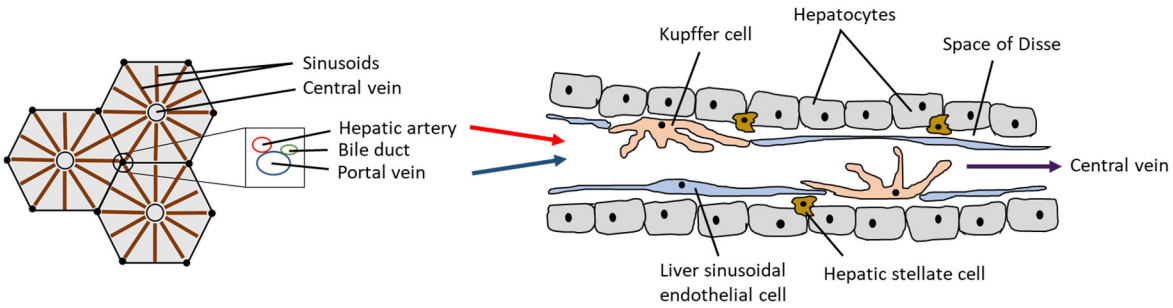

Figure 1. Liver architecture.
On the left, the schematic structure of a liver lobule is depicted: the portal fields that contain a portal vein, a hepatic artery, and a bile duct are located at the corner of the hepatic lobules. Blood from the hepatic artery and the portal vein mix in the sinusoids, the specialized capillary of the liver. A sectioned sinusoid is illustrated on the right: the capillary is lined by LSECs, the fenestrated endothelium of the liver. The space between hepatocytes and LSECs is called space of Disse and contains hepatic stellate cells that store vitamin A. The microvilli of hepatocytes reach into the space of Disse and take up nutrients from the blood plasma that enters the space via the fenestrated endothelium. Kupffer cells are part of the sinusoids. These liver-specific macrophages together with LSECs clear the blood of bacterial and waste products.

1.1.2 Liver antigen-presenting cells

Another important challenge of the liver – maintaining immune tolerance despite an abundance of foreign antigens – is accomplished by the specialized APCs. APCs are divided into professional and non-professional APCs: the former including dendritic cells (DCs) and the latter being liver-specific cells. Non-professional APCs in the liver are KCs and LSECs and under certain conditions hepatic stellate cells and hepatocytes.

KCs are liver-resident macrophages that make up approximately 35% of the non-parenchymal cells (NPCs) of the liver and 90% of all tissue macrophages [7]. They express different pattern recognition receptors, such as Toll-like receptors, mannose receptors, and NOD-like receptors enabling them to sense danger-associated molecular patterns and pathogen-associated molecular patterns. As such, they represent the first line of defense against bacterial products and antigens derived from the gut (reviewed in [7]). Apart from their important innate functions, KCs constitute a bridge towards the adaptive immune system, as they can present antigens to T cells. Under steady state conditions, they express low levels of major histocompatibility complex (MHC) II and co-stimulatory molecules and are thus less potent in mounting a T cell-specific immune response. Instead, they even inhibit T cell activation by DCs via production of prostaglandins, consequently favoring immune tolerance [8]. Interestingly, KCs were shown to secrete the inhibitory cytokines interleukin (IL)-10 and transforming growth factor (TGF)-β upon LPS exposure, an endotoxin constitutively present in the portal venous blood [9], which promote the tolerogenic milieu in the liver. In an *in vivo* model of low-dose peptide administration coupled to inert particles, Heymann et al. showed that KCs are the primary scavengers for particle-associated antigens. Antigen presentation by KCs led to cluster of differentiation (CD) 4 T cell arrest and expansion of regulatory T cells (Tregs) and could thus limit extrahepatic inflammation [10]. However, under inflammatory conditions in the liver, infiltrating macrophages activate T cells and KCs lose their tolerogenic phenotype [10]. In brief, KCs maintain a tolerogenic environment in the healthy liver due to phagocytosis of bacterial products, production of inhibitory cytokines, and their weak activation of T cells.

The second classical APC in the liver are the DCs, which mainly consist of three subtypes: conventional type 1 DCs, conventional type 2 DCs, and plasmacytoid DCs. The main subset found in the murine liver are plasmacytoid DCs with low MHC II expression [11]. Interestingly,

DCs isolated from healthy mouse liver are less potent in endocytosis and their capacity to activate T cells is reduced compared to splenic DCs (reviewed in [12]). A similar DC phenotype was seen when comparing human liver DCs to blood DCs. While both in an immature state, stimulation led to pro-inflammatory cytokine production in blood DCs, whereas liver DCs secreted substantial amounts of the anti-inflammatory cytokine IL-10, induced less potent CD4 T cell responses, and generated more suppressive Tregs [13]. Thus, intrahepatic DCs in both mouse and human differ substantially from their extrahepatic counterparts in having low endocytic potential and high IL-10 production. Their tolerogenic potential is also defined by the production of the prostaglandin E2, which leads to higher Indoleamine-pyrrole 2,3-dioxygenase (IDO) expression in DCs enhancing IL-10 production and Treg induction (reviewed in [14]). In an inflammatory context, the previously tolerogenic DCs develop an activating phenotype and prime pro-inflammatory T cell responses [12].

Notably, also non-professional APCs play an important role in maintaining liver tolerance. Despite not being considered "classical" APCs, LSECs are very efficient in endocytosing molecules, carry both scavenger and different C-type lectin receptors, and constitutively express low levels of MHC II [15, 16]. Upon stimulation, MHC II expression can be highly upregulated on LSECs [17]. Interestingly, CD4 T cells primed by LSECs preferably differentiate into cells that either have a classical Treg phenotype [18], or lack expression of CD25 and Forkhead box P3 (FoxP3), but still produce IL-10 [19]. In any case, priming of CD4 T cells by LSECs generates an anti-inflammatory response and stimulation of effector T cells by LSECs impairs production of interferon (IFN)-γ and IL-17 [20]. LSECs can also influence T cell activity via LSECtin, a C-type lectin on the cell surface that acts as a co-inhibitory molecule and downregulates T cell responses [21]. This tolerance-inducing capacity of LSECs can be harnessed by delivering autoantigen peptides specifically to LSECs *in vivo* and thus generating tolerance toward this antigen [22]. This tolerogenic role of antigen presentation via LSECs also applies to stimulation of CD8 T cells. Antigens derived from the blood stream are internalized by LSECs and cross-presented on MHC I to CD8 T cells resulting in tolerance. CD8 T cell tolerance is dependent on binding of the co-inhibitory receptor programmed cell death protein 1 (PD-1) on CD8 T cells to its ligand programmed cell death 1 ligand 1 (PD-L1) on LSECs. Interestingly, LSEC cross-presentation at high antigen concentration results in the generation

of functional effector CD8 T cells opening a role for LSECs to drive inflammatory responses e.g. in viral liver disease with high hepatic antigen load [23].

Hepatocytes only express low levels of MHC I in healthy liver, but were shown to express both MHC I and MHC II in chronic liver disease [24]. Stimulation via MHC II from hepatocytes activates CD4 T cells *in vitro* and generates a regulatory phenotype characterized by expression of IL-10 in the absence of Foxp3 [25]. In a minority of CD4 T cells, stimulation by hepatocytes induces conversion to Foxp3+ Tregs, which is increased in the presence of TGF-β, a cytokine produced by KCs [26]. Interestingly, in a mixed lymphocyte reaction setup, hepatocytes were shown to prevent proliferation of peripheral blood mononuclear cells (PBMCs) to an allogeneic stimulus in a dose-dependent manner outlining the immunoregulatory role of hepatocytes [27]. In brief, hepatocytes as parenchymal cells function as APCs under certain conditions and favor tolerogenic T cell responses.

The role of hepatic stellate cells is less clear. They are not efficient in endocytosis, but express MHC molecules for both peptides and lipids as well as co-stimulatory molecules. Accordingly, their function as APCs was shown in the capability to induce effector T cells [28]. However, contrasting research could not confirm their role as APCs due to the lack of co-stimulatory molecule expression and instead highlights their role as regulatory bystanders influencing the immune response by producing TGF-β and retinoic acid that favor the induction of Tregs [29, 30].

In conclusion, hepatic APCs prevent an overt immune reaction against the various innocuous antigens that the liver is presented with and generate a tolerogenic environment characterized by the presence of inhibitory cytokines, such as IL-10 and TGF-β. During (chronic) inflammatory processes, liver APCs can lose their tolerogenic phenotype and contribute to inflammation.

1.2 Autoimmune disease

Autoimmunity encompasses a variety of diseases that share a break of tolerance to self-antigens. Autoimmune pathologies are very frequent in the population with a prevalence of approximately 8% [31]. There are more than 80 different autoimmune diseases that are divided into organ-specific ones (e.g. thyreoditis or type 1 diabetes [T1D]) or systemic diseases (e.g. systemic lupus erythematosus [SLE] and rheumatoid arthritis [RA]) and there are mixtures between these two. Even the liver can be a target of autoimmunity despite its remarkable tolerogenic properties. Break of tolerance is seen in patients leading to autoimmune liver disease. The term autoimmune liver disease covers different disease patterns with autoimmune hepatitis (AIH), primary sclerosing cholangitis, and primary biliary cholangitis being the three most prominent. All three are classified as rare diseases (prevalence <1:2000) and the pathogeneses are not yet clear. Primary sclerosing cholangitis and primary biliary cholangitis are characterized by bile duct inflammation and cholestasis ultimately leading to liver cirrhosis if left untreated. In AIH, the hepatocytes themselves are the primary target of a cell-mediated immune response with CD4 T cells being the most frequent in the cellular infiltrate. Standard treatment of autoimmune diseases consists of anti-inflammatory and/or immunosuppressive drugs that, even though in most cases very effective, often have adverse effects especially when used over long periods.

The special role of T cells in autoimmunity became apparent through various studies that highlighted the genetic bias underlying many autoimmune diseases. Human leukocyte antigen (HLA) genes code for the MHC molecules and certain HLA types are strongly associated with autoimmune disease. A meta-analysis studying susceptibility to autoimmune disease in Latin Americans revealed shared HLA class II molecules in six autoimmune diseases: The class II HLA molecule HLA-DRB1*03:01 for example is associated with SLE, Sjögren's syndrome, and T1D, and HLA-DRB1*04:05 is a risk factor for AIH, RA, and T1D [32]. As T cell activation strongly depends on MHC signaling, this genetic association highlights the important role assigned to T cells. Apart from MHC molecules, other T cell-associated genes were identified that might drive autoimmunity. Genetic variants of the protein tyrosine phosphatase, non-receptor type 22, which is expressed primarily in lymphoid tissue, are associated with autoimmune diseases, such as RA or T1D, most likely due to hyperresponsive T cells because of reduced kinase activity [33]. Single nucleotide polymorphisms in the IL-2 receptor α gene were strongly associated with

multiple sclerosis (MS) [34], T1D [35], and Graves' disease [36], which suggests a role for CD4+CD25+ Tregs as they depend on high expression of CD25. A more direct connection to the role of T cells can be drawn from their higher abundance in patients suffering from autoimmune disease. In patients with relapsing-remitting MS, the frequency of certain CD4 subtypes is higher in the cerebrospinal fluid [37]. In RA, various immune cells are found in the synovial compartment, including expanded CD4 T cell clones that might drive disease development [38]. The role of CD4 T cells in autoimmunity will be further elaborated in 1.2.2.

1.2.1 CD4 T cell subsets

T cells are lymphocytes that develop in the thymus and play a central role in the adaptive immune system. They are characterized by expression of a T cell receptor (TCR), which recognizes antigen in the context of MHC molecules. There are two types of conventional, adaptive T cells: CD4 T cells, which are known as helper T cells (Th), and CD8 T cells, also termed cytotoxic T cells, which are known for their potential to kill virus-infected or tumor cells. Besides the classical T cells, innate-like T cells, such as NKT cells, mucosal-associated invariant T cells, and γδ T cells, are described. NKT cells recognize glycolipid antigen presented by the non-classical MHC molecule CD1d. Foreign (mostly bacteria-derived) antigens are presented to mucosal-associated invariant T cells via the MHC class I-related protein MR1. γδ T cells are a rare population of T cells that does not express the classical αβ TCR and seems to be independent of MHC molecules.

Within the conventional CD4 and CD8 T cells, different subsets were identified, which will be further described for CD4 T cells. Following T cell activation, naïve CD4 T cells differentiate into specialized subsets. A prerequisite for differentiation is recognition of an antigen peptide in the context of MHC II by the TCR next to co-stimulation [39]. Depending on TCR affinity to the antigen-MHC II complex and surrounding cytokine milieu, naïve CD4 T cells may differentiate into a specialized subset that is characterized by production of specific cytokines and is regulated by a master transcription factor.

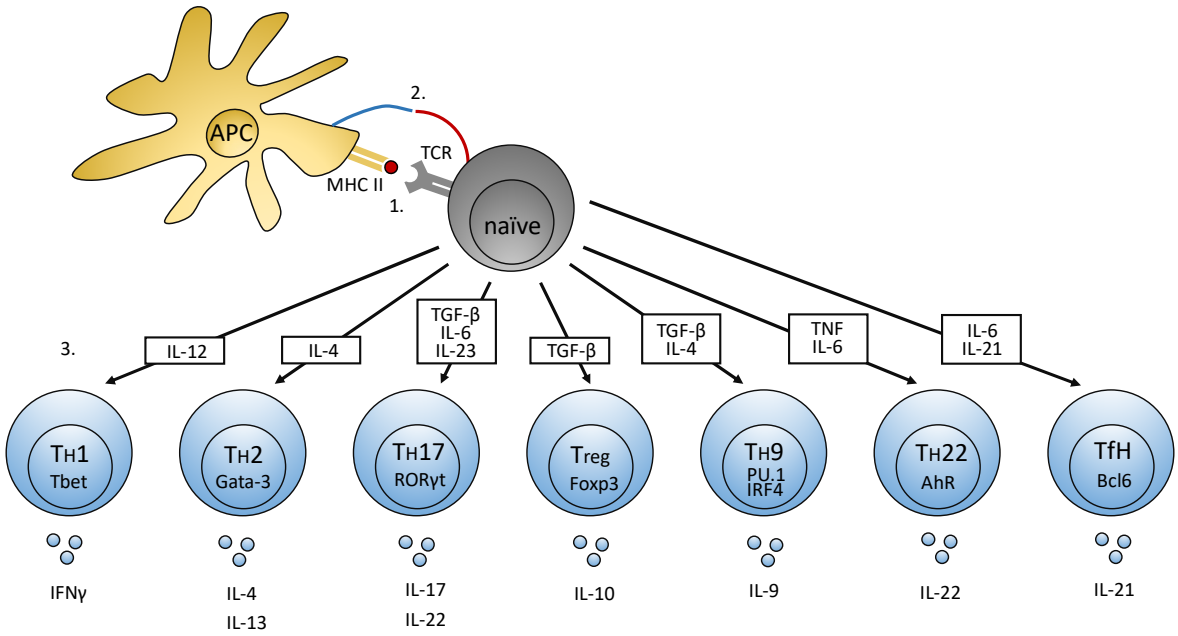

Figure 2. CD4 T cell subsets.
Naïve CD4 T cells differentiate into different subsets depending on three signals: 1. TCR stimulation via MHC II, 2. co-stimulation, and 3. cytokine milieu. Depicted are the subsets defined thus far including the cytokines needed for polarization, their master transcription factors, and key cytokines produced.

Already in 1985, two distinct subsets of CD4 T cells were identified according to their production of specific cytokines: Th1 and Th2 cells [40]. Further characterization identified Th1 cells to produce mainly IL-2 and IFNγ and thus preferentially initiate cellular immune responses directed against intracellular pathogens. Th2 cells secrete IL-4, IL-5, and IL-13, induce the humoral immune response, and act against extracellular pathogens [41, 42]. Immune responses were thought to be either Th1- or Th2-dominated as they mutually block each other. These effector populations were complemented by a subtype of suppressing CD4 T cells that was initially defined by surface expression of the IL-2 receptor α chain (also called CD25) and was able to down-regulate immune responses in a non-antigen-specific manner [43]. Subsequently, Foxp3 was identified as the master transcription factor of these regulatory T cells – in short: Tregs [44-46]. Tregs can already develop in the thymus and are then termed thymic-derived Tregs (tTregs) or develop in the periphery in the presence of TGF-β (peripheral Tregs, pTregs). In recent years, other effector T cells have been identified and named after their signature cytokine. Th17 cells mainly produce IL-17 and are regulated by retinoic acid receptor-related orphan receptor gamma t (RORγt) [47]. They confer protection against

microbial pathogens and are associated with various autoimmune disorders. Other subsets identified include Th9 cells that are characterized by high secretion of IL-9 [48, 49]. There is no master transcription factor identified for Th9 cells, but they share the necessity of Gata-3 expression with Th2 cells and additionally, PU.1 [50] and IRF4 [51] are needed for Th9 differentiation. As Th2 cells can be re-programmed by TGF-β, a cytokine that is crucial for Th17 and Treg development, to promote a Th9-phenotype [49], it is debatable whether Th9 cells constitute a specific subset of CD4 T cells or rather represent the plasticity within the CD4 T cell compartment. Th22 cells express high amounts of IL-22 and require Aryl hydrocarbon receptor expression for their differentiation. IL-22 is also a key cytokine secreted by Th17 cells. However, Th22 cells were proven to develop independently of Th17 cells, but show plasticity towards Th1 and Th2 cells under *in vitro* conditions [52]. Finally, there is a distinct class of CD4 T cells present in the B cell zone of secondary lymphoid organs and in the circulation. So-called T follicular helper cells (Tfh) play a decisive role in the formation of germinal centers and are dependent on expression of Bcl-6 [53-55].

1.2.2 Autoreactive T cells and autoimmune diseases

In the pathogenesis of autoimmune disease, T cells play an important role, as there is a fine balance between effector T cells needed to defend the body against foreign antigens and suppressive Tregs, which prevent excessive immune responses. However, the sole presence of autoreactive T cells in the peripheral blood does not cause autoimmune disease, as autoreactive T cell clones are also detectable in healthy individuals [56]. Indeed, it was shown in MS that the number of autoreactive T cells in the blood does not differ between patients and healthy controls, but their phenotype does. While CD4 T cells isolated from MS patients show enhanced production of IFNγ, IL-17, and GM-CSF, their expression of IL-10 is reduced compared to T cells isolated from healthy controls [57]. Within the classical Th1/Th2 paradigm, it was the Th1 cells that were attributed with generating autoimmune pathologies, for example in the context of experimental autoimmune encephalomyelitis (EAE) or experimental diabetes [58]. With increasing diversity in the CD4 T cell subsets, Th17 cells have gained particular relevance in the past decade, as they were shown to play a role in many autoimmune diseases. In MS, IL-17- and GM-CSF-producing Th17 cells are the main drivers of disease despite the

fact that Th1 cells can also transfer disease upon adoptive cell transfer in the EAE model [59]. Interestingly, fate mapping of IL-17-producing cells in EAE revealed a population of formerly IL-17-secreting cells that produce non-Th17 cytokines in chronic inflammation and are thus termed ex-Th17 cells [60]. This plasticity of CD4 T cell subsets makes it difficult to account one specific subset for a particular disease. However, the role of IL-17 also became apparent in RA, in which the frequencies of IL-17-producing T cells are increased in peripheral blood and in the synovium (reviewed in [61]). Moreover, treatment of diabetes-prone NOD mice with anti-IL-17 antibody reduced the incidence of T1D [62], highlighting the role of Th17 cells in diabetes and pointing to a role for Th17 inhibitors in treating autoimmune disease. Indeed, inhibitors of IL-17 and IL-23, a cytokine essential for the differentiation of Th17 cells, are applied successfully for the treatment of psoriasis (reviewed in [63]). Another approach to limit Th17 function is targeting their master transcription factor RORγt. A synthetic ligand for RORα and RORγt suppresses the receptor's transcriptional activity leading to inhibited development of murine Th17 cells, reduced IL-17 production in differentiated cells, and a mild decrease in severity of EAE [64]. Also IL-9-producing cells, including Th9 cells but also Th17 cells, gained interest as drivers of autoimmune disease as increased IL-9 expression is associated with SLE [65], RA [66], and EAE [67]. Jager et al. showed in the EAE model that *in vitro*-generated antigen-specific Th1, Th9, and Th17 cells can induce autoimmunity upon adoptive transfer with different pathologies [68]. The role for Th22 cells in autoimmunity is less clear. In RA, higher plasma levels of IL-22 were detected in patients as well as more IL-22+ CD4 T cells in the blood, which correlate positively with disease severity [69]. However, effector T cells isolated from peripheral blood of SLE patients showed decreased IL-22 production suggesting a protective role for IL-22 in SLE [70]. Also Tfh cells play a role in autoimmunity, as for example in SLE, it is known that autoantibodies are derived from reactions in the germinal centers, and animal models of SLE show an aberrant expansion of Tfh cells (reviewed in [71]).

The role of effector T cells is complemented by the action of Tregs forming an equilibrium to maintain immune tolerance. The importance of functional Tregs for immune homeostasis is reflected by the occurrence of autoimmune disease because of mutations in the *FOXP3* locus leading to dysfunctional FOXP3. In humans, over 70 mutations in the *FOXP3* gene are described leading to the immunodysregulation polyendocrinopathy enteropathy X-linked

(IPEX) syndrome [72]. Patients with this syndrome suffer from various autoimmune pathologies, such as autoimmune enteropathies, autoimmune skin conditions, or endocrinopathies. Without treatment, the disease is mostly lethal within the first two years of life. A cure is only possible via hematopoietic stem cell transplantation. A mouse model with a mutated *Foxp3* gene was generated, the so-called Scurfy mouse, which resembles IPEX patients in phenotype, confirming the importance of Tregs in mice [73]. Moreover, decreased Treg function has been observed in different autoimmune diseases. CD4+CD25hi Tregs from PBMCs in MS patients show decreased effector functions compared to healthy donors [74]. In T1D, the number of Tregs is not reduced, but their suppressive capacity is diminished compared to healthy controls [75]. In brief, a fine balance between effector and regulatory CD4 T cells is important for immune homeostasis and both effector CD4 T cells and Tregs can be altered in number and/or function during autoimmune pathologies.

1.3 CD4 T cell tolerance

In order to cope with the variety of harmful molecules within the body, the immune system must provide an enormous repertoire of TCRs that recognize various antigens in the context of MHC. This TCR repertoire is generated via a process called V(D)J recombination. The TCR consists of two subunits (mostly αβ, but γδ T cells also exist) that have a constant and a variable domain and are linked via a disulfide bond. The variable domain is encoded by variable (V) and joining (J) gene segments for the β chain and V, J, and diversity (D) gene segments for the α chain (summarized in [76]). V, J, and D segments are re-arranged with additional nucleotide additions or deletions ultimately leading to different amino acids in the antigen-binding region that can potentially generate 10^{15} to 10^{20} TCR clonotypes. However, the number of TCR clonotypes in the human body is far lower as there is only an estimated number of 10^{13} cells in the human body and some clonotypes are more abundant than others (reviewed in [77]). Inevitably, random somatic rearrangement will also generate TCRs recognizing self-antigens that need to be controlled in order to prevent an immune response against self. Self-tolerance mechanisms that limit immune responses directed against the host are divided into central and peripheral tolerance mechanisms.

1.3.1 Central tolerance

Development and maturation of T cells takes place in the thymus (reviewed in [78]). First, TCRs are arranged in the thymic cortex where – after successful TCR arrangement – positive selection occurs, ensuring that only cells with functional TCRs that are able to bind MHC undergo further development. Thymocytes that cannot bind MHC undergo apoptosis. Only at this step, lineage commitment occurs and so far double positive thymocytes mature into single CD4 or CD8 positive thymocytes. In the process of maturation, single positive cells upregulate the C-C chemokine receptor (CCR) 7 allowing entry into the thymic medulla. In the medulla, a process called negative selection or central tolerance is initiated. The transcription factor Aire drives expression of peripheral antigens in medullary thymic epithelial cells, which present endogenous peptides on MHC molecules to single-positive thymocytes. T cells with high affinity to these antigens will be deleted ensuring that autoreactive T cells will not enter the periphery. However, some autoantigen-specific T cells escape central tolerance creating the necessity for peripheral tolerance mechanisms.

1.3.2 Peripheral tolerance

Autoreactive T cells are detected in the periphery of both patients with autoimmune disease and in healthy individuals [56]. There are different mechanisms – summarized with the term peripheral tolerance – that restrain autoreactive immune responses. First, autoreactive T cells can be physically separate from tissue antigens. These immune-privileged sites include brain, eyes, testes, placenta, and the fetus. As autoreactive T cells are present in the periphery, but do not encounter their antigen, this tolerance mechanism is termed ignorance. Interestingly, in the eye as an immune-privileged site, it was shown that T cells gain expression of *Foxp3* and thus, differentiate into Tregs [79]. Second, TCR signaling alone does not elicit an immune response. Instead, co-stimulation via CD80/CD86 is necessary for T cells to express effector functions, and TCR stimulation in the absence of adequate co-stimulation leads to anergy (reviewed in [80]). Autoreactive T cells that encounter their antigen without co-stimulatory signal will thus not develop effector functions and become unresponsive for further stimulation. Third, inhibitory cells – most prominently Tregs – suppress T cell responses and thus prevent the development of autoimmune diseases. Exposure to TGF-β in the periphery can trigger

reprogramming of T cells to induce pTregs [81]. In brief, peripheral tolerance encompasses ignorance, anergy, and suppression by Tregs.

1.3.2.1 Regulatory T cells

Tregs play a pivotal role in the control of immune reactions and aberrant Treg functions lead to autoimmunity. Tregs are subdivided into tTregs that are differentiated in the thymus during negative selection and pTregs that develop in the periphery. Tregs are a heterogeneous subpopulation of T cells with CD4+CD25+Foxp3+ Tregs being the most extensively described in the literature. However, other less characterized subsets have been identified. Already in 1997, a Treg population was described that produces high IL-10 in the absence of Foxp3 signaling and was termed type 1 regulatory T cell (Tr1) [82]. While various surface markers and cytokines are described for Tr1 cells, research is hampered by the lack of a unique transcription factor. The co-inhibitory molecule Lymphocyte-activation gene 3 (Lag-3) and the integrin CD49b were described as indispensable surface markers for Tr1 identification [83]. Moreover, IL-10 signaling was proven essential for their function as impairment of IL-10 receptor signaling led to loss of suppressive activity [84].

As described before, there is a remarkable plasticity in the CD4 T cell subsets. Even cells that were previously thought to be solely inflammatory can have tolerogenic functions. For instance, Th17 cells that are associated with autoimmune disease can also play a protective role under certain conditions. Depending on cytokine polarization, differentiation into the protective subtype is promoted, i.e. polarization with TGF-β and IL-6 in the absence of IL-23 favors generation of so-called Treg17 cells. These are characterized by high secretion of IL-17 and IL-10, but low expression of IL-22 (summarized in [85]). Another group identified a similar population of Foxp3+RORγt+ cells that they propose as a novel lineage independent from Treg17 and Treg [86].

In the context of oral tolerance, another class of Foxp3+ Treg was identified that produces high amounts of TGF-β and varying amounts of IL-4 and IL-10: the so-called Th3 cells [87]. While first being described already in 1998, defining them as a specific subset remains difficult due to the lack of a specific marker. They share Foxp3 expression with conventional CD4+CD25+ Treg and depend on TGF-β analogous to Th17 cells. Notably, Th3 and Th17 cells might share

a common progenitor that expresses both Foxp3 and Rorγt and differentiates into a specific subset due to certain cytokines in the environment resulting in a suppressive population of Th3 cells or an inflammatory population of Th17 cells [88].

Modes of suppression by Tregs include contact-dependent and contact-independent mechanisms. Tregs can secrete inhibitory cytokines, such as IL-10, IL-35, and TGF-β to suppress effector T cell function and directly induce apoptosis in T cells via secretion of granzyme B [89]. They can also assert suppressive functions via the activation of tolerogenic DCs that express IDO. IDO activates the kynurenine pathway and thus limits the presence of tryptophan, an essential amino acid for T cell growth. Furthermore, the degradation products in the kynurenine pathway induce the generation of further Tregs resulting in a positive feedback loop [90]. Tregs can also directly interact with T cells via the expression of co-inhibitory signals, such as Lag-3 and T cell immunoreceptor with Ig and ITIM domains (TIGIT). Most importantly, activation of T cells requires three signals: TCR stimulation, co-stimulation, and cytokine polarization. Tregs can directly inhibit co-stimulation by the action of cytotoxic T-lymphocyte-associated protein 4 (CTLA-4) as this is homologous to the co-stimulatory protein CD28 that binds to CD80/CD86 on APCs. CTLA-4, however, binds CD80/CD86 with higher affinity and thus outcompetes CD28 and upon binding delivers co-inhibitory signals to T cells [91]. Lastly, Tregs were identified to assert their suppressive function via an IL-2 feedback loop (reviewed in [92]). IL-2 is essential for T cell proliferation and differentiation and is secreted by activated T cells to sustain their activation status [93]. However, IL-2 also activates Tregs that suppress the ongoing immune response, i.e. increasing levels of IL-2 under inflammatory conditions will activate Tregs and thus constitute a self-limiting mechanism of immune homeostasis. Additionally, it was suggested that Tregs compete with activated T cells for the secreted IL-2 and thus limit IL-2 availability for effector T cells [94]. Due to their exceptional suppressive capacity, Tregs are studied for therapeutical use in diseases, in which suppression of the immune system is desired, such as organ transplantation and autoimmunity. Injecting patients with mostly autologous polyclonally expanded Tregs showed promising results in different phase I and II studies for the treatment of T1D and Crohn's disease. Several ongoing phase I and II studies try to elucidate the potential of Tregs to prevent rejection in solid organ transplantation (reviewed in [95]).

1.3.2.2 Co-inhibitory signals

TCR stimulation does not suffice to activate T cells as TCR stimulation without co-stimulation leads to T cell anergy or deletion [39]. The best-characterized co-stimulatory molecule on T cells is CD28, which interacts with CD80/86 on APCs to deliver a secondary signal and enables T cells to become fully activated [96]. Another co-stimulatory molecule expressed on T cells is ICOS, which exerts its activating function when binding to ICOS-L on APCs [97]. In contrast to co-stimulatory receptors, co-inhibitory receptors (also termed immune checkpoint receptors) were identified that negatively regulate T cell responses when binding their ligands on APCs.

The most studied co-inhibitory receptor is CTLA-4, a homologue of CD28 that binds CD80/86 with higher affinity and thus outcompetes CD28 and dampens T cell activation [98]. Upon binding of its ligand, CTLA-4 induces endocytosis of the complex and reduces the chances of co-stimulation via CD28-CD80/86 ligation. Additionally, binding has direct effects on APCs, as CTLA-4 was shown to induce nuclear localization of the transcription factor Foxo3, which inhibited IL-6 and tumor necrosis factor (TNF) production in DCs leading to a rather tolerogenic DC phenotype [99]. While constitutively expressed on Tregs, surface expression of CTLA-4 is induced after TCR stimulation on activated T cells [100].

Another immune checkpoint receptor is PD-1 that is expressed on various cell types including CD4 T cells. Like CD28, ICOS, and CTLA-4, it belongs to the CD28 superfamily. PD-L1 and PD-L2 were identified as ligands for PD-1 that can be expressed on APCs and T cells [101]. Binding of PD-1 to its ligands ultimately leads to downregulation of TCR signaling through dephosphorylation of signaling molecules. This suppressive effect is mediated by an immunoreceptor tyrosine-based inhibitory motif (ITIM) and an immunoreceptor tyrosine-based switch motif [102].

T-cell immunoglobulin and mucin-domain containing-3 (Tim-3) was originally identified as a marker for Th1 cells that, when blocked, enhances the symptoms of EAE [103]. However, Tim-3 expression is not limited to Th1 cells, but was also described on Tregs, APCs, and other immune cells. Binding of galectin-9, a C-type lectin present on APCs, and Ceacam1, a glycoprotein present on T cells, leads to association of Tim-3 with phosphatases, such as CD45 and CD148 that via phosphorylation of two tyrosine residues lead to inhibition of TCR

signaling in T cells [104, 105]. Tim-3 is constitutively expressed in murine tTregs but absent in human Tregs under steady state conditions. However, upon stimulation, human Tregs upregulate Tim-3 expression together with gene expression of *CTLA4*, *FOXP3*, and *LAG3*, and Tim-3+ Treg were superior to Tim-3- Treg in suppressing CD4 T cells [106].

Lag-3 is expressed on activated T cells, natural killer cells (NK cells), and DCs and structurally resembles the CD4 receptor. Lag-3 competes with CD4 for MHC II binding and binds it with higher affinity [107]. Two other ligands for Lag-3 were identified: LSECtin that is highly expressed in the liver [108] and the lectin galectin-3 that was shown to suppress CD8 T cell responses via Lag-3 [109]. The molecular pathways underlying Lag-3 inhibition are not well understood. However, upon activation, Lag-3 associates with CD3 leading to a decreased calcium response and reduced T cell proliferation and cytokine production [110]. Apart from effector T cells, Lag-3 is also highly expressed in Tr1 cells [83] and loss of Lag-3 signaling in Tregs reduces their suppressive capacity [111]. Part of the inhibitory function Tregs have on DCs was attributed to their expression of Lag-3, as binding of Lag-3 on Tregs to MHC II on DCs inhibits DC activation and favors the generation of tolerogenic DCs [112].

Another member of the CD28 family is TIGIT that was identified to be expressed on activated and memory T cells and Tregs and also downregulates immune responses via binding of its ligands CD112 and CD155 [113]. The binding affinity to CD155 is high, whereas interactions with CD112 are with low affinity. Both ligands are shared with the co-stimulatory receptor CD226 [114]. Similar to CTLA-4, TIGIT binds the shared ligands with higher affinity and in doing so, inhibits co-stimulation and can also directly interact with CD226 and inhibit its dimerization [115]. The cytoplasmic tail of TIGIT contains an ITIM and an immunoglobulin tail tyrosine-like motif that mediate cell intrinsic inhibitory function by downregulation of TCR signaling molecules and the TCR complex itself [116, 117]. The inhibitory role of TIGIT was shown in mice where TIGIT-deficient CD4 T cells produce more pro-inflammatory cytokines [117]. Comparable to other co-inhibitory molecules, TIGIT is also highly expressed on Tregs.

TIGIT+ Tregs express higher levels of Treg signature genes, such as *Foxp3* and *Il2ra* and show a higher lineage stability as well as increased suppressive capacity [118, 119].

Apart from the co-inhibitory molecules discussed above, there are others that were shown to downregulate T cell responses and are considered as immune checkpoints, such as BTLA [120], VISTA [121], 4-1BB [122], PSGL-1 [123], PROCR, and podoplanin [124] that are mostly studied in the context of CD8 T cell inhibition in cancer. Exhausted T cells – i.e. dysfunctional T cells that are found in cancer as well as in chronic infections – are characterized by high expression of co-inhibitory molecules accompanied by a loss of effector functions, ultimately leading to apoptosis. Whereas transient expression of co-inhibitory receptors is seen in activated T cells, the expression of multiple co-inhibitory molecules over an extended period of time was described as a sign for both CD4 and CD8 T cell exhaustion in humans and mice (reviewed in [125]).

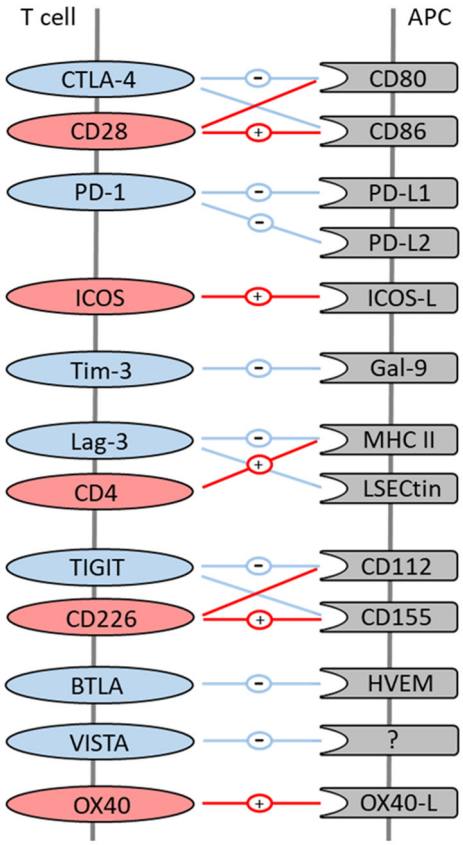

Figure 3. Selected co-inhibitory and co-stimulatory receptors and their respective ligands.
Efficient T cell activation requires a second signal delivered by binding of co-stimulatory molecules (red) on CD4 T cells to their respective ligands on APCs (grey). Co-inhibitory receptors (blue) instead suppress T cell activation by delivering negative signals. Certain co-inhibitory and co-stimulatory receptors share the same ligands on APCs. Binding of CTLA-4 to CD80/86 on APCs delivers an inhibitory signal, whereas CD28 ligation to CD80/86 is an important secondary signal needed for T cell activation. The co-inhibitory receptor Lag-3 and the co-stimulatory receptor CD4 share binding of MHC II and also TIGIT and CD226 bind to the same ligands on APCs with TIGIT delivering negative signals and CD226 assisting in T cell activation.

The importance of co-inhibitory receptors for maintaining peripheral tolerance is illustrated by the detrimental effects when these inhibitory signals are lost. A CTLA-4 knockout (KO) in mice leads to lymphoproliferation and death within three to four weeks of life due to multiple organ failure [126]. A PD-1 KO in mice leads to a lupus-like disease [102]. Another group showed that PD-1-deficient mice suffer from autoimmune dilated cardiomyopathy, and two thirds of the homozygous KO mice, as compared to only 10% of the heterozygous KO mice, died by the age of 30 weeks [127]. Loss of other receptors may not lead to spontaneous autoimmunity, but favors the development of autoimmune disease in various mouse models. A loss in TIGIT signaling increases the susceptibility to EAE [117], whereas Lag-3 KO mice are more prone to develop diabetes in the NOD mouse model [128]. Also in humans, an association between reduced co-inhibition and the development of autoimmunity was observed. Indeed, heterozygous mutations in *CTLA4* cause a variety of autoimmune phenotypes due to decreased Treg function, increased T cell activity, and infiltration of cells into different non-lymphoid organs, such as brain, lung, and gastrointestinal tract [129]. Polymorphisms in the *PDCD1* gene, coding for PD-1, favor the development of different autoimmune diseases, such as MS [130, 131], SLE [132], and RA [133]. Mutations in *Hepatitis A virus cellular receptor 2 (HAVCR2)*, coding for Tim-3, have been associated with MS [134] and RA [135] as well.

The importance of co-inhibitory signaling in preserving peripheral tolerance led to a strong interest in therapeutic interventions. Treatment with monoclonal antibodies directed against various co-inhibitory receptors is promising in cancer to reverse T cell exhaustion and thus boost the immune response against the tumor (reviewed in [136]). However, negative side effects of treatment have been observed and are summarized under the term immune-related adverse events. These include a variety of autoimmune pathologies in various organ systems, such as gastrointestinal tract, liver, skin, lung, and others, with increasing risk in combination therapy using multiple antibodies directed against multiple co-inhibitory receptors (reviewed in [137]). As a loss in co-inhibitory signaling is associated with the development of autoimmune disease, the use of agonists is suggested to induce signaling through these receptors for the treatment of autoimmunity (reviewed in [138]). One example of successful translation of co-inhibitory receptor activation into the clinics is the use of Abatacept to treat RA. Abatacept is a recombinant fusion protein combining human CTLA-4 with the Fc region of immunoglobulin G (IgG) 1,

and treatment of patients with Abatacept improves RA symptoms and disease activity [139]. This CTLA-4Ig blocks binding of APCs to CD28, thus inhibits co-stimulation, and could compensate for the loss of CTLA-4 signaling in a patient with a point mutation in *CTLA4* [140]. In SLE, however, disease outcome was not improved in patients receiving standard treatment in conjunction with Abatacept compared to a placebo [141] revealing a disease-dependent effect of treatment. Co-inhibitory receptors are thus of major importance to maintain immune homeostasis and are interesting targets for immune interventions.

1.4 Mouse models of hepatic tolerance and autoimmunity

1.4.1 Induction of hepatic tolerance in CRP-MBP mice

Luth et al. studied whether the extraordinary capacity of the liver to induce immune tolerance could be harnessed for the protection of extrahepatic tissues from autoimmune attacks using the EAE mouse model [142]. EAE is a T cell-driven autoimmune disease causing demyelination in the central nervous system (CNS) and is studied as a mouse model for MS. In B10.PL mice, the encephalitogenic epitope of MBP is the aminoterminal acetylated peptide Ac1-9. To increase MHC II binding affinity, the lysine at position 4 was replaced by tyrosine [143]. The modified MBP was constantly expressed in the liver under control of the hepatocyte-specific human C-reactive protein (CRP) promoter rendering the mice completely resistant to induction of autoimmune disease when immunized to MBP [142]. Disease prevention was also verified when MBP was only transiently expressed in the liver, either via hydrodynamics-based or adenoviral gene transfer [142]. Clonal deletion of encephalitogenic T cells was ruled out by crossing MBP-transgenic mice to T cell-receptor-transgenic tg4 mice that express a restricted Vβ8.2+ TCR recognizing Ac1-9 [144]. These mice showed similar peripheral antigen-specific T cell numbers compared to tg4 mice, in which expression of MBP is restricted to the CNS. Upon immunization to Ac1-9, these mice were also protected from EAE [142]. Tolerance in this model seemed to be associated with Tregs, which were increased in numbers [18] and could confer tolerance upon transfer [142]. However, preliminary work of our group showed that tolerance is maintained despite depletion of Tregs via anti-CD25 antibody and impairment of pTreg generation via crossing of CRP-MBP mice to dominant negative TGF-β receptor mice

[145]. Thus, Tregs are able to confer tolerance, but are dispensable for liver-induced tolerance raising the question, which mechanisms safeguard tolerance in this model. Preliminary work of our group, conducted by Alena Laschtowitz [146] and Lisa Leypoldt [145], suggested a role for Tr1 cells and the co-inhibitory molecules PD-1 and CTLA-4.

1.4.2 Induction of hepatic tolerance via autoantigen peptide-loaded nanoparticles

The generation of antigen-specific immune tolerance is a major goal for treatment of autoimmune diseases. In recent years, synthetic nanoparticles (NP) have gained interest, as they are readily taken up by APCs, and can thus alter the immune system. Kishimoto and Maldonado [147] summarize the current knowledge on tolerogenic NPs and define three classes with different mechanisms of action. First, NPs can deliver the sole antigen to initiate natural tolerance mechanisms. Secondly, antigen-delivering NPs can simultaneously target tolerogenic receptors and lastly, NPs can carry pharmacological agents that favor a tolerogenic APC phenotype. Harnessing the tolerogenic capacity of the liver falls into the first category of using natural tolerance mechanisms. As LSECs bear an exceptional potential to induce Tregs (described in 1.1.2), targeting autoantigens to LSECs *in vivo* was suggested as a potential tool for antigen-specific treatment of autoimmune diseases. Indeed, in the EAE model, delivery of MBP to LSECs via poly(maleic anhydrate-alt-1-octadecene)-coated NPs completely protected from disease development and could even alleviate established disease [22]. NPs were selectively taken up by LSECs, a tropism that was favored by their small size, as particles >0.5 μm were shown to be phagocytosed by KCs and smaller particles were found inside LSECs [16]. Tolerance induced by LSEC-targeting peptide-loaded NPs was associated with the induction of Tregs, as Treg numbers in spleens of mice treated with antigen peptide-loaded NPs were higher than in controls and depletion of Tregs via antibody abrogated tolerance [22].

Recently, Liu et al. [148] generated LSEC-targeting NPs that carry surface ligands of scavenger and mannose receptors expressed on LSECs. Due to their size of 200-300 nm, they were preferably taken up by LSECs – a tropism that was increased by expression of surface ligands. The NPs used were poly(lactic-co-glycolic acid) nanocarriers, which transported the murine allergen ovalbumin (OVA) to the liver. Sensitization with OVA is a model for pulmonary

allergen sensitization that is characterized by anti-OVA IgE responses, airway eosinophilia, and a Th2 cytokine profile. Prophylactic treatment with OVA-loaded nanoparticles could alleviate all of the mentioned symptoms. Beneficial effects were increased when nanoparticles with attached surface ligands were used. In brief, the tolerogenic effect of LSEC-targeting antigen-loaded NPs was increased by attachment of ligands targeting scavenger and mannose receptors on LSECs.

1.5 Aims of the study

The remarkable tolerogenic capacity of the liver is evidenced by its ability to protect extrahepatic tissue. However, the underlying tolerance mechanisms are not yet fully understood. The aim of this study was to elucidate the mechanisms behind tolerization of antigen-specific T cells in the liver. Therefore, hepatic tolerance was studied in two mouse models in which the myelin antigen MBP served as MHC II-restricted autoantigen expressed in the liver:

1) The transgenic CRP-MBP model is characterized by ectopic expression of MBP in the liver under control of the human C-reactive protein promoter [142].

2) The model of autoantigen delivery to LSECs via nanoparticles exploits the tolerogenic capacity of LSECs by targeting MBP specifically to these cells in the liver [22].

Whereas the CRP-MBP model as a transgenic mouse model represents an ideal tool to study potential peripheral tolerance mechanisms, the translational aspect of autoantigen delivery to LSECs via nanoparticles allowed for the verification of identified tolerance mechanisms in a model of high therapeutic relevance with potential translation into the clinics. Of note, in both models, hepatic MBP presentation to T cells completely protected mice from the development of MBP-induced autoimmune neuroinflammation. Tolerance in both models was associated with an increase in CD25+Foxp3+ Treg numbers [18, 22]. However, preliminary work of our group showed that Tregs were dispensable for the maintenance of hepatic tolerance in CRP-MBP mice [145]. Therefore, this study aimed at identifying additional hepatic tolerance mechanisms apart from Tregs that might suppress autoreactive CD4 T cell responses and protect from autoimmune disease in extrahepatic tissues, such as the CNS. Specifically, the following mechanisms should be addressed:

- T cell migration to the liver
- T cell differentiation within the liver with a focus on Tr1 cells
- Cytokine production of MBP-specific T cells
- Activation status of MBP-specific T cells with regard to co-inhibitory receptor expression

Moreover, as an additional aim, prognostic biomarkers associated with the induction of antigen-specific tolerance in the liver and protection from autoimmunity should be identified.

2. Materials and Methods

2.1 Materials

2.1.1 Devices

Table 1. Devices

Device	Manufacturer
Analytical scale	Ohaus
Autoclave VX-120	Systec GmbH
Centrifuge 5417R	Eppendorf
Centrifuge 5810R	Eppendorf
Centrifuge Megafuge 2.0	Heraeus Instruments
CO_2 incubator	SANYO Biomedica
Cobas Integra 400 Plus	Roche
Dispenser Multipipette Stream	Eppendorf AG
Dissecting set	VWR International GmbH
Flow cytometer LSRII	BD Biosciences
Flow cytometer FACSAria Illu	BD Biosciences
Flow cytometer Fortessa	BD Biosciences
Fluoresence microscope BZ-9000	Keyence
Light microscope Axiovert 40 CFL	Carl Zeiss
Magnetic holder	Miltenyi Biotec
Microme HM550 Cryostat	Thermo Fisher Scientific
Microplate reader	Tecan Trading AG
Microtome CUT 5062	SLEE medical
Nanodrop 2000	Thermo Fisher Scientific
Neubauer counting chamber	Optik Labor Frischknecht
Peqstar thermocycler	VWR International GmbH
Perfusion pump	Dynex Technologies
Pipets	Eppendorf AG
Pipetting aid	Hirschmann Laborgeräte
Safety workbench Lamin Air	Thermo Fisher Scientific
Tabletop centrifuge Biofuge pico	Heraeus Instruments
Thermocycler	Biometra
Tissue Cool Plate COP 20	MEDITE
ViiA 7 Real-Time PCR System	Applied Biosystems

2.1.2 Consumables

Table 2. Consumables

Consumables	Manufacturer
Cannulas BD Microlance 26G x ½	BD Bioscience
Cannulas 19G x 1 ½, 21G x 1 ½, 26G x 1, 27G x ¾, 30G x 1 ½	B. Braun
Cell Strainer 100 µm, 40 µm	Greiner bio-one
Cell culture plates 96-well	Sarstedt
Combitips advanced 0.2 mL, 1 mL, 5 mL, 10 mL	Eppendorf
Coverslips	Sarstedt
CryoPure tubes 1.6 mL	Sarstedt
Cryotome blades C53	Feather
LS columns	Miltenyi Biotec
MACS Pre-Separation Filters	Miltenyi Biotec
MicroAmp Fast 96-well reaction plate 0.1 mL	Applied Biosystems
Micropistille for 1.5 mL tubes	Carl Roth
Microscope slides	Thermo Fisher Scientific
Microtome blades S35	Feather
Multiply-µStrip Pro 8-strip	Sarstedt
Petri dish, 75 mm	Sarstedt
Pipet tips	Sarstedt
Polystyrene tube 12x75 mm for flow cytometry	Sarstedt
Reaction tubes 0.5 mL, 1.5 mL, 2 mL, 5 mL	Sarstedt
Reaction tubes 15 mL, 50 mL	Greiner bio-one
Serological pipets	Greiner bio-one
Syringes 1 mL, 2 mL, 10 mL	B. Braun
Tissue embedding cassettes	Kabe Labortechnik

2.1.3 Substances

Table 3. Substances

Substance	Manufacturer
4Y-MBP (Acetyl-ASQYRPSQR-COOH)	Panatecs
Ammonium chloride (NH_4Cl)	Merck
Annexin V Binding Buffer, 10x concentrate	BD Biosciences
Antibody diluent	Zytomed
Aqua Braun	B. Braun

Avidin-Biotin-Block	Dako
Bovine serum albumin (BSA)	Carl Roth
Complete Freund's Adjuvants	Difco Laboratories
CD4 microbeads	Miltenyi Biotec
CD11c microbeads	Miltenyi Biotec
Citrate buffer (unmasking solution)	Vector laboratories
Ethylenediaminetetraacetic acid (EDTA)	Roth
Entellan	Merck
Eosin	Roth
Ethanol absolute	ChemSolute ® Th. Geyer GmbH & Co. KG
FACS Clean Solution	BD Biosciences
FACSFlow Sheath Fluid	BD Biosciences
FACSRinse Solution	BD Biosciences
Fc block (CD16/32)	eBioscience
FCS	PAA Laboratories GmbH
Fluorescence mounting medium	Dako
GolgiPlug	BD Biosciences
Hematoxylin	Carl Roth GmbH & Co. KG
Heparin-sodium-25000	Ratiopharm
Hoechst 33258	Invitrogen
Hydrochloric acid	Carl Roth
Ionomycin calcium salt from *S. conglobatus*	Sigma-Aldrich
Ketamine	aniMedica GmbH
M. Tuberculosis H37 RA	Difco Laboratories
OneComp eBeads	Invitrogen by Thermo Fisher Scientific Inc.
OptiPrep	Sigma-Aldrich
OptiPrep	Stemcell Technologies
Pacific Orange Succinimidyl Ester (PacO-NHS)	Invitrogen by Thermo Fisher Scientific Inc.
Panserin	PAN-Biotech GmbH
Paraformaldehyde	Carl Roth
Penicillin/Streptomycin 10,000 U/mL	Gibco Life Technologies
Percoll	GE Healthcare
Pertussis Toxin from Bordetella Pertussis	Sigma-Aldrich
Poly(maleic anhydrate-alt-1-octadecene)-coated nanoparticles	Topas Therapeutics
Phorbol-12-myristat-13-acetat (PMA)	Sigma-Aldrich

Potassium chloride (KCl)	Merck
Potassium hydrogen carbonate ($KHCO_3$)	Carl Roth
Potassium dihydrogenphosphate (KH_2PO_4)	Merck
Rompune 2%	Bayer Vital GmbH
RotiHistoFix	Carl Roth
Saponin	Sigma-Aldrich
Sodium chloride (NaCl)	Carl Roth
Sodium hydrogen phosphate (Na_2HPO_4)	Carl Roth
Trypane Blue 0.4%	Gibco Life Technologies
Xylol	ChemSolute Th. Geyer GmbH & Co. KG
β-mercaptoethanol	Sigma-Aldrich

2.1.4 Kits

Table 4. Kits

Kit	**Manufacturer**
Foxp3 Staining Buffer Set	eBioscience
High Capacity cDNA Reverse Transcription Kit	Applied Biosystems
In Situ Cell Death Detection Kit, TMR Red	Roche
KAPA Probe Fast qPCR Kit	Sigma-Aldrich
NucleoSpin RNA	Macherey Nagel
Permanent AP Red Kit	Zytomed
POLAP Kit	Zytomed
Vector M.O.M. Immunodetection Kit	Vector Laboratories

2.1.5 Antibodies

2.1.5.1 Flow cytometry

Table 5. Fluorochrome-labelled antibodies for flow cytometry

Antibody	**Color**	**Clone**	**Manufacturer**
Annexin V	PE	N/A	BD Biosciences
CD4	PE-Dazzle	RM4-5	BioLegend
CD4	PerCP	RM4-5	BD Biosciences
CD45	AF700	30-F11	BioLegend
CD11b	FITC	M1/70	BD Biosciences
CD11c	PE-Dazzle	N418	BioLegend
CD25	APC	PC61	BioLegend

CD45.1	AF700 PE-Cy7	A20	BioLegend
CD49b	PE PerCPCy5.5	HMa2	BioLegend
CD69	BV421	H1.2F3	BioLegend
CD146	PE-Cy7	ME-9F1	BioLegend
CTLA-4 (ICS [149])	PE	UC10-4F10-11	BD Biosciences
CXCL9	PE	MIG-2F5.5	BioLegend
CXCR3	APC	CXCR3-173	BioLegend
F4/80	APC/Fire	BM8	BioLegend
Foxp3	FITC	FJK-16S	eBioscience
IFNγ	AF700 FITC	XMG1.2	BioLegend
IL-10	PE	JES5-16E3	BioLegend
IL-17	APC BV421	eBio17B7	eBioscience
Ki-67	BV421	16A8	BioLegend
Lag-3	APC PerCPCy5.5	C9B7W	BioLegend
PD-1	APC/Fire BV421	29F.1A12	BioLegend
PD-L1	BV421	10F.9G2	BioLegend
TIGIT	BV421	1G9	BD
Tim-3	PE-Cy7	RMT3-23	BioLegend
TNFα	BV421 FITC	MP6-XT22	BioLegend

2.1.5.2 Histology

Table 6. Antibodies for histology

Antibody	**Color**	**Clone**	**Manufacturer**
CD4	PE	RM4-5	BioLegend
CD45.1	AF647	A20	BioLegend
CD45.2	FITC	104	BioLegend
Rabbit anti-rat IgG Biotin-conjugated	N/A	Polyclonal	Thermo Fisher Scientific
Rat anti-mouse Ki-67	N/A	SolA15	eBioscience

2.1.5.3 In vivo blockade

Table 7. Antibodies for in vivo blockade

Antibody	Clone	Manufacturer
CTLA-4	UC10-4F10-11	BioXCell
IFNγ	XMG1.2	BioXCell BioLegend
Anti-IL-10 receptor	1B1.3A	BioXCell
Armenian hamster IgG	Polyclonal	BioXCell
Rat IgG, anti-horseradish peroxidase, isotype control	HRPN	BioXCell

2.1.6 Taqman probes

All TaqMan probes were purchased from Thermo Fisher Scientific.

Table 8. Taqman probes

Gene	Encoded protein	Probe
Aoc3	VAP-1	Mm00839624_m1
Ctla4	CTLA-4	Mm00486849_m1
Ccr7	CCR7	Mm99999130_s1
Cd274	PD-L1	Mm03048248_m1
Cxcl9	CXCL9	Mm00434946_m1
Cxcr3	CXCR3	Mm99999054_s1
Havcr2	Tim-3	Mm00454540_m1
Hprt	HPRT	Mm00446968_m1
Icam1	ICAM-1	Mm00516023_m1
Ido1	IDO1	Mm00492590_m1
Il2	IL-2	Mm00434256_m1
Lag3	Lag-3	Mm00493071_m1
Madcam	MAdCAM-1	Mm00522088_m1
Pdcd1	PD-1	Mm01285676_m1
Tigit	TIGIT	Mm03807522_m1
Vcam1	VCAM-1	Mm01320970_m1

2.1.7 Buffers

Table 9. Buffers

Buffer	Formula
1x PBS, pH 7.4	KCl 2.7 mM KH_2PO_4 1.5 mM NaCl 137 mM Na_2HPO_4 6.5 mM
1x ACK (Ammonium-chloride-potassium)	NH_4Cl 150 mM $KHCO_3$ 10 mM EDTA 100 mM
MACS buffer	1x PBS 0.5% BSA EDTA 2.5 mM
Saponin buffer	1x PBS 1% BSA 0.5% Saponin

2.1.8 Mice

Table 10. Mice

Mouse line	Background	Characterization
tg4	B10.PL-H2uH2-T18a/(73NS)SnJ (B10.PL)	MBP-specific T cell receptor, CD45.1-CD45.2+
(CRP-MBP x B10.PL) F1 – CD45.1/2	C57BL/6 x B10.PL	Expression of MBP in the liver, CD45.1+CD45.2+
(B6.SJL/BoyJ x B10.PL) F1 – CD45.1/2	C57BL/6 x B10.PL	CD45.1+CD45.2+
(tg4 x $IL10^{eGFP}$ $Foxp3^{mRFP}$) F1 – CD45.1	C57BL/6 x B10.PL	MBP-specific T cell receptor and reporter for IL-10 and Foxp3

For adoptive transfer experiments, (CRP-MBP x B10.PL) F1 mice with hepatic MBP expression [142] or (B6.SJL/BoyJ x B10.PL) F1 were used as recipients. MBP-specific CD4 T cells were isolated from T cell-receptor-transgenic tg4 mice [144]. As indicated, the tg4 T cells had additional mutations, such as IL-10 [150] and Foxp3 reporter activity [151] (tg4 x $IL10^{eGFP}$ $Foxp3^{mRFP}$ reporter mice). All mice were bred and kept in the animal facility of the University Medical Center Hamburg-Eppendorf under specific pathogen-free conditions and used for the

experiments at the age of 8-20 weeks. Animal experiments comply with the ARRIVE guidelines [152] and were approved by the review board of the State of Hamburg, Germany.

2.1.9 Software

Table 11. Software

Software	**Manufacturer**
BD FACS Diva 8	BD Biosciences
BZ-II Analyzer	Keyence
BZ-II Viewer	Keyence
Endnote X8	Alfasoft GmbH
FlowJo V10	Flowjo
GraphPad Prism 6.01	GraphPad Software Inc.
ImageJ	Wayne Rasband, National Institutes of Health
Microsoft Office 2013	Microsoft Corporation
NanoDrop 2000/2000c; 1.6.198	Thermo Fisher Scientific
TierBase TBv610b42	Abase, P. Nielsen
ViiA 7 Software 1.2.4	Applied Biosystems

2.2 Methods

2.2.1 Isolation of primary cells

2.2.1.1 Isolation of cells from spleen

Mice were anesthetized with ketamine and rompune (ketamine : rompune : phosphate-buffered saline [PBS] = 1 : 0.8 : 1; 100 µL/10 g body weight) via intraperitoneal (i.p.) injection and killed via cervical dislocation. Spleens were taken out and fat was removed before generating a single cell suspension. A maximum of four spleens was pooled per isolation. After standard centrifugation (5 min, 400 g, room temperature [RT]), the cell pellet was resuspended in 1 mL of ACK buffer for 90 s to lyse erythrocytes. Lysis was stopped by adding 20 mL of PBS. After centrifugation, cells were resuspended in 1 mL of PBS and counted in a Neubauer counting chamber. Until further use, cells were left at 4°C.

2.2.1.2 Isolation of NPCs from liver

Mice were anesthetized and killed via cervical dislocation. Livers were perfused with PBS (6 mL/min) for approximately 20 s via the vena portae. The gall bladder was removed and the liver was removed from the abdominal cavity. A single cell suspension was generated and centrifuged at 40 g for 4 min to remove hepatocytes. The supernatant was transferred in a new falcon tube and centrifugation was repeated. The final supernatant was centrifuged at 400 g for 7 min. The cell pellet was resuspended in 4.5 mL of PBS and mixed with 2.5 mL OptiPrep at ambient temperature in a 15 mL Falcon tube to generate a 21% OptiPrep gradient. The suspension was carefully covered with 1 mL of PBS and subjected to density gradient centrifugation at 400 g for 20 min without brake. The interphase containing the NPCs and erythrocytes was removed and transferred into a 15 mL Falcon tube. After erythrocyte lysis as described before (see 2.2.1.1), the cell pellet was resuspended in 1 mL of PBS and counted in a Neubauer counting chamber. Until further use, cells were left at 4°C.

2.2.1.3 Whole blood cell analysis

Mice were anesthetized and killed via cervical dislocation. Blood was drawn from the vena cava inferior and transferred to an Eppendorf tube containing 5 µL heparin 5000 U/mL. Erythrocyte lysis was performed for 10 min in ACK buffer. The cell pellet was resuspended in 1 mL of PBS and kept at 4°C until further use.

2.2.1.4 Isolation of T cells from spinal cord

Mice were anesthetized and killed via cervical dislocation. The chest was cut open to expose the heart and the right atrium was cut. Mice were perfused via the left ventricle with PBS (6 mL/min) until the effluent from the atrium was clear. The spinal column was isolated and removed from the body cavity by cutting at the base of the head and close to the tail. A 19G x 1 ½ needle was attached to a 10 mL syringe filled with PBS. The needle was inserted into the spinal canal at the caudal end of the spinal column and the spinal cord was flushed out of the spinal canal into a petri dish. A single cell suspension was generated and centrifuged at 350 g for 10 min. The cell suspension was resuspended in 4 mL 40% Percoll and laid on top of 4 mL 67% Percoll. Density gradient centrifugation was performed at 400 g for 20 min at RT with slow acceleration and no brake. T cells were located in the interphase and were transferred into a 15 mL Falcon tube and washed with PBS/1%FCS. After centrifugation at 350 g for 10 min, cells were resuspended in PBS/1%FCS and left at 4°C until staining.

2.2.2 Magnetic-activated cell sorting (MACS)

To isolate CD4 T cells from spleens, cells were isolated as described (see 2.2.1.1). Erythrocyte lysis was omitted. After cell counting and standard centrifugation (400 g, 5 min, RT), cells were resuspended in 1 mL of MACS buffer per 10^8 cells. 100 µL of CD4 microbeads were added per 10^8 cells for 10 min at 4°C. After further centrifugation, cells were resuspended in 1 mL of MACS buffer per 10^8 cells. A suitable column (here: LS column) was placed in the magnetic field of the MACS separator and was rinsed with 3 mL of MACS buffer. The cell suspension was first filtered through a 30 µm pre-separation filter and then added to the column, which was afterwards rinsed three times with 3 mL of MACS buffer. CD4+ T cells remained in the column while CD4- cells were in the flow through. The column was removed from the separator and 5 mL of MACS buffer were pipetted on the column. By pushing the plunger into the column, CD4 T cells were flushed out. To increase the purity, this eluted fraction was added to a second column following the same protocol. In some experiments, CD4+CD25- cells were needed. For this, prior to positive selection for CD4, cells were negatively selected for CD25. 100 µL of CD25 microbeads in 1 mL of MACS buffer were added per 10^8 cells and incubated for 10 min at 4°C. After standard centrifugation, the cell suspension was added to an

equilibrated column and the flow through containing CD25- cells was collected. The column was washed twice with 3 mL of MACS buffer and the flow through was collected in the same tube. After centrifugation, this flow through was subjected to positive selection for CD4 (as described) to obtain CD4+CD25- cells.

An updated version of the protocol omits the centrifugation after microbead incubation and demands only one washing step on the column.

2.2.3 Flow cytometry

Flow cytometry allows the simultaneous measurement of cell size, granularity, and different fluorescence channels and thus allows the analysis of cellular concentration of fluorescent-labelled molecules. Samples are in a flow and focused, so that only one cell at a time is captured by a laser beam. The scattering light allows the analysis of size and granularity. If cells are fluorescently labelled, lasers can be used to excite different fluorochromes. Detectors record the characteristic band of wavelengths that is emitted, which enables analysis of markers in cells on protein level [153].

2.2.3.1 Live/dead staining

Dead cells were excluded via staining with Pacific Orange Succinidyl Ester (PacO-NHS). As this dye only enters dead cells and stains free amines, live cells remain unstained. A suitable amount of cells (1-2 x 10^6) was transferred into a 5 mL polystyrene tube. PacO-NHS was diluted 1:1000 and the cell pellet was resuspended in 200 µL of solution. Incubation was done for 20 min at 4°C in the dark.

2.2.3.2 Surface staining

To stain surface markers, cells were washed after live/dead staining and resuspended in 100 µL PBS containing 1 µL of each antibody of interest. Incubation was done at 4°C for 15 min. Afterwards, cells were washed with PBS and either directly measured at the flow cytometer, fixated with paraformaldehyde (4% for 15 min) and stored for later measurement, or used for further intracellular staining. If Lag-3 was part of the antibody cocktail, cells were first incubated at 37°C for 15 min followed by 15 min of incubation at RT.

2.2.3.3 Intracellular staining

In order to stain for cytokines and other intracellular factors, cells need to be permeabilized to make the inner part of the cell accessible for staining. Therefore, after fixation, cells were washed with 1 mL of saponin buffer to permeabilize the cell membrane. 1 µL of each antibody of interest was added in 100 µL of saponin buffer and cells were incubated for 30-60 min at 4°C. After washing, cells were resuspended in PBS and either directly measured at the flow cytometer or stored at 4°C until measurement. If the transcription factor Foxp3 was included in the staining, the eBioscience Foxp3 / Transcription Factor Staining Buffer Set was used after surface staining for all intracellular stainings according to manufacturer's instructions.

2.2.3.4 Stimulation of cells

To detect cytokine production, re-stimulation of the cells was necessary. For this, 1-2 x 10^6 cells were resuspended in 1 mL Panserin media with 50 µL FCS and PMA (100 ng/mL) and ionomycin (1 µg/mL) were added to unspecifically activate the cells. PMA diffuses through the cell membrane and directly activates the protein kinase C [154] and ionomycin elevates the intracellular calcium level [155], which is needed for T cell activation. Golgi Plug (1 µl/mL) is added as a protein transport inhibitor, so that cytokines accumulate in the Golgi apparatus and are thus better detectable via flow cytometry. Incubation was done at 37°C/5% CO_2 for 4h.

2.2.3.5 Annexin V staining

Apoptotic cells were detected via staining of Annexin V, which binds to phosphatidylserine presented on the outer leaflet of the plasma membrane on apoptotic cells [156]. When apoptotic cells were stained, first, surface staining of desired proteins was performed. Afterwards, cells were resuspended in 100 µL 1x binding buffer and 3 µL of Annexin V antibody and PacO (1:1000) was added. Incubation was done for 15 min at RT in the dark. After washing, cells were resuspended in 200 µL 1x binding buffer and measured at the flow cytometer within 1h.

2.2.3.6 Measuring at the flow cytometer

When emission spectra of different dyes overlap, compensation is necessary. This was done by separately measuring OneComp eBeads, which were stained with each color used in the experiment. One drop of beads was added into a 5 mL polystyrene tube and was stained with

1 µL of antibody. To compensate for PacO, remaining cells were killed via incubation at 56°C for 30 min and stained for PacO as described (see 2.2.3.1).

In order to analyze a specific population of cells, a defined gating strategy was applied (Fig. 4). First, doublets were excluded by plotting FSC-A against FSC-H. Secondly, lymphocytes were gated according to their characteristic size and granularity in FSC-A vs. SSC-A. Dead cells were excluded by analyzing the dead cell marker PacO and only further looking at the PacO-negative cells. This basic gating strategy was applied to all samples. Further gating steps depended on the target cells in the respective experiment.

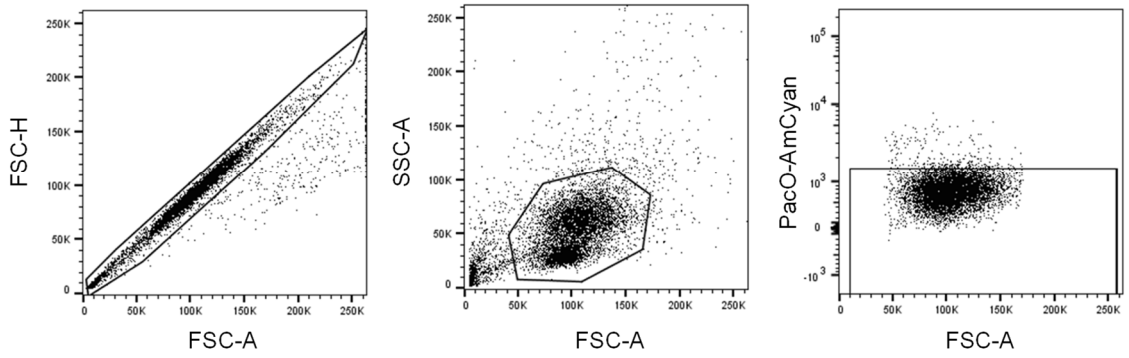

Figure 4. Gating strategy.
In all flow cytometric analyses, doublets were excluded (left), the target population was gated according to size (FSC-A) and granularity (SSC-A) (middle), and dead cells were excluded (right).

2.2.3.7 T-SNE

T-distributed stochastic neighbor embedding (t-SNE) is an algorithm that allows the illustration of high-dimensional data sets in a low-dimensional space with only two or three dimensions [157]. This unsupervised nonlinear reduction algorithm is implemented as a Plugin in FlowJo and can be used to analyze high dimensional flow cytometric data sets. First, classic gating needs to be performed on the samples to remove doublets, dead cells, and debris. Further gating is performed to include only the cells of interest, i.e. CD4+CD45.1- MBP-specific tg4 T cells, here. To reduce computation time, the number of events is reduced by downsampling to a desired amount of cells, such as 5000 cells per sample. It is important to merge samples that should be compared, as running the algorithm twice will lead to a different two-dimensional map. This process is called concatenation and allows the direct comparison of samples within the same t-SNE data space. Dimension reduction is performed on the concatenated sample by

choosing the compensated fluorescence-based parameters of interest, such as the colors used for staining of the co-inhibitory receptors. The output can be modified by changing the technical options, such as the number of iterations, perplexity, and Eta (learning rate). Analysis was performed with default settings of 1000 iterations, a value of 20 for perplexity, and a learning rate of 200 for analysis of co-inhibitory receptors, and 2000 iterations, a value of 50 for perplexity, and a learning rate of 500 for analysis of IL-10-producing cells.

2.2.4 EAE induction and scoring

Age- and sex-matched mice were injected subcutaneously at the base of the tail with 200 µg MBP peptide Ac1-9 [6] in 0.1 mL of an emulsion of PBS and complete Freund's adjuvant containing 4 mg/mL heat-killed *Mycobacterium tuberculosis*, strain H37RA. At the day of immunization and two days later, 200 ng of pertussis toxin was injected i.p. in 0.25 mL of PBS. EAE was monitored daily for up to 30 days post immunization. The severity of EAE was scored as follows: 0, no clinical signs; 1, flaccid tail; 2, partial hind-limb paralysis; 3, complete hind limb paralysis; 4, fore- and hind-limb paralysis; 5, moribund. Treatment with anti-IFNγ antibody leads to atypical EAE symptoms in some mice. These are scored as follows: 0, no clinical signs; 1, slight head tilt; 2, severe head tilt; 3, slight axial rotation/staggered walking; 4, severe axial rotation/spinning; 5, moribund [158]. Mice were sacrificed when reaching a score of 4 due to ethical reasons. The cumulative disease score is the sum of individual daily scores for each animal.

2.2.5 Adoptive T cell transfer

In order to analyze the antigen-specific T cell response, MBP-specific CD4 T cells were isolated from spleens of tg4 mice via MACS as described (see 2.2.2.1) and adoptively transferred into recipient mice. 5-6 x 10^6 CD4 T cells were injected intravenously into immunized mice one day after immunization.

2.2.6 Nanoparticle treatment of mice

MBP peptide-loaded poly(maleic anhydrate-alt-1-octadecene)-coated NPs and empty control NPs were provided by Topas Therapeutics. On the day of immunization, mice were injected i.p. with NPs containing 20 μg MBP in 150 μL 100 mM NaCl (MBP-NP). A solution of empty NPs in 100 mM NaCl with the iron content adjusted to MBP peptide-loaded NPs was injected i.p. as control (NP). Before administration, NPs were filtered via a 30 μm filter.

2.2.7 In vivo antibody blockade

For in vivo blockade of IFNγ, CTLA-4, and IL-10R, 300 μg of antibody was administered i.p. in 0.2 mL of PBS twice a week. Rat IgG1 anti-horseradish peroxidase (HRPN) was used in equal concentration and volume as isotype control for anti-IFNγ and anti-IL-10R. Armenian hamster IgG was used as isotype control for anti-CTLA-4.

2.2.8 RNA isolation and qPCR

Total ribonucleic acid (RNA) was prepared from liver tissue or NPCs with the NucleoSpin RNA Kit according to manufacturer's instructions. The quantity and quality of the RNA was determined with a Nanodrop2000. 1 μg of RNA was reverse-transcribed to complementary deoxyribonucleic acid (cDNA) with the High-Capacity cDNA Reverse Transcription Kit. cDNA was diluted 1:4 in water and stored at -20°C or directly used for quantitative polymerase chain reaction (qPCR). To determine the relative expression level of each gene of interest, qPCR was performed with TaqMan probes and the KAPA Probe Fast qPCR Master Mix (2x) Kit. qPCR reactions were performed in duplicates and measured on the ViiA 7 Real-Time PCR System using a pre-set protocol (see table 12). To calculate the relative expression for each target gene, first, the ΔCt value was calculated by subtracting the threshold cycle of the housekeeper (here: hypoxanthine-guanine phosphoribosyltransferase [Hprt]) from the target gene. The relative expression was determined using the following formula: $\frac{1}{2^{\Delta Ct}}$.

Finally, the relative expression was normalized to the control group, i.e. the relative expression in wildtype (wt) or empty NP-treated mice, using the following formula:

$$\frac{1}{\text{mean relative expression control}} \text{ x relative expression sample} = \text{normalized expression}$$

Table 12. qPCR program

Temperature	Time	No. of cycles
95°C	20 s	1
95°C	1 s	40
60°C	20 s	

2.2.9 Histology

After perfusion, livers were immediately frozen for subsequent immunofluorescence staining or embedded in paraffin for hematoxylin and eosin staining (HE), histological stainings, or terminal deoxynucleotidyl transferase dUTP nick end labeling (TUNEL).

2.2.9.1 Sample preparation and cutting at the microtome

After perfusion, half of or the full left liver lobe (Lobus sinister) was placed into a histology grid and was fixated for 24h in Roti-Histofix (4%, 4°C). Samples were dewatered at the pathology of the UKE and embedded in paraffin.

Table 13. Protocol for dewatering tissue samples

	Formalin	**Ethanol**							**Xylol**		**Paraffin**			
		80%		96%		100%			I	II	A	B	C	D
Time (min)	60	30	40	30	40	30	40	50	40	60	20	30	40	60

To generate 3 µm thick cuts, samples were placed on a cooling plate at -8°C and after cooling down placed on ice. After short incubation on ice, samples were cut and placed in a water bath at 37°C before being transferred to the microscope slide and dried at 37°C over night.

2.2.9.2 HE staining

To visualize infiltration of cells, liver slides were stained with HE. The organ slices were deparaffinized in xylol (3x 4 min) before being rehydrated by incubation in solutions with

decreasing alcohol concentration (100%, 90%, 70%, 50% ethanol, each 4 min). After rinsing with de-ionized water, slices were incubated in hematoxylin solution for 10 min. Incubation in running tap water led to the staining of acidic (basophilic) structures, such as nuclei in a purple color. After short wash in de-ionized water, slices were stained in eosin for 1-2 min (depending on age and acidity of the eosin solution) to stain basic (acidophilic) structures, such as proteins in the cell plasma, collagen, or mitochondria. After short washing in de-ionized water, organ slices were dewatered by incubation in solutions with increasing alcohol concentration (<30 s in 50%, 30 s in 70%, 1 min in 90%, 2x 2 min in 100% ethanol). After incubation in xylol (3x 4 min), the organ sections were mounted using Entellan and stored at room temperature.

2.2.9.3 Ki-67 staining

Ki-67 was stained in paraffin sections. First, slides were deparaffinized in xylol and rehydrated in solutions with decreasing alcohol concentration (see 2.2.9.2). Slides were washed in H_2O (3x 3 min) before antigen retrieval in citrate buffer was performed. Slides were heated in the microwave (5x 5min, 600 watt) and cooled for 30 min at RT. After washing in H_2O and PBS (each 3x 5 min), unspecific binding sites were blocked by incubation for 10 min in blocking buffer (POLAP kit). A second blocking step was performed using Avidin-Biotin block, each for 10 min at RT separated by washing with PBS (2 x 4 min). The primary antibody (rat anti mouse Ki-67, 1:500, diluted in Zytomed buffer) incubated at 4°C in a humidity chamber overnight. After washing with PBS (3x 5 min), the secondary antibody (polyclonal rabbit anti-rat IgG biotin, 1:300, diluted in Zytomed buffer) incubated at RT in a humidity chamber for 30 min. Washing with PBS (3x 5 min) was followed by incubation with anti-rabbit alkaline phosphatase (POLAP kit) at RT in a humidity chamber for 30 min. After washing with PBS (3x 5 min) and rinsing in H_2O, the alkaline phosphatase permanent red kit was used according to manufacturer's instructions. Slides were rinsed with H_2O, stained with hematoxylin for 3 min and incubated in running tap water for 5-10 min. Slides were dipped in 0.1% HCl for 5 s and dipped in tap water three times. Dewatering was performed with increasing alcohol concentration (dipping in 50% and 70%, 30 s in 90% and 2x 1 min in 100% ethanol). After incubation in xylol (3x 3 min), slides were mounted with entellan and stored at RT.

2.2.9.4 TUNEL

TUNEL is a method to detect double strand breaks in the DNA in tissue sections as a marker of apoptosis. The terminal deoxynucleotidyl transferase is an enzyme that specifically binds double strand breaks and catalyzes the attachment of fluorescently labelled deoxynucleotides to the 3'-hydroxyl termini of DNA double strand breaks. In order to stain for apoptotic cells in paraffin sections, the In Situ Cell Death Detection Kit, TMR Red (Roche) was used according to manufacturer's instructions.

2.2.9.5 Sample preparation and cutting at the cryotome

After perfusion, half of the Lobus hepatis dexter medialis was embedded in Tissue-Tek O.C.T. Compound on dry ice. Frozen samples were stored at -80°C. 6 µm sections were prepared at the cryotome with the chamber and the object cooling at -15°C. Cuts were either directly stained or stored at -80°C until staining.

2.2.9.6 Immunofluorescence

Liver slides were fixated in ice-cold acetone for 15 min. After washing with PBS (3x 3 min), unspecific binding sites were blocked by incubation with PBS/1%BSA/Fc block (1:50) for 30 min at RT. Slides were washed with PBS (3x 3 min) and subsequently stained with antibodies of interest for 1h at RT. After washing with PBS (3x 3min), nuclei were stained with Hoechst33258 (1:10,000 in PBS; 1 min). Final washing steps in PBS (2 x 5 min) were followed by mounting with fluorescence mounting medium. CD45.1 was stained with the Vector M.O.M. immunodetection kit according to manufacturer's instructions.

2.2.10 Assessment of liver damage

Autoimmune hepatitis development was assessed by measurement of serum alanine aminotransferase (ALT) levels in the serum or plasma using an automated procedure (Cobas Integra 400 plus, done by Carsten Rothkegel, UKE) and by histological quantification of liver inflammation in HE-stained slides according to the modified hepatic activity index (mHAI) by a pathologist (Sören Weidemann, Institute of Pathology, UKE).

2.2.11 Statistics

Statistical analyses between two data sets were conducted with the Mann-Whitney U test. For comparisons of three or more groups, a one-way ANOVA with or without Sidak's multiple comparisons test was performed. A p value <0.05 was considered statistically significant: *p<0.05; **p<0.01; ***p<0.001; ****p<0.0001. All data were analyzed using GraphPad Prism 6.01.

3. Results

3.1 Tolerance mechanisms in the CRP-MBP model

In the first part of this thesis, the immune mechanisms underlying tolerance in the CRP-MBP mouse model should be investigated. Therefore, the CRP-MBP model and especially the role of CD4 T cells in this model was characterized before examining different potential tolerance mechanisms in detail. Previous data suggested a pivotal role for Tregs in tolerance induction, as they were increased in CRP-MBP mice compared to wt mice [18] and confer tolerance to wt mice upon transfer [142]. However, Tregs seemed to be dispensable for the maintenance of tolerance in CRP-MBP mice, as shown by depletion experiments [145], indicating that they are not the only drivers of tolerance. Thus, additional tolerance mechanisms seemed to control autoantigen-specific T cells in the absence of Tregs. Based on preliminary work of Alena Laschtowitz [146] and Lisa Leypoldt [145], Tr1 cells and co-inhibitory receptor expression on antigen-specific T cells were to be further analyzed here.

3.1.1 Transfer of MBP-specific T cells does not break tolerance

In order to study the autoreactive CD4 T cell response, MBP-specific CD4 T cells from spleens of tg4 mice were adoptively transferred into wt mice. Recipient mice were immunized to MBP to activate the MBP-specific T cells *in vivo* and induce EAE. Transfer of MBP-specific tg4 T cells was able to accelerate the disease in wt mice compared to transfer of non-antigen-specific CD4 T cells, illustrating the pathogenic potential of the transferred MBP-specific T cells (Fig. 5A). Transfer of wt CD4 T cells did not alter the EAE score, as compared to transfer of PBS as control. Only transfer of MBP-specific but not polyclonal T cells thus accelerated disease.

In order to study the antigen-specific T cell response in the presence of hepatic MBP, MBP-specific T cells were transferred into immunized wt or CRP-MBP mice, respectively. Expression of MBP in the liver protected from development of EAE despite transfer of tg4 T cells, as indicated by the lack of clinical symptoms in CRP-MBP mice compared to wt mice (Fig. 5B).

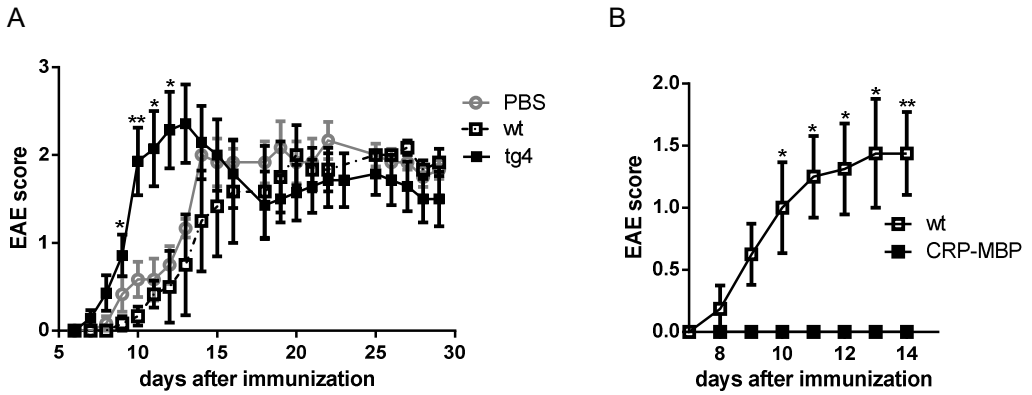

Figure 5. Tg4 T cell transfer aggravates EAE in wt mice, but does not impair tolerance in CRP-MBP mice.

A. MBP-specific CD4 T cells, wt CD4 T cells, or PBS were transferred into wt mice one day after immunization to MBP (n = 6-7). Clinical course of disease was followed for 30 days. B. MBP-specific CD4 T cells were transferred into wt or CRP-MBP mice one day after immunization to MBP (n = 6-8). Clinical course of disease was followed for 14 days. Data correspond to mean ± SEM. P values were calculated via Mann-Whitney U test comparing transfer of wt and MBP-specific CD4 T cells (A), or transfer of MBP-specific T cells into wt or CRP-MBP mice (B) on individual days after immunization. *p<0.05; **p<0.01.

Interestingly, HE analysis of the liver on day seven after immunization showed infiltrating cells in CRP-MBP mice, which were mostly located near the portal fields (Fig. 6A). Liver damage was assessed independently by Sören Weidemann (Institute of Pathology, UKE) by determining the mHAI, which includes a scoring for interface hepatitis, confluent necrosis, focal necrosis/apoptosis, and portal inflammation (Fig. 6B). Out of the maximum score of 18, wt mice reached a score of 1.3 and CRP-MBP mice had a mean score of 5.3 revealing a mild liver damage ($p < 0.001$). Accordingly, the serum transaminase ALT was slightly, but significantly elevated in CRP-MBP mice compared to wt mice (77.8 U/L vs. 28.7 U/L; $p = 0.0025$) (Fig. 6C). This enzyme is produced in hepatocytes and its presence in the serum is a sign of liver damage. Taken together, transfer of antigen-specific T cells did not impair tolerance in CRP-MBP mice, but induced mild hepatitis characterized by periportal lymphocytic infiltrates and increased ALT levels.

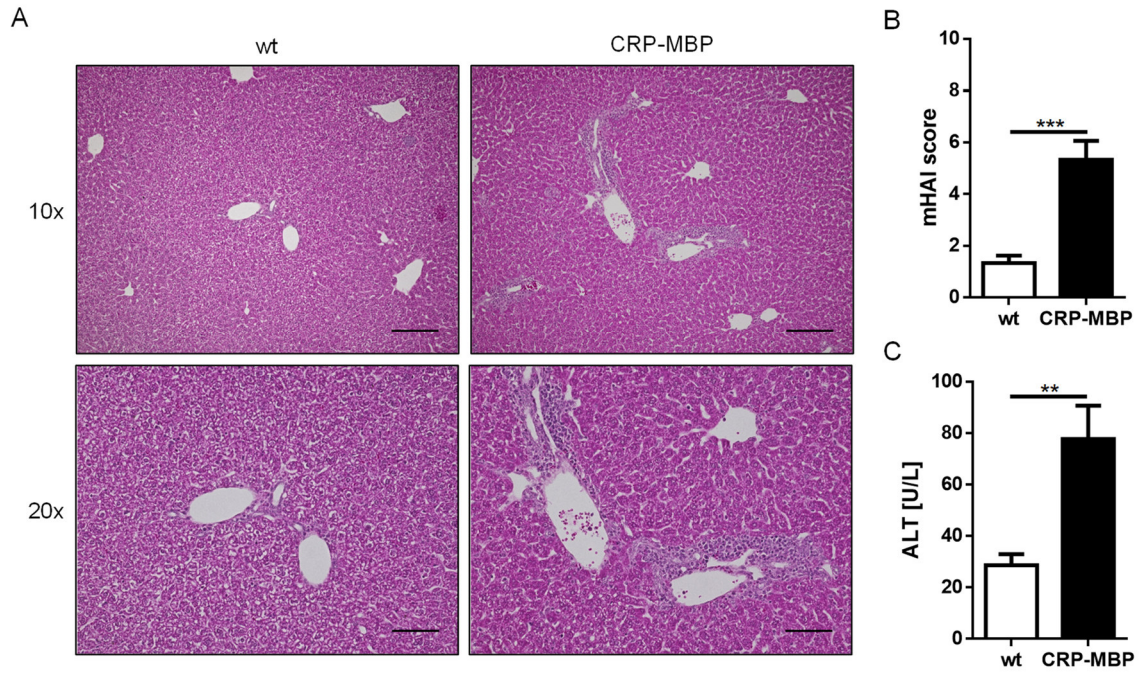

Figure 6. Transfer of MBP-specific T cells results in mild hepatitis in CRP-MBP mice.
MBP-specific CD4 T cells were transferred into wt or CRP-MBP mice one day after immunization to MBP. Livers of mice were perfused and histological sections were stained with HE on day 7 after immunization. Representative images are shown in A. Scale bar: 200 µm (10x); 100 µm (20x). B. Based on HE staining, the mHAI score was assessed in a blinded fashion. C. ALT levels were measured in the serum. Pooled data of two independent experiments are shown (n = 9). Data correspond to mean ± SEM. P values were calculated via Mann-Whitney U test. **p<0.01; ***p<0.001.

3.1.2 MBP-specific T cells accumulate in livers of CRP-MBP mice

The infiltrating cells observed in the livers of CRP-MBP mice were to be further investigated via flow cytometric analysis. Isolation of NPCs from the liver revealed an increase in NPC numbers in CRP-MBP mice corresponding to the inflammation seen in HE staining (13.4 x 10^6 in CRP-MBP vs. 5.5 x 10^6 in wt; p = 0.0008) (Fig. 7A). The use of a congenic mouse model with different isoforms of CD45 allowed for the differentiation between transferred (MBP-specific) and endogenous (non-MBP-specific) cells. Endogenous T cells in recipient mice carried both isoforms of CD45, CD45.1 and CD45.2, whereas the transferred tg4 T cells only carried CD45.2 and were negative for CD45.1 (Fig. 7B). Both, in percentage of living cells and in absolute cell numbers, more transferred tg4 T cells (CD4+CD45.1-) were observed in CRP-MBP mice (Fig. 7C+D). In wt recipients, 1.3% of the living NPCs isolated from the liver were transferred, MBP-specific CD4 T cells, whereas this population made up 14.2% in

CRP-MBP mice ($p < 0.0001$). In absolute numbers, there was a more than 20-fold increase of transferred, MBP-specific T cells in CRP-MBP livers compared to wt livers (1.7×10^6 cells in CRP-MBP vs. 7.4×10^4 cells in wt; $p < 0.0001$) (Fig. 7D). In the spleen, transferred cells made up between 1-2% in both wt and CRP-MBP mice ($p = 0.2138$) (Fig. 7E). Thus, MBP-specific T cells accumulated specifically in the livers of CRP-MBP mice.

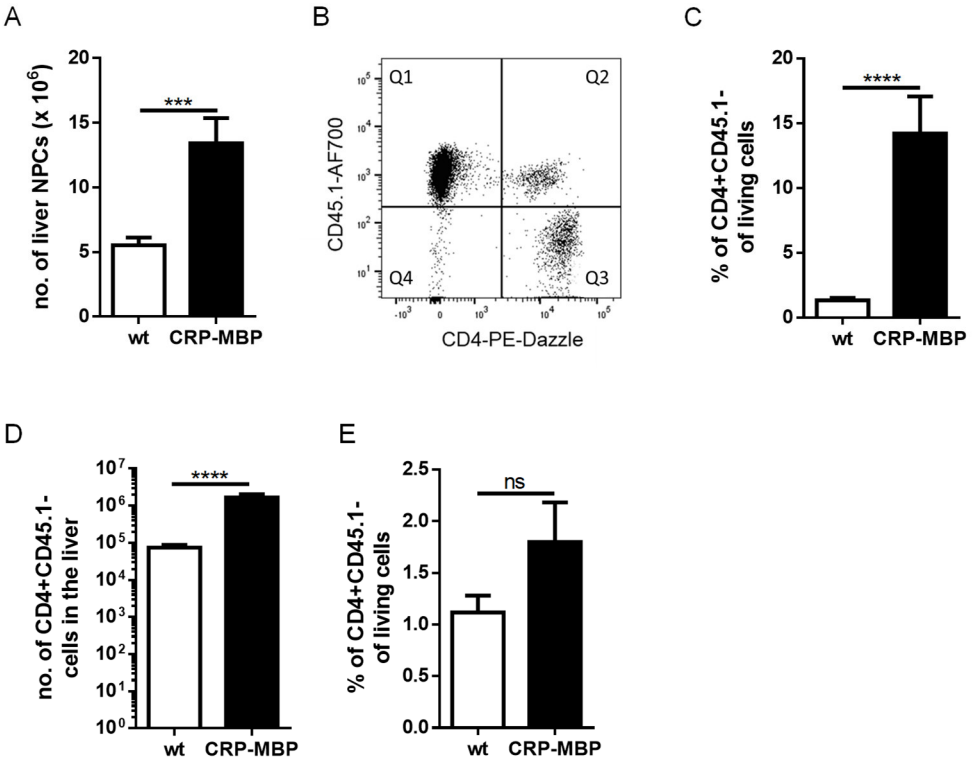

Figure 7. MBP-specific T cells accumulate in livers of CRP-MBP mice.
MBP-specific CD4 T cells were transferred into wt or CRP-MBP mice one day after immunization to MBP. A. Livers were perfused and NPCs were isolated and counted. B. Representative FACS plot illustrating two populations of CD4 T cells: endogenous CD45.1+ (Q2) and transferred, MBP-specific CD45.1- cells (Q3). C. Quantitative analysis of transferred (CD4+CD45.1-) cells from livers of wt and CRP-MBP mice. D. Absolute numbers of transferred, MBP-specific T cells in wt and CRP-MBP mice. E. Analysis of transferred, MBP-specific T cells from spleens of wt and CRP-MBP mice. Pooled data of two independent experiments are shown (n = 9). Data correspond to mean ± SEM. P values were calculated via Mann-Whitney U test. ***p<0.001; ****p<0.0001. ns – not significant.

The presence of MBP-specific T cells in the liver was confirmed via immune fluorescence staining of CD4 and CD45.1 in wt and CRP-MBP mice. Large infiltrates are seen in CRP-MBP mice that are mostly composed of CD4 T cells that are CD45.1-, i.e. transferred, MBP-specific T cells (Fig. 8).

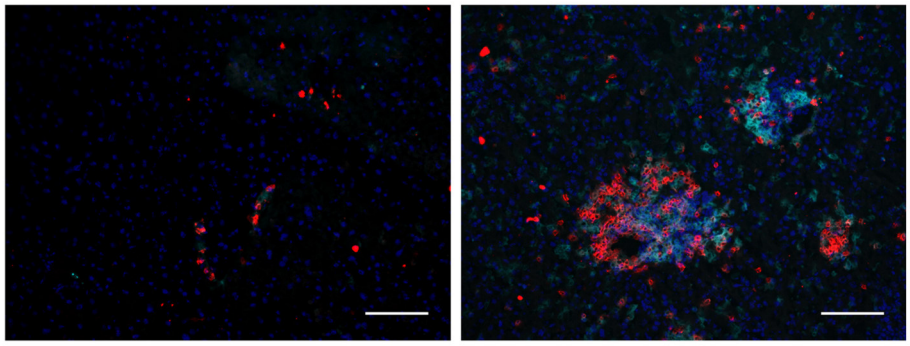

Figure 8. MBP-specific T cells accumulate in livers of CRP-MBP mice.
MBP-specific CD4 T cells were transferred into wt or CRP-MBP mice one day after immunization to MBP. Livers were perfused and freshly frozen at day 7 after immunization. Histological sections were stained with antibodies against CD4 (red), CD45.1 (light blue), and Hoechst 33258 nuclear stain (blue). Shown are representative images for wt (left) and CRP-MBP livers (right), respectively. Scale bar: 100 µm.

3.1.3 Hepatitis in CRP-MBP mice is transient

In order to study the kinetics of transferred, MBP-specific T cells, different time points after cell transfer were analyzed. As early as five days after immunization, transferred cells made up approximately 1% of NPCs in both wt and CRP-MBP mice. Whereas these cells accumulated in livers of CRP-MBP mice, cell numbers were decreasing from day seven after immunization in wt mice. 14 days after immunization, hardly any MBP-specific T cells were detectable in wt mice. Peaking at day seven after immunization, donor cells were also depleted from CRP-MBP mice and 14 days after immunization, transferred cells made up <0.15% of NPCs in both groups (Fig. 9A). However, despite the low frequency of MBP-specific T cells, there were still ten times more cells in the livers of CRP-MBP mice compared to wt mice (7116 vs. 706; $p = 0.0476$) (Fig. 9B). In accordance with low T cell numbers seen in flow cytometric analysis, there were only small infiltrates visible in HE staining of CRP-MBP liver on day 14 after transfer (Fig. 9C) and ALT levels were comparable to wt mice (25.9 U/L in wt vs. 24.1 U/L in CRP-MBP; $p = 0.3810$) (Fig. 9D). Hence, the mild hepatitis induced in CRP-MBP mice via immunization and subsequent cell transfer was only transient and resolved by day 14 despite a remaining small population of MBP-specific T cells.

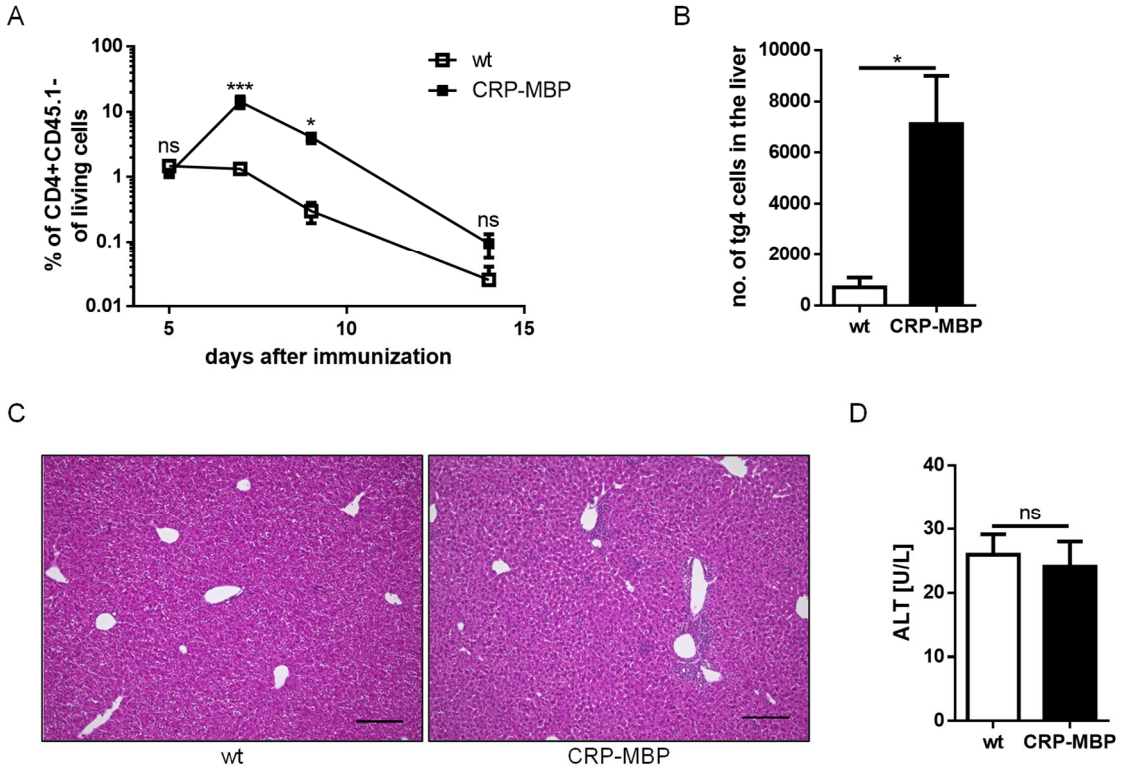

Figure 9. Hepatitis in CRP-MBP mice is transient.
MBP-specific CD4 T cells were transferred into wt or CRP-MBP mice one day after immunization to MBP (n = 3-9). A. Livers were perfused and the percentage of transferred cells from living cells was determined on day 5, 7, 9, and 14 after immunization. B. Absolute number of transferred cells in the livers of wt and CRP-MBP mice on day 14 after immunization. C. Representative HE staining of livers of wt (left) and CRP-MBP mice (right) on day 14 after immunization and D. corresponding ALT measured in the serum. Data correspond to mean ± SEM. Scale bar: 200 µm. P values were calculated via Mann-Whitney U test. *p<0.05; ***p<0.001. ns – not significant.

3.1.4 MBP-specific T cells proliferate in CRP-MBP mice

As the kinetics depicted in Fig. 9 illustrates, MBP-specific T cells seemed to proliferate in the livers of CRP-MBP mice. qPCR analysis of whole liver tissue revealed elevated *Il2* expression in CRP-MBP mice (four-fold induction compared to wt; p = 0.0288) and accordingly, the IL-2 receptor α chain (CD25) was elevated on MBP-specific T cells in CRP-MBP mice in the liver (22.3% in CRP-MBP vs. 9.6% in wt; p = 0.0179) (Fig. 10).

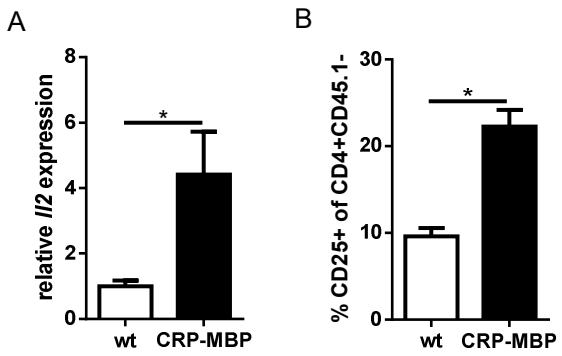

Figure 10. *Il2* gene expression and CD25 surface expression is elevated in CRP-MBP mice.
MBP-specific CD4 T cells were transferred into wt or CRP-MBP mice one day after immunization to MBP. Analysis on day 7 after immunization revealed A. elevated *Il2* gene expression in whole liver tissue of CRP-MBP mice compared to wt mice (n = 8-9) and B. higher CD25 expression on MBP-specific CD4 T cells from livers of CRP-MBP mice compared to wt mice (n = 4-5). Data correspond to mean ± SEM. P values were calculated via Mann-Whitney U test. *p<0.05.

IL-2 primarily acts as a T cell growth factor and is essential for the proliferation and survival of T cells [93]. To further study the proliferative capacity of MBP-specific T cells, Ki-67 was analyzed in flow cytometry and histology. Ki-67 expression is limited to proliferating cells and can be detected in all phases of the cell cycle, but not in resting cells [159]. While 5.9% of transferred cells in wt mice expressed Ki-67 in the liver, 23.2% were positive for this marker in CRP-MBP mice at day 7 (p = 0.1000) (Fig. 11A). This finding was supported by immunohistochemical staining of Ki-67 in paraffin sections of the liver. In both wt and CRP-MBP mice, infiltrating cells rather than hepatocytes were positive for Ki-67 and the number of proliferating cells was much higher in MBP-expressing mice (Fig. 11B).

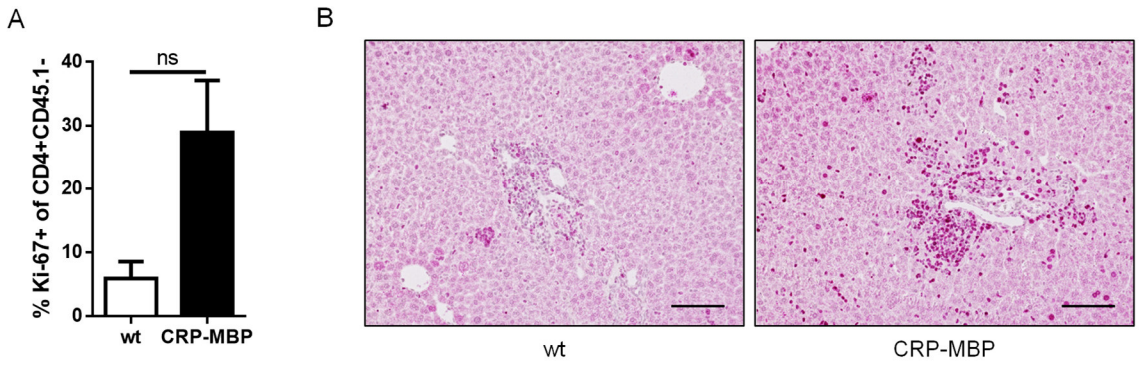

Figure 11. MBP-specific T cells proliferate in livers of CRP-MBP mice.
MBP-specific CD4 T cells were transferred into wt or CRP-MBP mice one day after immunization to MBP. Proliferation was analyzed via staining of Ki-67 in A. MBP-specific T cells in the liver via flow cytometry (n = 3) and in B. liver histology (n = 5) on day 7 after immunization. Data corresponds to mean ± SEM. Scale bar: 100 µm. Data was analyzed via Mann-Whitney U test. ns – not significant.

3.1.5 Increased apoptosis in MBP-specific T cells in CRP-MBP mice

There was a remarkable decrease of MBP-specific T cell numbers in the livers of CRP-MBP mice from day nine to day 14 (Fig. 9A). To study whether MBP-specific T cells in CRP-MBP mice were eliminated via apoptosis, the expression of the apoptosis marker Annexin V was analyzed on the surface of MBP-specific and endogenous T cells on day nine after immunization. Annexin V is able to bind phosphatidylserine, which is presented on the outer leaflet of the plasma membrane in apoptotic cells [156]. Indeed, while <5% of MBP-specific Tcells in wt mice were apoptotic, >10% in CRP-MBP mice were Annexin V+ (p = 0.0286) (Fig. 12A). When comparing apoptotic cells in transferred (CD45.1-) and endogenous (CD45.1+) T cells, it became apparent that transferred, MBP-specific T cells were more prone to apoptosis than endogenous CD4 T cells in CRP-MBP mice (11.5% vs. 5.5%; p = 0.0286), whereas there was no difference in wt mice (3.7% vs. 3.4%; p = 0.8286) (Fig. 12B+C).

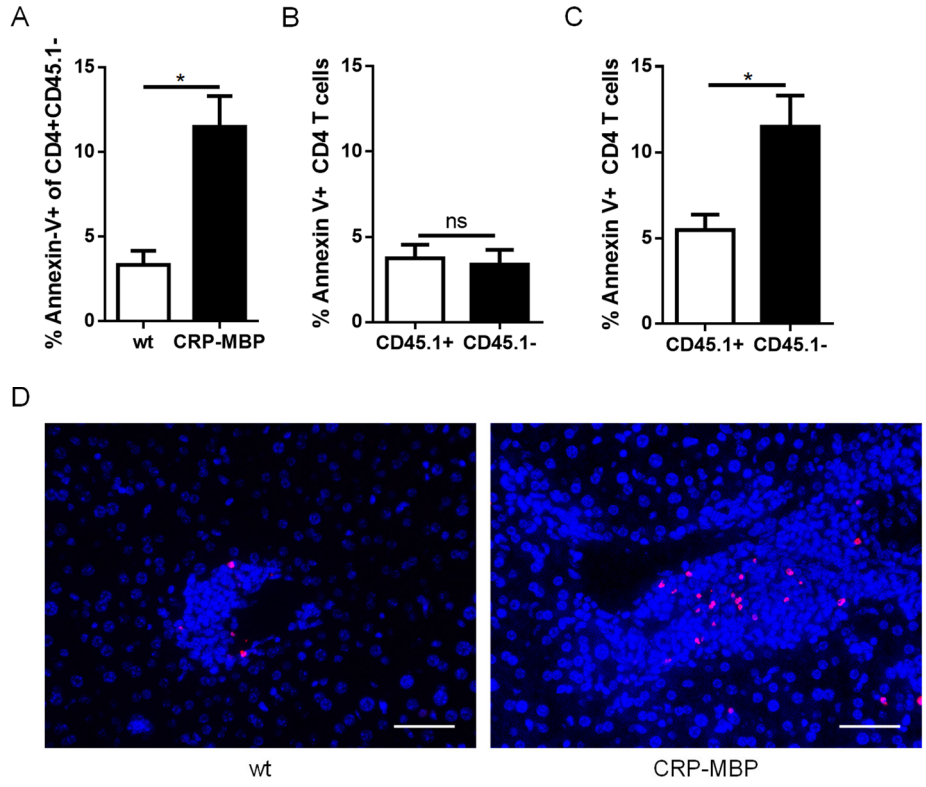

Figure 12. Only a fraction of MBP-specific T cells in the liver is cleared via apoptosis.
MBP-specific CD4 T cells were transferred into wt or CRP-MBP mice one day after immunization to MBP (n = 4). A. The percentage of Annexin-V+ cells in MBP-specific T cells from the liver was determined on day 9 after immunization and Annexin-V was analyzed in endogenous (CD45.1+) and transferred (CD45.1-) CD4 T cells isolated from the liver of wt (B) or CRP-MBP mice (C). D. TUNEL staining was performed on liver paraffin sections on day 7 after immunization. Scale bar: 50 µm. Data correspond to mean ± SEM. P values were calculated via Mann-Whitney U test. *p<0.05. ns – not significant.

This finding was confirmed in a TUNEL assay, where double strand breaks in the DNA are detected as a characteristic feature of apoptosis. While only few positive cells were seen in wt mice, more cells especially in the infiltrates of CRP-MBP mice were apoptotic (Fig. 12D). However, similar to the flow cytometric analysis, the majority of cells was not eliminated via apoptosis at this point.

3.1.6 MBP-specific T cells produce more IFNγ in CRP-MBP mice

To further characterize the phenotype of transferred, MBP-specific T cells in wt and CRP-MBP mice, NPCs, splenocytes, and peripheral blood cells were re-stimulated with PMA/ionomycin *ex vivo* seven days after immunization and CD4 T cells were analyzed for their production of IFNγ, IL-17, and TNFα. MBP-specific T cells in livers of both wt and CRP-MBP mice appeared to be activated, as approximately 70% produced TNFα and 55% produced IL-17 (Fig.13A). However, in the liver, the only difference in cytokine production by MBP-specific T cells in wt compared to CRP-MBP mice was seen concerning production of IFNγ. 26.6% of MBP-specific T cells produced IFNγ in wt mice compared to 55.0% in CRP-MBP mice ($p = 0.0019$) (Fig. 13A). IFNγ and TNFα levels in the spleen were not affected by expression of MBP in the liver, but IL-17 production was significantly reduced in MBP-specific T cells retrieved from the spleens of CRP-MBP mice (24.5% in CRP-MBP vs. 45.5% in wt; $p = 0.0401$) (Fig. 13B). Analysis of cytokine production in MBP-specific T cells from the blood showed higher production of IFNγ (34.7% vs. 5.7%; $p = 0.0286$) and TNFα (52.0% vs. 24.3%; $p = 0.0286$) in CRP-MBP mice compared to wt mice also indicating an activated phenotype of circulating MBP-specific T cells (Fig. 13C).

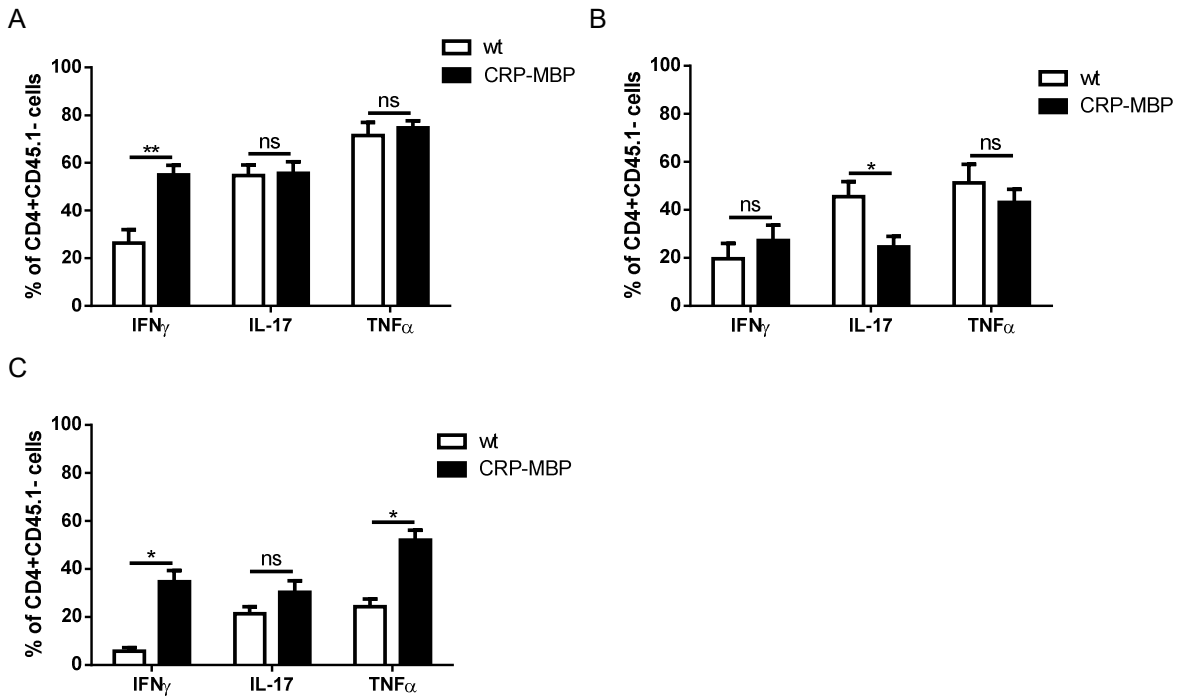

Figure 13. Cytokine analysis of MBP-specific T cells *ex vivo*.
MBP-specific CD4 T cells were transferred into wt or CRP-MBP mice one day after immunization to MBP (liver and spleen, n = 8; blood, n = 4). On day 7 after immunization, NPCs from the liver and splenocytes were isolated. NPCs (A), splenocytes (B), and cells from whole blood (C) were re-stimulated with PMA/ionomycin for 4h before intracellular cytokine staining for IFNγ, IL-17, and TNFα. Data correspond to mean ± SEM. P values were calculated via Mann-Whitney U test. *p<0.05; **p<0.01. ns – not significant.

3.1.7 Analysis of IFNγ-inducible genes

IFNγ is the sole member of the type II class of interferons and, as the other members of the IFN family, induces many gene products known as interferon-stimulated genes (ISGs) [160]. As IFNγ upregulation was observed in MBP-specific T cells from livers of CRP-MBP mice, the expression of selected ISGs was analyzed in whole liver tissue or NPCs isolated from the liver on day seven after immunization. In accordance with increased IFNγ levels in livers of CRP-MBP mice, *Cxcl9* was increased in whole liver tissue and NPCs isolated from the liver of CRP-MBP mice (five-fold and 60-fold induction, respectively; p = 0.0006 and p = 0.0286) (Fig. 14A+B). Expression of the respective receptor, *Cxcr3,* was also elevated in whole liver tissue of CRP-MBP mice (five-fold induction; p = 0.0039) (Fig. 14C). Expression of the ISG CXC chemokine ligand (CXCL) 9 – or Monokine induced by Gamma-Interferon (MIG) – is induced by IFNγ and regulates the differentiation of naïve T cells into pro-inflammatory Th1 cells and

the migration of immune cells to sites of inflammation via interaction with its receptor CXCR3 [161].

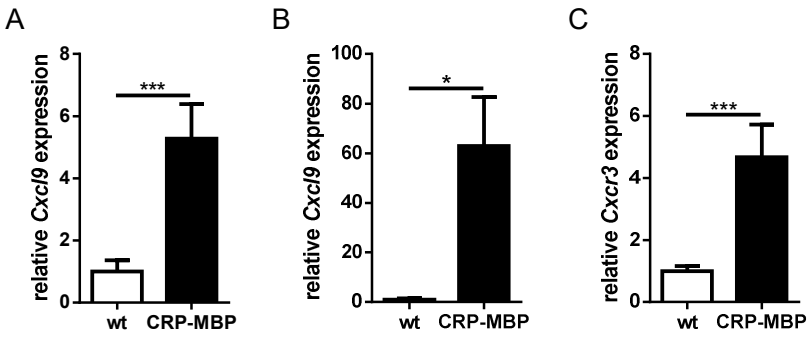

Figure 14. Hepatic expression of *Cxcl9* and *Cxcr3* is elevated in CRP-MBP mice.
MBP-specific CD4 T cells were transferred into wt or CRP-MBP mice one day after immunization to MBP. On day 7 after immunization, *Cxcl9* expression was analyzed in A. whole liver tissue (n = 8) and B. NPCs (n = 4). C. *Cxcr3* expression was analyzed in whole liver tissue (n = 8). Data correspond to mean ± SEM. P values were calculated via Mann-Whitney U test. *p<0.05; ***p<0.001.

Also on protein level, higher CXCR3 was detected on MBP-specific T cells in CRP-MBP mice in liver, spleen, and blood (Fig. 15A-C). In wt mice, only approximately 30% of transferred, MBP-specific T cells expressed CXCR3 in all three organs compared to approximately 60% in liver and spleen of CRP-MBP mice, whereas 80% of transferred cells in the blood of CRP-MBP mice express CXCR3 ($p = 0.0286$ for liver, spleen, and blood). Different cell types were described to be able to produce CXCL9 upon stimulation in the liver, such as hepatocytes and LSECs [162]. Here, CXCL9 was stained intracellularly in LSECs revealing a higher number of CXCL9-producing LSECs in livers of CRP-MBP mice compared to wt mice (4.9% vs. 1.2%; $p = 0.0159$) (Fig. 15D). In brief, production of IFNγ was induced in MBP-specific T cells in livers of CRP-MBP mice, which led to secretion of CXCL9 by LSECs. MBP-specific T cells upregulated the respective receptor CXCR3 and were bound to the liver via the IFNγ-CXCL9-CXCR3 axis.

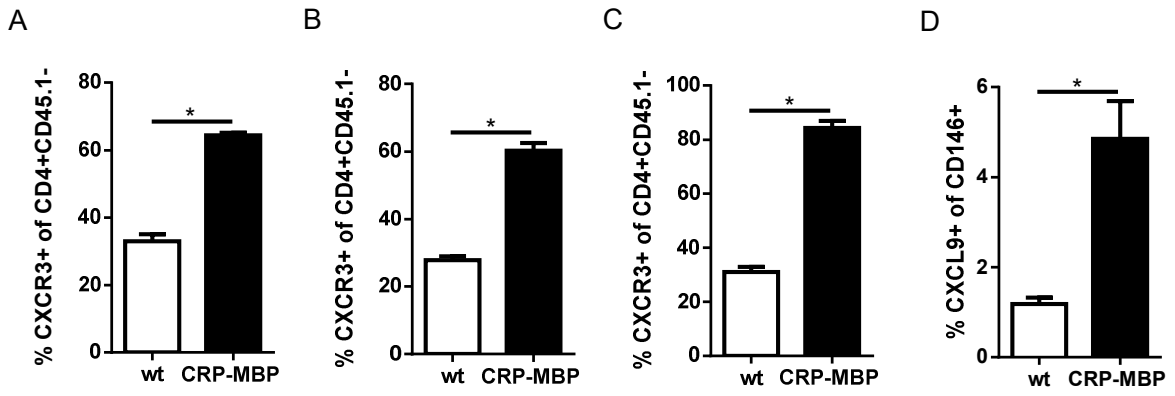

Figure 15. CXCR3 and CXCL9 protein expression is elevated in CRP-MBP mice.
MBP-specific CD4 T cells were transferred into wt or CRP-MBP mice one day after immunization to MBP. On day 7 after immunization, protein expression of CXCR3 was determined on MBP-specific T cells in liver (A), spleen (B), and blood (C) via flow cytometry (n = 4). D. CXCL9 production was analyzed in LSECs (n = 4-5). Data correspond to mean ± SEM. P values were calculated via Mann-Whitney U test. *p<0.05.

Two additional ISGs were analyzed in the following: PD-L1 and IDO1. PD-L1 is the primary ligand for the co-inhibitory receptor PD-1 and plays an important role in preventing excessive immune responses and maintaining immune tolerance [163]. IDO1 is involved in tryptophan catabolism and has immunosuppressive function [164]. *Cd274*, encoding PD-L1, was only slightly elevated in whole liver tissue in CRP-MBP mice (1.4-fold induction compared to wt mice; p = 0.2288), but induction was observed in liver NPCs isolated from CRP-MBP mice compared to NPCs isolated from wt mice (2.8-fold induction; p = 0.0109) (Fig. 16A+B). No or very low expression of *Ido1* was detected in whole liver tissue of wt mice, but expression was induced in livers of CRP-MBP mice (24.5-fold induction compared to wt mice; p = 0.0018) (Fig. 16C).

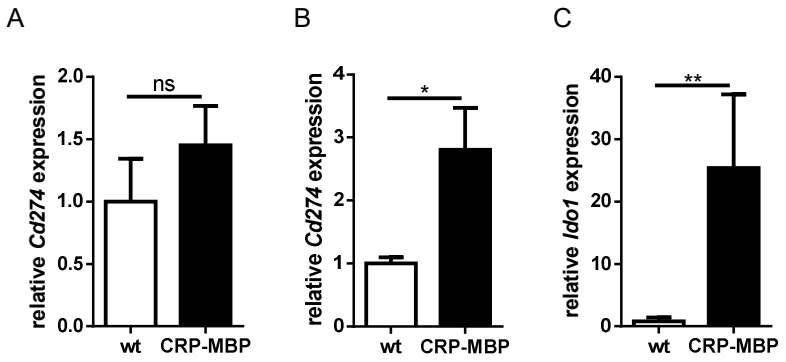

Figure 16. *Cd274* and *Ido1* expression are increased in CRP-MBP mice.
MBP-specific CD4 T cells were transferred into wt or CRP-MBP mice one day after immunization to MBP. On day 7 after immunization, *Cd274* expression was analyzed in whole liver tissue (A) and liver NPCs (B), and *Ido1* expression (C) was analyzed in whole liver tissue (n = 5-11). Data correspond to mean ± SEM. P values were calculated via Mann-Whitney U test. *p<0.05; **p<0.01. ns – not significant.

PD-L1 protein expression was subsequently studied in different hepatic cell populations. There was no detection of PD-L1+ cells in neither endogenous nor transferred CD4 T cells (data not shown). Strikingly, almost all Kupffer cells expressed PD-L1 in both wt and CRP-MBP mice with a mild trend towards higher expression in CRP-MBP mice (97.0% in CRP-MBP vs. 90.0% in wt; p = 0.1111) (Fig. 17A). However, differential expression of PD-L1 was seen in DCs (23.0% in wt vs. 33.4% in CRP-MBP; p = 0.0159) and LSECs (9.3% in wt vs. 18.3% in CRP-MBP; p = 0.0159) (Fig. 17B+C). These data indicate that IFNγ derived from MBP-specific T cells induced upregulation of PD-L1 on hepatic DCs and LSECs in CRP-MBP mice.

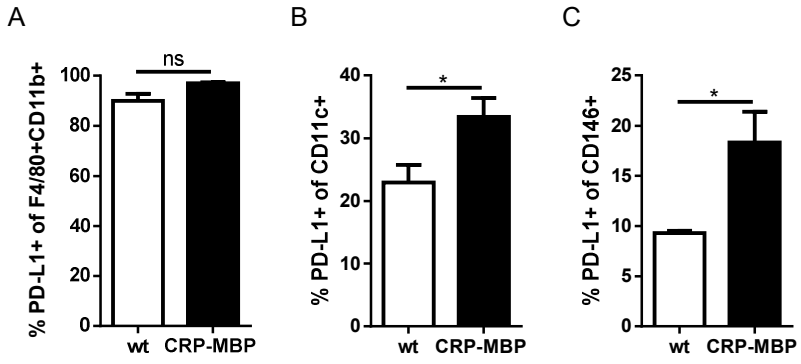

Figure 17. PD-L1 expression is elevated in KCs, DCs, and LSECs in CRP-MBP mice.
MBP-specific CD4 T cells were transferred into wt or CRP-MBP mice one day after immunization to MBP (n = 4-5). On day 7 after immunization, NPCs were isolated and PD-L1 expression was analyzed in KCs (A), DCs (B), and LSECs (C) via flow cytometry. Data correspond to mean ± SEM. P values were calculated via Mann-Whitney U test. *p<0.05; ns – not significant.

3.1.8 Homing of MBP-specific T cells to the liver

Besides regulation via chemokines and their respective receptors, immune cells are targeted to the liver via interaction of adhesion molecules on the liver endothelium with their respective ligands on circulating cells [165]. Tissue homing of MBP-specific T cells to the livers of CRP-MBP mice was favored by increased CXCL9 production in the liver and increased CXCR3 expression on MBP-specific T cells (Fig. 14+15). Additional adhesion molecules are known to be important for homing of lymphocytes to the liver. Thus, the expression of *Icam1*, *Vcam1*, *Madcam1*, and *Amine oxidase, copper containing 3 (Aoc3)* (coding for vascular adhesion protein 1 (VAP-1)) was analyzed in whole liver tissue in wt and CRP-MBP mice (Fig. 18A). *Madcam1* (4.2-fold induction; $p = 0.0040$) and *Aoc3* (3.7-fold induction; $p = 0.0267$) were higher expressed in livers of CRP-MBP mice. Only a mild trend for higher *Icam1* (1.7-fold induction; $p = 0.0680$) and *Vcam1* (1.5-fold induction; $p = 0.1044$) expression in CRP-MBP mice, compared to wt mice, was seen. Interestingly, cells homing to the liver seemed to be retained there, as gene expression of *Ccr7*, which is important for T cell homing into secondary lymphoid organs and essential for T cells to exit peripheral tissues [166], was reduced in NPCs isolated from CRP-MBP mice compared to wt mice (0.2-fold expression; $p = 0.0286$) (Fig. 18B). Accordingly, CD69, a molecule that is associated with increased dwell-time in organs, as it suppresses S1P1-mediated egress [167], was upregulated on MBP-specific T cells in the liver of CRP-MBP mice (26.7% in CRP-MBP vs. 9.7% in wt; $p = 0.0286$) (Fig. 18C). Taken together, homing of MBP-specific T cells to the livers of CRP-MBP mice was promoted via the CXCL9-CXCR3 axis and upregulation of several adhesion molecules on the liver endothelium. Once in the liver, cells might be retained there as indicated by the lack of *Ccr7* expression in NPCs and elevated CD69 expression on MBP-specific T cells in CRP-MBP mice.

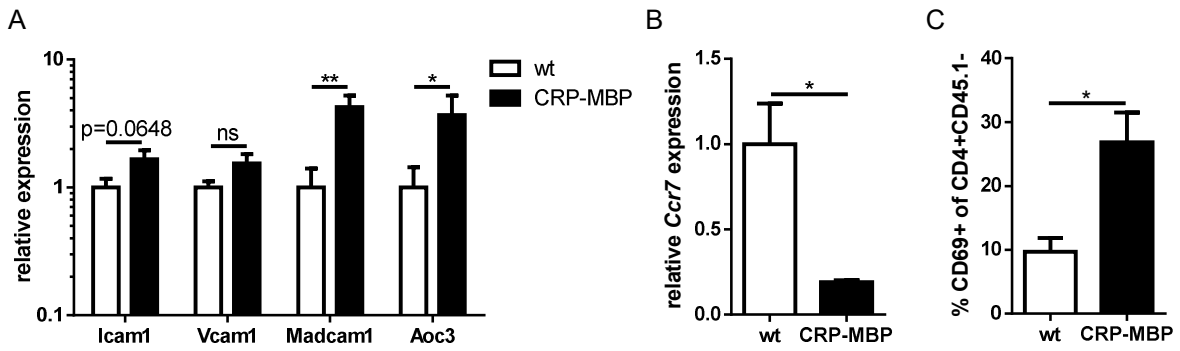

Figure 18. Expression of adhesion molecules, *Ccr7*, and CD69 in wt and CRP-MBP mice.
MBP-specific CD4 T cells were transferred into wt or CRP-MBP mice one day after immunization to MBP. On day 7 after immunization, A. expression of adhesion molecules in whole liver tissue was analyzed via qPCR (n = 8-9). B. NPCs were isolated and expression of *Ccr7* was analyzed via qPCR (n = 4). C. Protein expression of CD69 was analyzed on hepatic MBP-specific T cells (n = 4). Data correspond to mean ± SEM. P values were calculated via Mann-Whitney U test. *p<0.05; **p<0.01. ns – not significant.

3.1.9 Analysis of Tr1 cells

As these findings indicated that MBP-specific T cells seemed to accumulate in the livers of CRP-MBP mice, the question was, whether their retention in the liver had an effect on their function. Therefore, the retained MBP-specific T cells were further characterized via flow cytometry. Confirming previous results [145, 146], a striking difference was observed in the number of Lag-3+CD49b+ cells, which have been described as Tr1-like cells [83]. While 5% of MBP-specific T cells in the livers of wt mice were double positive for these markers, they made up >15% of the CD4 T cell population in CRP-MBP mice (p = 0.0079) (Fig. 19A+B). This increase in Lag-3+CD49b+ cells was not specific to the liver, as there was also a significant increase of double positive cells in the spleen (7.7% in CRP-MBP vs. 1.7% in wt; p = 0.0159) (Fig. 19C).

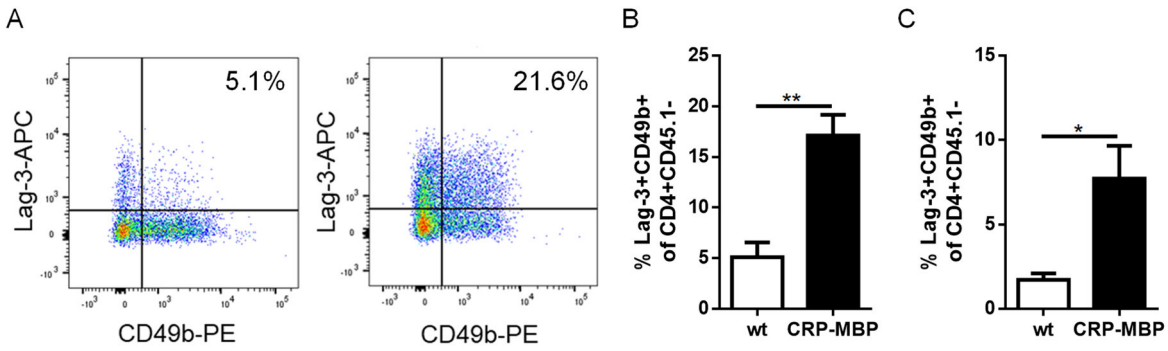

Figure 19. Lag-3+CD49b+ cells are increased in MBP-specific T cells in CRP-MBP mice.
MBP-specific CD4 T cells were transferred into wt or CRP-MBP mice one day after immunization to MBP. On day 7 after immunization, NPCs and splenocytes were isolated and analyzed via flow cytometry (n = 5). A. Representative images of Lag-3 and CD49b surface staining on MBP-specific T cells from livers of wt (left) or CRP-MBP mice (right). Quantitative analysis of Lag-3+CD49b+ cells in MBP-specific T cells from liver (B) and spleen (C). Data correspond to mean ± SEM. P values were calculated via Mann-Whitney U test. *p<0.05; **p<0.01.

However, it was shown that surface expression of Lag-3 and CD49b alone is not sufficient to characterize Tr1 cells. Instead, these cells are also dependent on IL-10 signaling to fulfill their suppressive capacity [84]. For that reason, double IL-10^{eGFP} Foxp3^{mRFP} reporter mice were crossed to tg4 mice to more thoroughly study MBP-specific Tr1 cells. Use of IL-10^{eGFP} Foxp3^{mRFP} x tg4 mice as donor mice showed that, indeed, below 5% in wt mice and approximately 13% in CRP-MBP mice of the Lag-3+CD49b+ Tr1-like cells were positive for IL-10 and were thus bona fide Tr1 cells (Fig. 20A-C), confirming the need for additional IL-10 staining to characterize Tr1 cells. Nevertheless, significantly more MBP-specific Lag-3+CD49b+ Tr1-like cells produced IL-10 in CRP-MBP mice, as compared to wt mice, in both liver (12.9% in CRP-MBP vs. 4.3% in wt; p = 0.0159) and spleen (12.0% in CRP-MBP vs. 3.7% in wt; p = 0.0159).

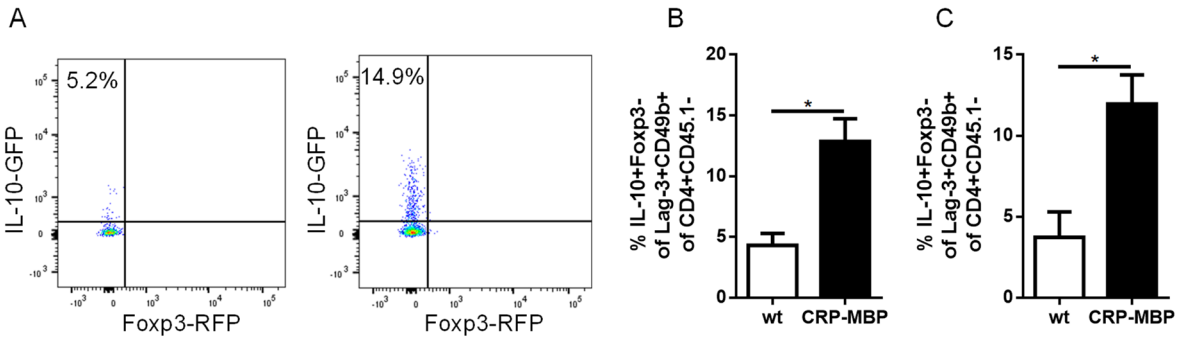

Figure 20. IL-10 production in MBP-specific Lag-3+CD49b+ cells.
MBP-specific CD4 T cells were transferred into wt or CRP-MBP mice one day after immunization to MBP. On day 7 after immunization, NPCs and splenocytes were isolated and analyzed via flow cytometry (n = 5). A. Representative images of IL-10 production in Lag-3+CD49b+ MBP-specific T cells from livers of wt (left) or CRP-MBP mice (right). Quantitative analysis of IL-10+Foxp3- cells in Lag-3+CD49b+ MBP-specific T cells from liver (B) and spleen (C). Data correspond to mean ± SEM. P values were calculated via Mann-Whitney U test. *p<0.05.

Thus, even though overall Tr1 numbers were lower when including IL-10 expression, still the numbers of bona fide Tr1 cells detected in the livers of CRP-MBP mice were almost 200-fold higher than in wt mice (94,587 Tr1 cells in CRP-MBP vs. 483 Tr1 cells in wt; p = 0.0079) (Fig. 21A). Also in the spleen, the number of Tr1 cells was 100-fold increased in CRP-MBP mice as compared to wt controls (26,364 Tr1 cells in CRP-MBP vs. 270 Tr1 cells in wt; p = 0.0079) (Fig. 21B).

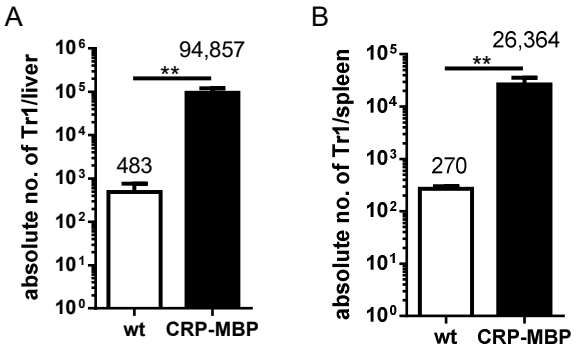

Figure 21. MBP-specific Tr1 cells are increased in CRP-MBP mice.
MBP-specific CD4 T cells were transferred into wt or CRP-MBP mice one day after immunization to MBP. On day 7 after immunization, NPCs and splenocytes were isolated and analyzed via flow cytometry (n = 5). The absolute number of MBP-specific Tr1 cells (defined as Lag-3+CD49b+IL-10+) were calculated for liver (A) and spleen (B). Data correspond to mean ± SEM. P values were calculated via Mann-Whitney U test. **p<0.01.

Of note, only 20% of the IL-10-producing MBP-specific CD4 T cells in the liver carried Lag-3 and CD49b on their surface in both wt and CRP-MBP mice, revealing a high proportion of more than 70% of IL-10+ cells that were not expressing the described Tr1 markers (Fig. 22A). In the spleen, the proportion of IL-10-producing cells lacking Tr1 markers was even higher (more than 75%; Fig. 22B). Indeed, only 22.6% of IL-10-producing MBP-specific T cells derived from spleens of CRP-MBP mice vs. 9.5% in wt mice were Lag-3+CD49b+ ($p = 0.0079$).

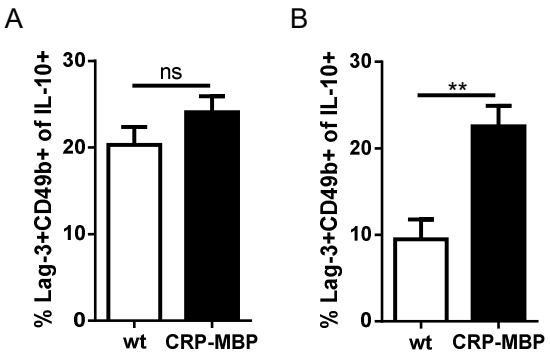

Figure 22. Lag-3+CD49b+ cells in IL-10-producing MBP-specific T cells.
MBP-specific CD4 T cells were transferred into wt or CRP-MBP mice one day after immunization to MBP. On day 7 after immunization, NPCs and splenocytes were isolated and analyzed via flow cytometry (n = 5). Lag-3+CD49b+ cells were analyzed in IL-10+ MBP-specific CD4 T cells from livers (A) and spleens (B) of wt and CRP-MBP mice. Data correspond to mean ± SEM. P values were calculated via Mann-Whitney U test. **p<0.01. ns – not significant.

In order to more closely study the IL-10+ cells, MBP-specific T cells from livers of wt and CRP-MBP mice were subjected to t-SNE analysis on the basis of median fluorescence intensity of IL-10, the Tr1 marker Lag-3 and CD49b, and the co-inhibitory receptors PD-1, TIGIT, and Tim-3. Six separate clusters of IL-10-producing CD4 T cells were gated in CRP-MBP mice with each cluster representing ≥ 0.5% of antigen-specific IL-10+ cells (Fig. 23A). Additional IL-10+ cells are scattered throughout the plot and were thus not analyzed. In CRP-MBP mice, 1997 IL-10+ cells (8.3% of MBP-specific T cells) fall into these six clusters compared to 267 cells in wt mice (1.1% of MBP-specific T cells). The largest cluster in both groups is cluster 1 constituting 4.95% of MBP-specific T cells in CRP-MBP and 0.68% in wt mice. To characterize these IL-10+ clusters, the histograms of different markers were compared to examine the presence of Tr1 cells and co-inhibitory receptor expression in wt and CRP-MBP mice (Fig. 23B+C).

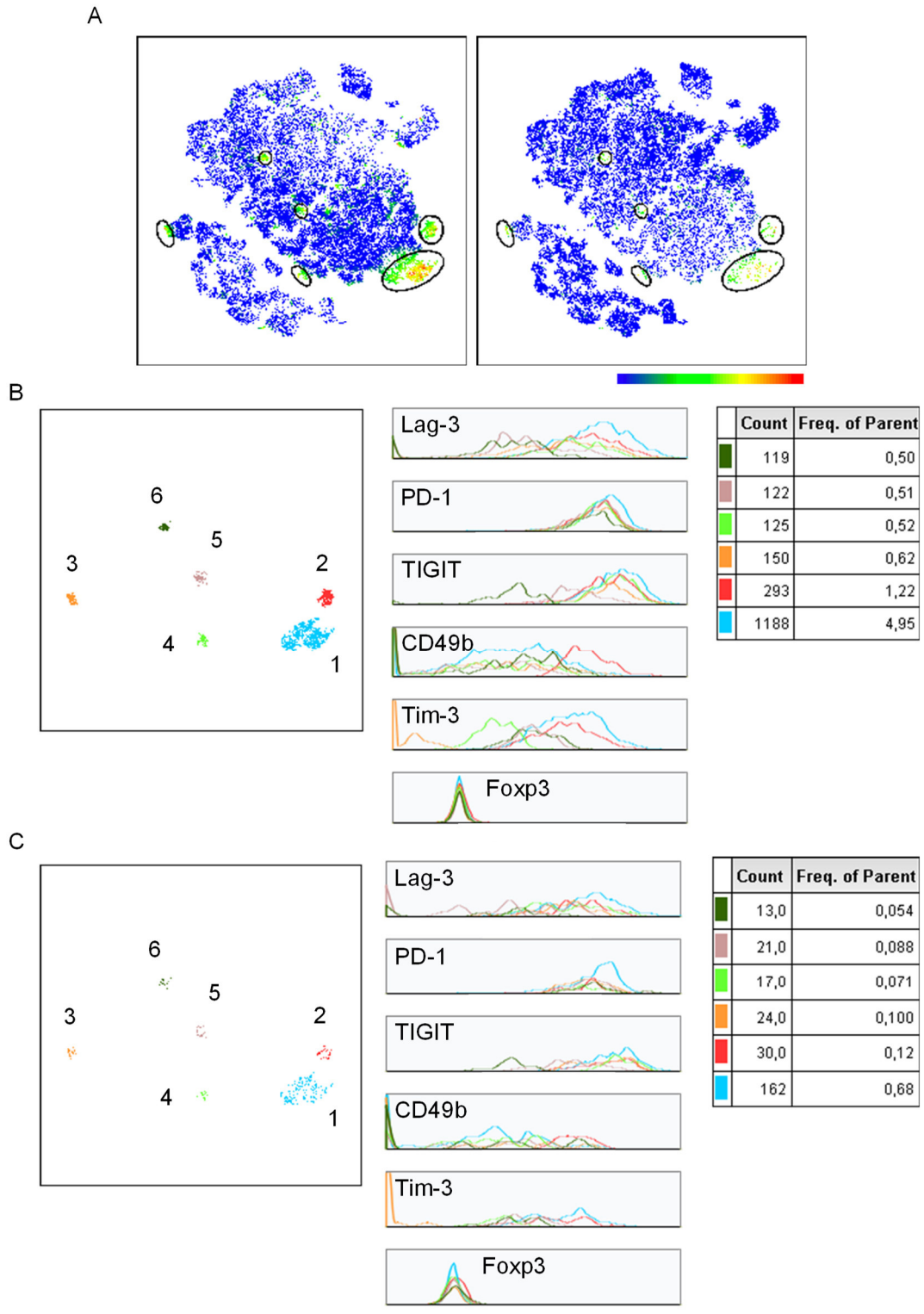

Figure 23. T-SNE analysis of IL-10-producing CD4 T cells.
MBP-specific CD4 T cells were transferred into wt or CRP-MBP mice one day after immunization to MBP. On day 7 after immunization, NPCs were isolated and analyzed via flow cytometry for the expression of IL-10, Lag-3, CD49b, PD-1, Tim-3, and TIGIT (n = 5). T-SNE analysis was performed based on expression of the aforementioned markers. A. T-SNE plot for CRP-MBP (left) and wt (right) with a color axis for IL-10 expression. IL-10+ clusters were gated, overlayed, and histograms were analyzed for the expression of Lag-3, PD-1, TIGIT, CD49b, Tim-3, and Foxp3 in CRP-MBP (B) and wt mice (C). Total T cell count and frequency of CD4+CD45.1- is stated in the associated table.

As expected, none of the clusters included classical Tregs, as seen by negative staining for Foxp3. In CRP-MBP mice, all clusters, except cluster 5 and 6, were positive for Lag-3. However, only cluster 2 showed high expression of CD49b, and thus was composed of Tr1 cells, which are defined by co-expression of Lag-3 and CD49b [83]. All clusters showed high expression of PD-1, but TIGIT was absent from cluster 6 and lower within cluster 5 compared to the other clusters. In addition, Tim-3 expression was different between the clusters. Tim-3 expression was very high in cluster 1 and 2, intermediate in cluster 5 and 6, very low in cluster 4 and absent in cluster 3. The same clusters were analyzed in MBP-specific T cells from wt mice. While cell numbers were much lower, a similar phenotype could be observed within the respective clusters. Cluster 2 included Tr1 cells and cluster 1 and 2 were high in co-inhibitory receptors. Here, cluster 1 showed markedly higher PD-1 expression compared to the other clusters. Tim-3, as seen before, was highly expressed in cluster 1 and 2 and absent in cluster 3, whereas TIGIT expression was reduced in cluster 6 compared to the other clusters. In brief, t-SNE analysis of IL-10+ hepatic MBP-specific T cells showed remarkable heterogeneity within the IL-10-producing cells with distinct expression patterns of co-inhibitory receptors and varying expression of the Tr1-characterizing surface markers Lag-3 and CD49b.

Interestingly, of the IL-10+ population, many cells co-expressed the pro-inflammatory cytokine IFNγ in both liver (64.7% in wt vs. 75.8% in CRP-MBP; p = 0.2286) and spleen (47.4% in wt vs. 62.2% in CRP-MBP; p = 0.6286) indicating that MBP-specific T cells had both pro-inflammatory and anti-inflammatory capacities (Fig. 24).

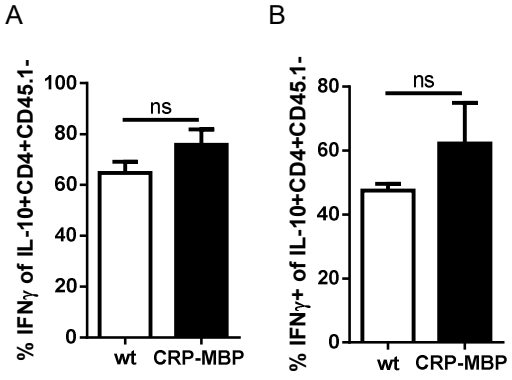

Figure 24. IFNγ+ of IL-10+ MBP-specific T cells.
MBP-specific CD4 T cells were transferred into wt or CRP-MBP mice one day after immunization to MBP. On day 7 after immunization, NPCs and splenocytes were isolated and analyzed via flow cytometry (n = 5). Expression of IFNγ was analyzed in IL-10+ MBP-specific T cells from liver (A) and spleen (B) of wt and CRP-MBP mice. Data correspond to mean ± SEM. P values were calculated via Mann-Whitney U test. ns – not significant.

The high number of Tr1 cells and other IL-10-producing cells suggested a role of these cells for tolerance induction in CRP-MBP mice. To analyze the importance of IL-10 signaling on tolerance, wt and CRP-MBP mice were immunized, given MBP-specific T cells by adoptive transfer, and anti-IL-10 receptor antibody to impair IL-10 signaling. However, despite inhibition of IL-10 signaling, CRP-MBP mice remained protected from EAE (Fig. 25). To confirm this finding, a dominant-negative IL-10 receptor was bred onto CRP-MBP x tg4 background to obtain mice with MBP-specific T cells that were insensitive to IL-10 signaling together with ectopic expression of MBP in the liver. Upon immunization to MBP, these mice remained protected from EAE despite their T cell insensitivity to IL-10 [146]. These findings indicated that IL-10 signaling was dispensable for the maintenance of tolerance despite the increase of IL-10-producing Tr1 and other CD4 T cells in CRP-MBP mice.

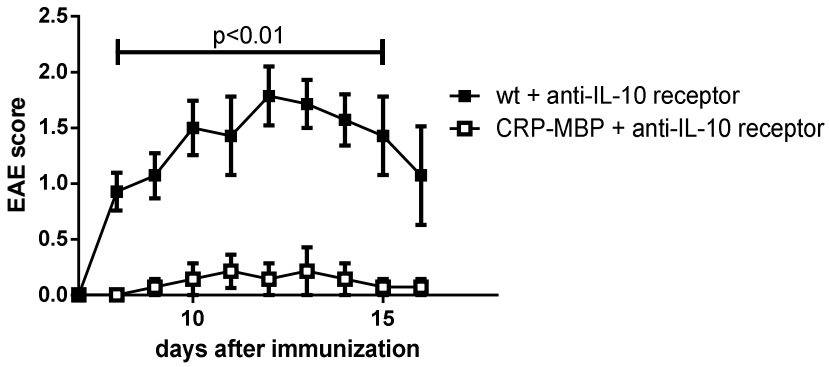

Figure 25. IL-10 signaling is dispensable for tolerance induction in CRP-MBP mice.
MBP-specific CD4 T cells were transferred into wt or CRP-MBP mice one day after immunization to MBP. Mice were i.p.-injected with 300 µg of anti-IL-10R antibody twice a week and the EAE score was followed for 16 days (n = 7). P values were calculated via Mann-Whitney U test.

3.1.10 Expression of co-inhibitory receptors on MBP-specific T cells

As described earlier, Lag-3 expression is not only associated with Tr1 cells, but Lag-3 is a co-inhibitory molecule described to downregulate T cell responses [107, 110]. Besides Lag-3, other co-inhibitory receptors have been described and the expression of co-inhibitory receptors on effector T cells is an important mechanism to ensure immune homeostasis. After immunization and adoptive T cell transfer, the expression of different co-inhibitory receptors was determined in whole liver tissue and normalized to expression in wt mice. Previous work of our group showed that *Pdcd1* and *Ctla4* expression were highly upregulated in livers from

CRP-MBP mice compared to wt mice [145]. Three other co-inhibitory receptors, Lag-3, TIGIT, and Tim-3, were analyzed here. Apart from *Lag3* (11.3-fold induction; $p < 0.0001$), also *Tigit* (7.6-fold induction; $p < 0.0001$), and *Havcr2* (Tim-3) (3.5-fold induction; $p = 0.0002$) were higher expressed in CRP-MBP mice compared to wt mice (Fig. 26).

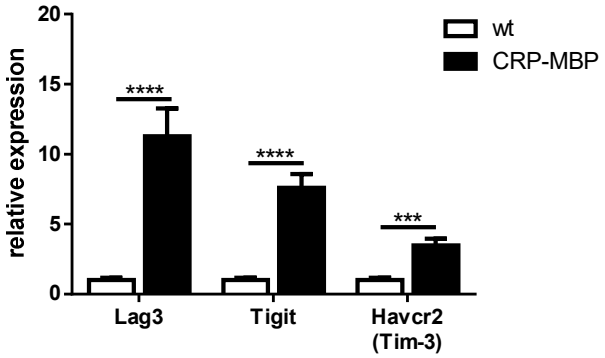

Figure 26. Gene expression of co-inhibitory receptors in wt and CRP-MBP mice.
MBP-specific CD4 T cells were transferred into wt or CRP-MBP mice one day after immunization to MBP. On day 7 after immunization, whole liver tissue was analyzed for the expression of *Lag3*, *Tigit,* and *Havcr2* via qPCR. Pooled data of two independent experiments are shown (n = 8-10). Data correspond to mean ± SEM. P values were calculated via Mann-Whitney U test. ***p<0.001; ****p<0.0001.

Subsequently, protein expression of these co-inhibitory receptors was assessed on MBP-specific CD4 T cells in wt and CRP-MBP mice in liver, spleen, and blood. Previous work suggested an upregulation of PD-1 and CTLA-4 on MBP-specific T cells from liver and spleen, but due to low sample size and high variation, no conclusion could be drawn [145]. Thus, staining for PD-1 and CTLA-4 were included in this study. In accordance with gene expression, protein expression of all co-inhibitory receptors tested was upregulated on liver-derived MBP-specific T cells in CRP-MBP mice (Lag-3: 47.0% vs. 9.9%; $p < 0.0001$; PD-1: 96.9% vs. 75.3%; $p < 0.0001$; TIGIT: 55.1% vs. 26.6%; $p = 0.0002$; Tim-3: 40.1% vs. 18.5%; $p = 0.0002$; CTLA-4: 27.6% vs. 15.6%; $p = 0.0042$) (Fig. 27A). Interestingly, also in the periphery in splenic-derived MBP-specific T cells, Lag-3 (26.0% vs. 10.1%; $p < 0.0001$), PD-1 (91.1% vs. 81.7%; $p = 0.0073$), and TIGIT (39.0% vs. 27.1%; $p = 0.0288$) were upregulated in MBP-expressing mice compared to wt mice (Fig. 27B). CTLA-4 expression in MBP-specific T cells in the spleen was lower than in the liver, but also twice as high in CRP-MBP compared to wt mice even though this difference did not reach statistical significance (12.4% vs. 6.9%; $p = 0.0865$). Analysis of co-inhibitory receptor-expressing cells from the peripheral blood,

however, showed highly induced expression of Lag-3 (26.3% vs. 6.1%; p = 0.0003) and CTLA-4 (49.6% vs. 20.9%; p = 0.0003) on MBP-specific T cells in CRP-MBP mice as compared to wt mice (Fig. 27C). Additionally, also Tim-3 was slightly elevated (29.7% in CRP-MBP vs. 25.2% in wt; p = 0.0037).

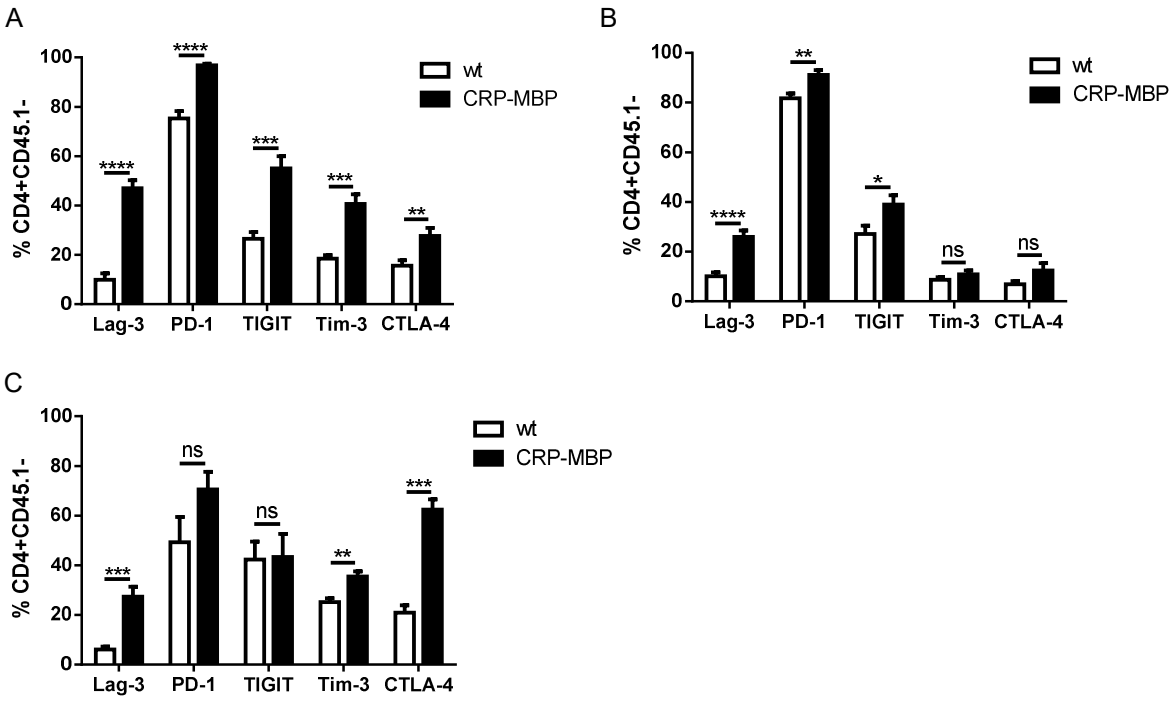

Figure 27. Co-inhibitory receptors are upregulated on MBP-specific T cells in CRP-MBP mice.
MBP-specific CD4 T cells were transferred into wt or CRP-MBP mice one day after immunization to MBP. On day 7 after immunization, expression of Lag-3, PD-1, TIGIT, Tim-3, and CTLA-4 was determined on MBP-specific T cells in liver (A), spleen (B), and blood (C). Pooled data of two independent experiments are shown (n = 7-10). Data correspond to mean ± SEM. P values were calculated via Mann-Whitney U test. *p<0.05; **p<0.01; ***p<0.001; ****p<0.0001. ns – not significant.

In brief, all five co-inhibitory receptors tested were elevated on liver-derived MBP-specific T cells in mice with hepatic expression of MBP, as compared to wt mice. In splenic-derived T cells, Lag-3, PD-1, and TIGIT were upregulated, whereas higher protein expression of Lag-3, Tim-3, and TIGIT was measured on MBP-specific T cells from the peripheral blood. Thus, depending on the organ tested, co-inhibitory receptor expression on MBP-specific T cells differed, but at least three receptors were higher expressed in MBP-expressing mice compared to wt mice in cells derived from liver, spleen, or blood.

Including all co-inhibitory markers in one staining panel allowed for flow cytometric analysis of the co-expression of these receptors on MBP-specific T cells in the liver via t-SNE analysis. The

density plots already highlight the different phenotype that MBP-specific T cells acquire in livers of wt and CRP-MBP mice, respectively. The area of highest cell density in each sample is encircled and corresponds to approximately 60% of cells in the respective group (Fig. 28A). The expression of co-inhibitory receptors on MBP-specific T cells is illustrated by color code in separate plots for wt (Fig. 28B) and CRP-MBP mice (Fig. 28C). Interestingly, some cells show co-expression of multiple co-inhibitory receptors and this population is higher in CRP-MBP compared to wt mice (17.3% vs. 2.4%). Notably, t-SNE analysis of liver-derived MBP-specific T cells generated many separate clusters illustrating the diversity in this population.

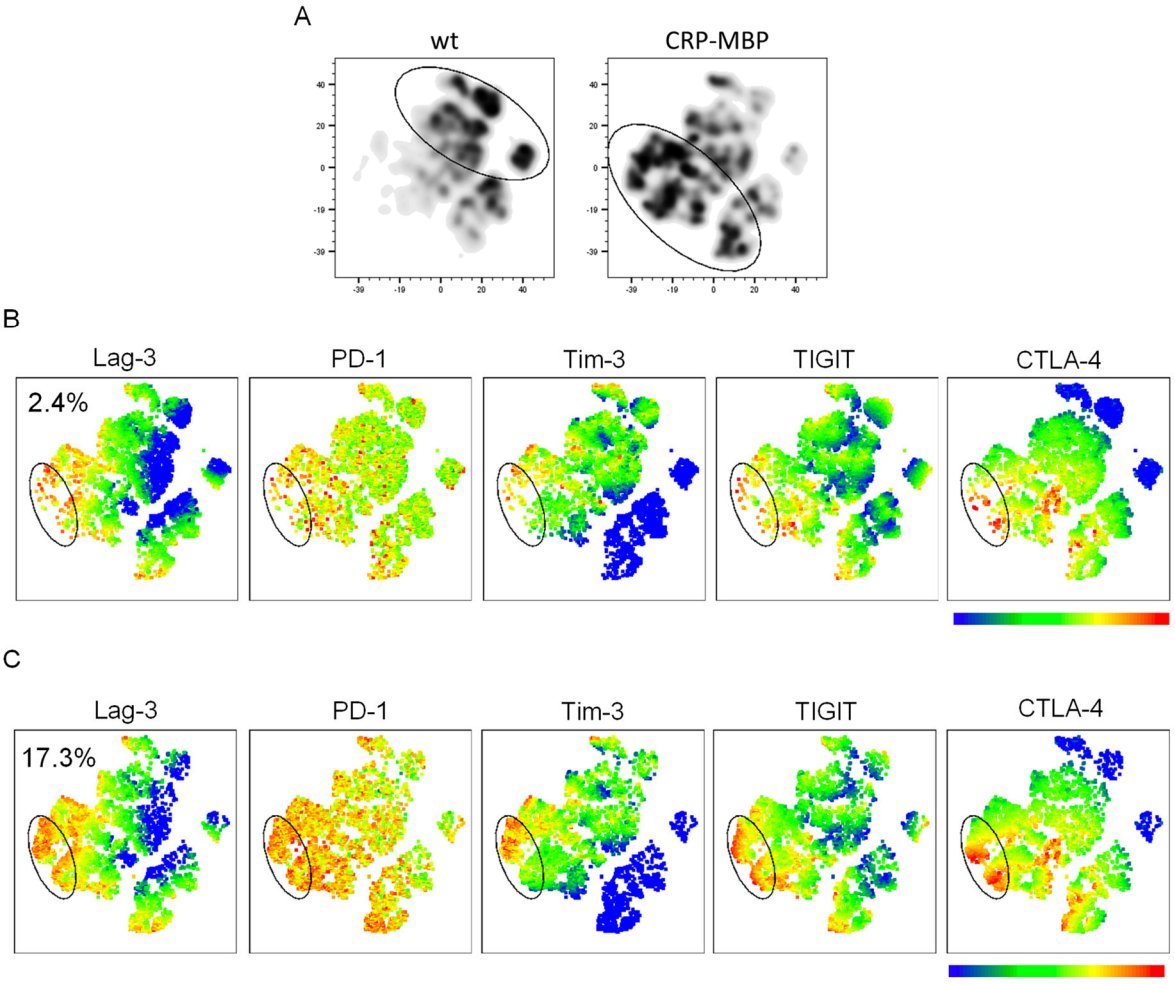

Figure 28. T-SNE analysis of liver-derived MBP-specific T cells.
MBP-specific CD4 T cells were transferred into wt or CRP-MBP mice one day after immunization to MBP (n = 5). On day 7 after immunization, NPCs were isolated from the liver and stained for the co-inhibitory receptors Lag-3, PD-1, TIGIT, Tim-3, and CTLA-4. Illustrated is a t-SNE analysis of MBP-specific T cells based on the median fluorescence intensity of the co-inhibitory receptors. A. Separate density plots depict the highest cell density in wt (left) and CRP-MBP mice (right). The encircled area corresponds to approximately 60% of cells. B. Analysis of co-inhibitory receptor expression in MBP-specific T cells from wt (B) and CRP-MBP mice (C). Circles indicate a population of co-inhibitory receptor high cells.

3.1.11 Depletion of IFNγ impairs protection from EAE in CRP-MBP mice

IFNγ production by MBP-specific T cells in the liver was associated with increased *Cd274* and *Ido1* expression (Fig. 16B+C) and upregulation of *Cxcl9* in the liver (Fig. 14A+B). MBP-specific T cells accumulated in the livers of CRP-MBP mice via the IFNγ-CXCL9-CXCR3 axis (Fig. 7+15) and developed a tolerant phenotype characterized by simultaneous expression of multiple co-inhibitory receptors (Fig. 27+28). In the following, the importance of this cascade for tolerance was to be examined. Therefore, an inhibitory antibody to IFNγ was administered during the course of EAE, which led to a mild break of tolerance in CRP-MBP mice (Fig. 29A). There was no significant difference between anti-IFNγ- or isotype-treated wt mice, but anti-IFNγ-treated CRP-MBP mice had a higher cumulative disease score than isotype-treated CRP-MBP mice (10 in anti-IFNγ-treated vs. 0 in isotype-treated CRP-MBP mice; p = 0.0152) (Fig. 29B).

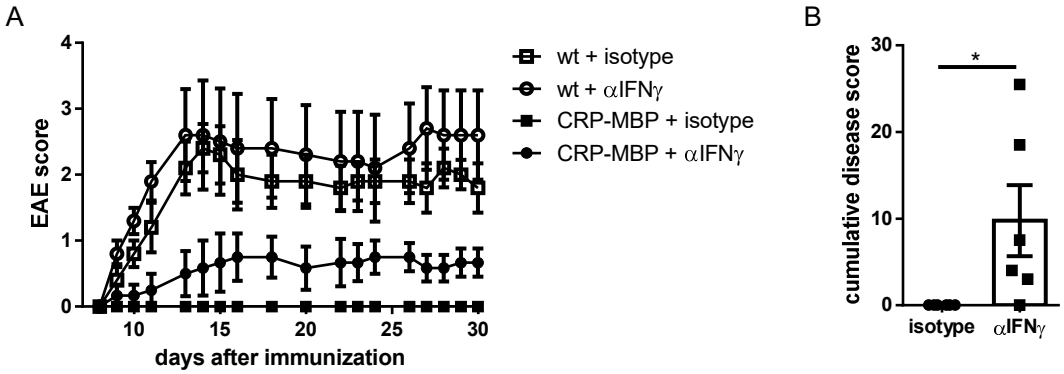

Figure 29. Blockade of IFNγ leads to mild EAE in CRP-MBP mice.
MBP-specific CD4 T cells were transferred into wt or CRP-MBP mice one day after immunization to MBP (n = 5-6). On day 3 and 6 after immunization, mice were injected with 300 µg of anti-IFNγ or isotype antibody i.p. A. EAE score was monitored for 30 days. B. The cumulative disease score was determined for CRP-MBP mice treated with isotype or anti-IFNγ antibody. Data correspond to mean ± SEM. P value was calculated via Mann-Whitney U test. *p<0.05.

Analysis of liver histology via HE staining revealed a reduced number of liver-infiltrating cells in CRP-MBP mice treated with anti-IFNγ antibody on day seven after immunization (Fig. 30A). This was also reflected by reduced ALT levels (24.7 U/L in anti-IFNγ-treated CRP-MBP vs. 106.6 U/L in isotype-treated CRP-MBP; p = 0.0007) (Fig. 30B).

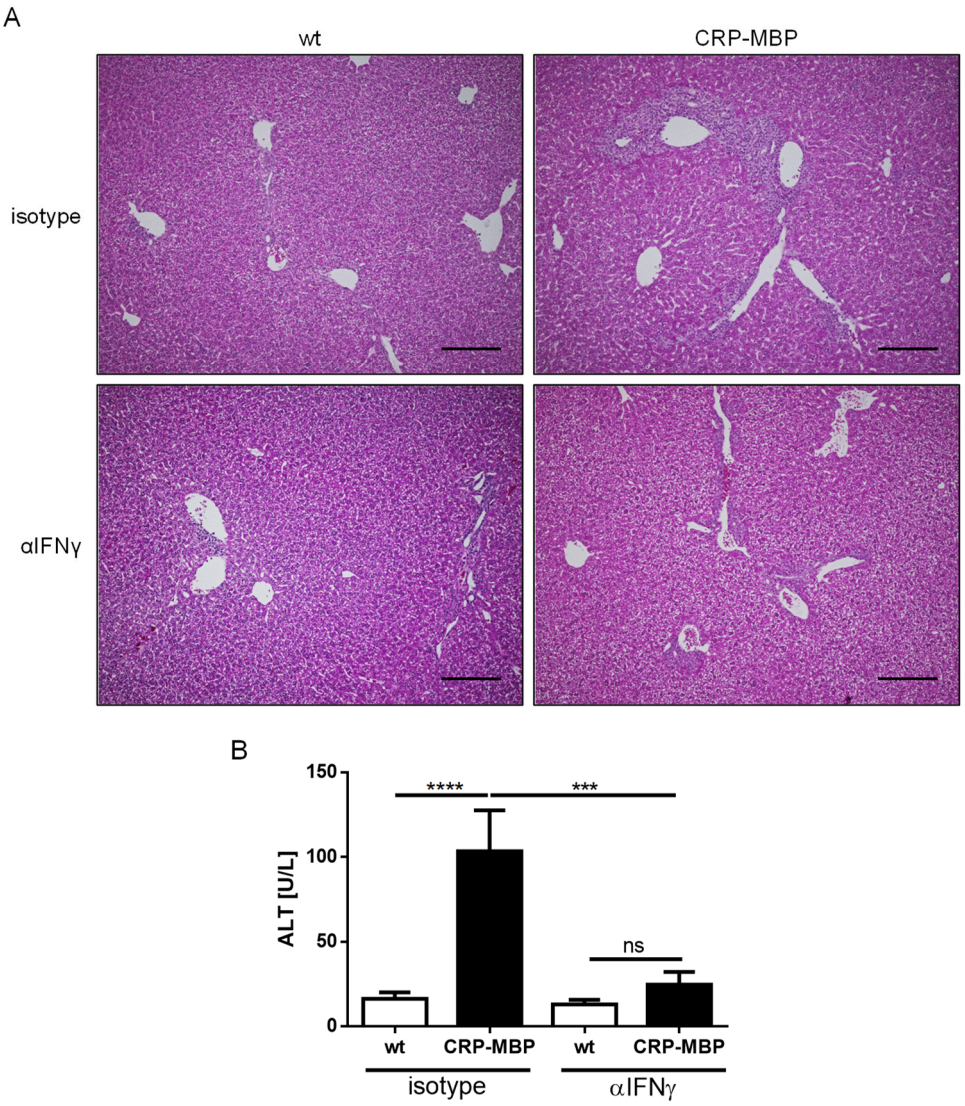

Figure 30. Blockade of IFNγ attenuates hepatitis in CRP-MBP mice.
MBP-specific CD4 T cells were transferred into wt or CRP-MBP mice one day after immunization to MBP. On day 3 and 6 after immunization, mice were injected with 300 µg of anti-IFNγ or isotype antibody. On day 7 after immunization, liver pathology was analyzed via A. HE staining and B. ALT serum levels. Data correspond to mean ± SEM. Scale bar: 200 µm. Pooled data of three independent experiments are shown (n = 10-12). P values were calculated via one-way ANOVA with Sidak's multiple comparisons test. ***p<0.001; ****p<0.0001. ns – not significant.

The absolute number of transferred, MBP-specific T cells that could be retrieved from the liver was also reduced in CRP-MBP mice treated with anti-IFNγ. In isotype-treated wt mice, approx. 0.1 x 10^6 MBP-specific T cells were found in the liver six days after cell transfer compared to 1.6 x 10^6 in isotype-treated CRP-MBP mice ($p < 0.0001$), highlighting hepatic accumulation of MBP-specific T cells in CRP-MBP mice (Fig. 31A). However, blockade of IFNγ reduced the number of MBP-specific T cells in CRP-MBP mice compared to isotype-treated CRP-MBP

mice (0.7x 10^6 vs. 1.6x 10^6; p = 0.0049). This reduction in T cell numbers in the liver might be explained by the striking decrease of *Cxcl9* expression when IFNγ signaling was blocked (Fig. 31B). Isotype-treated CRP-MBP mice expressed 48x more *Cxcl9* in the liver than wt mice (p < 0.0001) and expression levels in CRP-MBP mice with impaired IFNγ signaling were comparable to wt mice (1.5-fold induction in anti-IFNγ-treated CRP-MBP compared to wt; p = 0.9989). Thus, blockade of IFNγ signaling very effectively lowered *Cxcl9* expression to the level of wt mice. *Cxcr3* expression was increased by four times in CRP-MBP mice compared to wt mice in isotype controls (p = 0.0005). A reduction in expression almost to the level of wt mice was also seen for *Cxcr3* in CRP-MBP mice treated with anti-IFNγ (isotype- vs. anti-IFNγ-treated CRP-MBP mice; p = 0.0322) (Fig. 31C). Taken together, blockade of IFNγ reduced expression of *Cxcl9* and *Cxcr3* and therefore prevented hepatic accumulation of MBP-specific T cells in CRP-MBP mice.

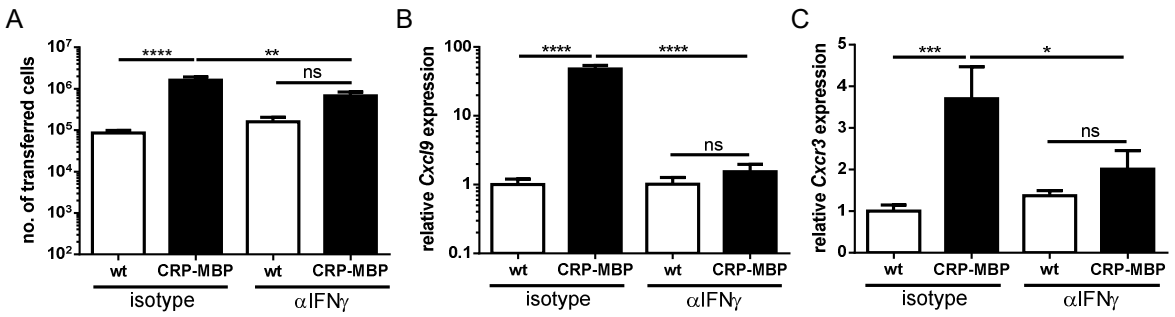

Figure 31. Blockade of IFNγ reduces hepatic accumulation of MBP-specific T cells.
MBP-specific CD4 T cells were transferred into wt or CRP-MBP mice one day after immunization to MBP. On day 3 and 6 after immunization, mice were injected with 300 µg of anti-IFNγ or isotype antibody i.p. A. The absolute number of MBP-specific T cells was determined in the liver of wt and CRP-MBP mice treated with isotype or anti-IFNγ antibody on day 7 after immunization. In whole liver tissue, *Cxcl9* (B) and *Cxcr3* (C) expression was determined. Pooled data of three independent experiments are shown (n = 8-12). Data correspond to mean ± SEM. P values were calculated via one-way ANOVA with Sidak's multiple comparisons test. **p<0.01; ***p<0.001; ****p<0.0001. ns – not significant.

Functional IFNγ depletion was also confirmed when analyzing PD-L1 and IDO1, two other ISGs that were previously seen to be upregulated in CRP-MBP mice compared to wt mice (Fig. 16). Both, *Cd274*, encoding PD-L1, and *Ido1* expression was reduced in liver NPCs when IFNγ signaling was impaired (Fig. 32). Expression of *Cd274* was reduced to levels of wt mice (2.8-fold induction in isotype-treated CRP-MBP mice compared to isotype-treated wt mice vs. 0.9-fold induction in anti-IFNγ-treated CRP-MBP mice compared to isotype-treated wt mice;

p = 0.0044). *Ido1* expression was not detectable in anti-IFNγ-treated mice, whereas there was expression in isotype-treated mice (0 vs. 0.0053 relative to *Hprt*; p = 0.0286).

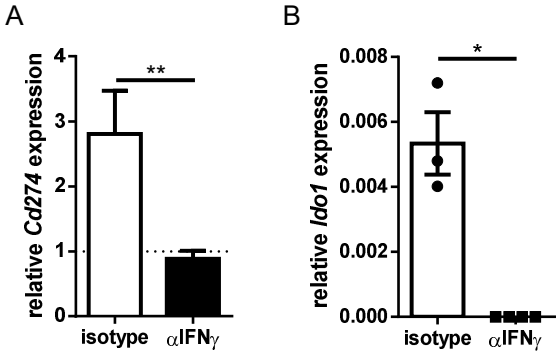

Figure 32. Blockade of IFNγ impedes induction of *Cd274* and *Ido1* in CRP-MBP mice.
MBP-specific CD4 T cells were transferred into wt or CRP-MBP mice one day after immunization to MBP. On day 3 and 6 after immunization, mice were injected with 300 µg of anti-IFNγ or isotype antibody i.p. Expression of *Cd274* (A; n = 8-10) and *Ido1* (B; n = 3-4) was analyzed in liver NPCs from CRP-MBP mice on day 7 after immunization. *Cd274* expression was normalized to wt mice treated with isotype antibody (dotted line). *Ido1* expression was analyzed relative to *Hprt*. Data correspond to mean ± SEM. P values were calculated via Mann-Whitney U test. * p<0.05; **p<0.01.

Thus, IFNγ signaling was effectively blocked, which reduced the amount of MBP-specific T cells in the liver and the expression of several ISGs. In the following, it was investigated whether this affected the tolerogenic phenotype of the MBP-specific T cells. To this end, the expression of co-inhibitory receptors on transferred T cells was studied (Fig. 33). As seen before (Fig. 27), in isotype-treated mice, all co-inhibitory receptors were upregulated on MBP-specific cells in the livers of CRP-MBP mice compared to wt mice. In anti-IFNγ-treated CRP-MBP mice, Lag-3 (44.3% vs. 55.7%; p = 0.0348) and CTLA-4 (47.6% vs. 56.9%; p = 0.0330) were significantly reduced compared to isotype-treated CRP-MBP mice, but still strongly increased compared to wt mice. Expression of TIGIT was reduced on MBP-specific T cells in anti-IFNγ-treated CRP-MBP mice compared to isotype-treated mice, even though this difference was not statistically significant (61.8% vs. 72.4%; p = 0.0557). Taken together, blockade of IFNγ signaling reduced expression of three co-inhibitory receptors on MBP-specific T cells in livers of CRP-MBP mice, but expression was not reduced to expression in wt mice.

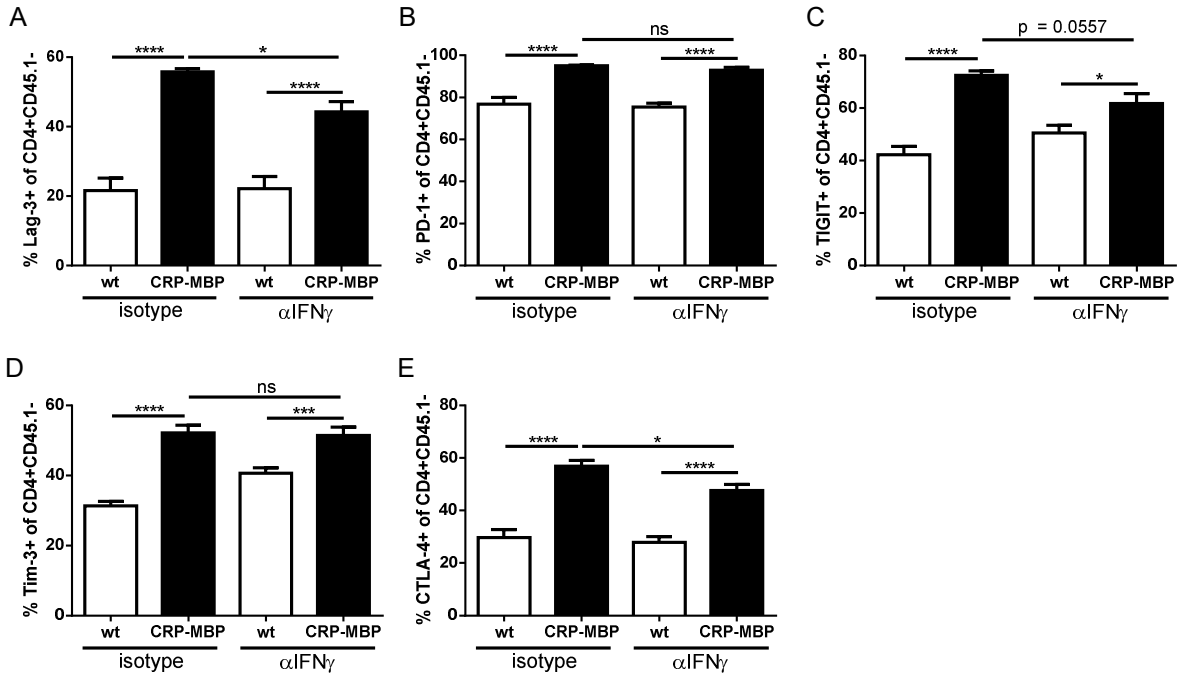

Figure 33. Expression of co-inhibitory receptors on liver-derived MBP-specific T cells.
MBP-specific CD4 T cells were transferred into wt or CRP-MBP mice one day after immunization to MBP. On day 3 and 6 after immunization, mice were injected with 300 μg of anti-IFNγ or isotype antibody i.p. Expression of Lag-3 (A), PD-1 (B), TIGIT (C), Tim-3 (D), and CTLA-4 (E) was analyzed on MBP-specific T cells from livers of wt and CRP-MBP mice on day 7 after immunization. Pooled data of three independent experiments are shown (n = 11-12). Data correspond to mean ± SEM. P values were calculated via one-way ANOVA with Sidak's multiple comparisons test. *p<0.05; ***p<0.001; ****p<0.0001. ns – not significant.

To sum up, in CRP-MBP mice, blockade of IFNγ led to mild EAE associated with 1) reduced accumulation of MBP-specific T cells in the liver, 2) reduced *Ido1* and *Cd274* expression in liver NPCs, and 3) mild reduction of co-inhibitory receptor expression on MBP-specific T cells in the liver.

3.1.12 Concomitant blockade of CTLA-4 and IFNγ impairs tolerance in CRP-MBP mice

As the co-inhibitory receptor CTLA-4 was induced in CRP-MBP mice after immunization (Fig. 27) and considering that a decrease of CTLA-4 was associated with a mild disease score during anti-IFNγ-treatment (Fig. 33), it was hypothesized that combined treatment of CRP-MBP mice with anti-IFNγ and anti-CTLA-4 antibodies might lead to a complete loss of tolerance. Indeed, while anti-CTLA-4 antibody alone did not lead to clinical EAE in CRP-MBP mice, combined administration of both antibodies led to clinical disease comparable to wt mice that were treated with an isotype antibody (cumulative disease score of 18.9 in CRP-MBP mice treated with anti-IFNγ/CTLA-4 vs. 19.3 in wt mice treated with isotype antibody; $p > 0.9999$) (Fig. 34B). Anti-IFNγ/CTLA-4-treated wt mice, showed a higher disease score compared to control wt mice even though that difference was not significant when studying the cumulative disease score (31.7 in anti-IFNγ/CTLA-4-treated wt mice vs. 19.3 in isotype-treated wt mice; $p = 0.1252$).

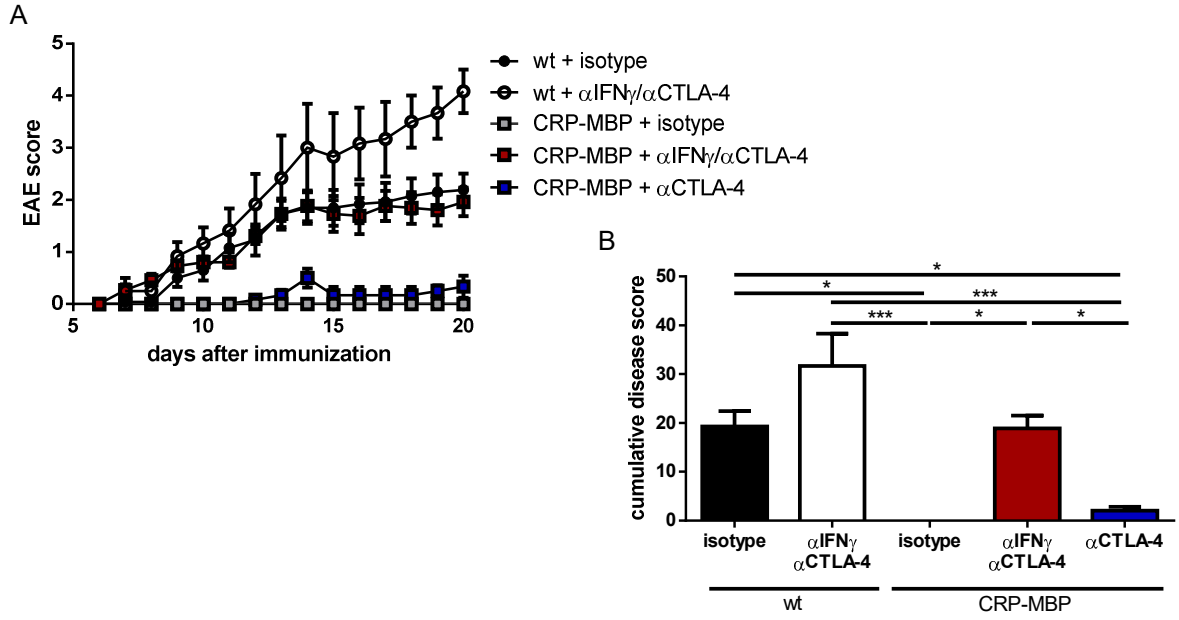

Figure 34. Blockade of IFNγ and CTLA-4 impairs tolerance in CRP-MBP mice.
MBP-specific CD4 T cells were transferred into wt or CRP-MBP mice one day after immunization to MBP. Mice were injected with 300 µg of isotype, anti-CTLA-4, or a mixture of anti-IFNγ and anti-CTLA-4 antibodies on day 3, 6, 9, and 12 after immunization. A. EAE score was monitored for 20 days. B. The cumulative disease score was calculated. Pooled data of two independent experiments are shown (n = 4-13). Data correspond to mean ± SEM. P values were calculated via one-way ANOVA. Statistically not significant results are not depicted. *p<0.05; ***p<0.001.

As EAE is a T cell driven disease, T cells were isolated from spinal cords and their frequency was determined. Combining all experimental groups shown in Fig. 34 in one graph, correlation analysis showed a moderate correlation between the presence of CD4 T cells in the spinal cord and the clinical EAE score (Fig. 35A). A closer look on CRP-MBP mice revealed that less than ten CD4 T cells were isolated from spinal cords of mice treated with an isotype antibody, of which none developed symptoms of disease. In CRP-MBP mice that were treated with anti-IFNγ/CTLA-4 antibodies and had an average disease score of 1.75 at day of analysis, the number of T cells retrieved from the spinal cord was almost 100 T cells (Fig. 35B). The clinical symptoms observed in CRP-MBP mice treated with anti-IFNγ/CTLA-4 antibodies were thus associated with the presence of CD4 T cells in the spinal cord.

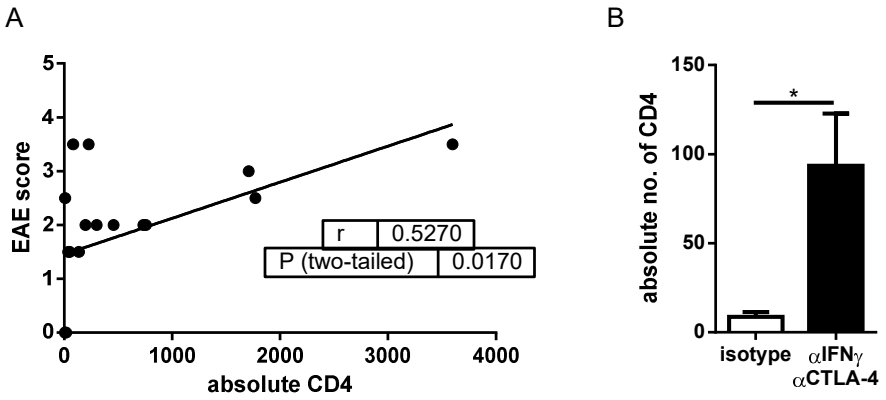

Figure 35. Analysis of CD4 T cells in spinal cord.
MBP-specific CD4 T cells were transferred into wt or CRP-MBP mice one day after immunization to MBP. Mice were injected with 300 µg of isotype, or anti-IFNγ/-CTLA-4 antibodies on day 3, 6, 9, and 12 after immunization. Mice were sacrificed at day 20 after immunization and cells were isolated from spinal cords. A. Correlation analysis between number of CD4 T cells in spinal cord and EAE score (n = 20). B. Absolute number of CD4 T cells isolated from spinal cords of CRP-MBP mice treated with isotype antibody or anti-IFNγ/CTLA-4 antibodies (n = 4-6). Data correspond to mean ± SEM (B). Data was analyzed calculating the Pearson correlation coefficient (A) or via Mann-Whitney U test (B), as appropriate. *p<0.05.

Notably, blockade of IFNγ and CTLA-4 led to an increase in IL-17 production by MBP-specific T cells in CRP-MBP mice. In the liver, 54.7% of MBP-specific CD4 T cells produced IL-17 compared to 33.2% in isotype-treated mice (p = 0.0351) (Fig. 36A). Spleen-derived MBP-specific T cells also produced more IL-17 in anti-IFNγ/CTLA-4-treated CRP-MBP mice, but this difference was neither significant compared to isotype-treated mice (17.1% vs. 12.2%; p = 0.1398) nor compared to anti-IFNγ-treated mice (17.1% vs. 10.7%; p = 0.0749) (Fig. 36B).

The strongest induction of IL-17 production was seen in the peripheral blood, where IL-17 expression was more than doubled by blockade of IFNγ and CTLA-4 (22.1% vs. 9.2%; p = 0.0017) (Fig. 36C). Interestingly, in peripheral blood, IL-17 production in isotype-treated CRP-MBP mice was lower than in disease-prone wt mice conflicting previous results where IL-17 expression was not altered (Fig. 13C).

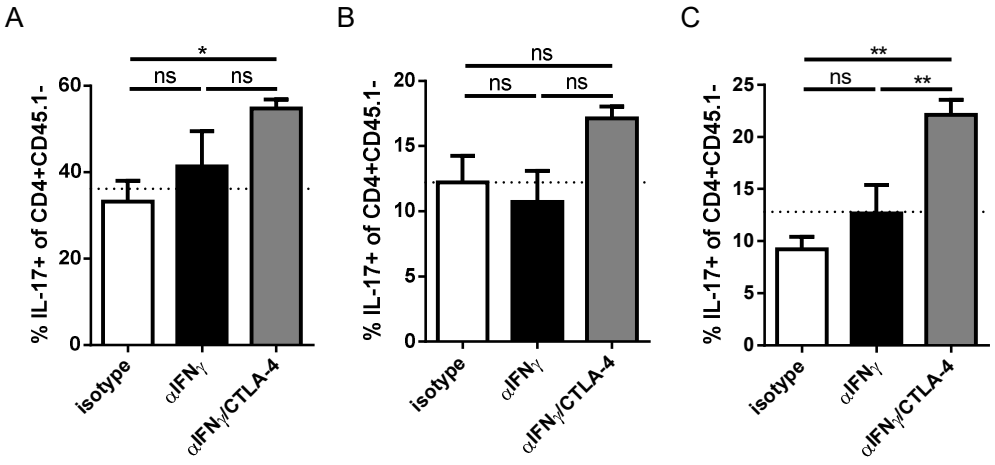

Figure 36. Concomitant blockade of IFNγ and CTLA-4 induces IL-17 production in MBP-specific T cells in CRP-MBP mice.
MBP-specific CD4 T cells were transferred into wt or CRP-MBP mice one day after immunization to MBP. Mice were injected with isotype, anti-IFNγ, or a combination of anti-IFNγ and anti-CTLA-4 antibody (n = 4-5). On day 7 after immunization, IL-17 protein expression was analyzed in MBP-specific CD4 T cells in liver (A), spleen (B), and whole blood (C). Data correspond to mean ± SEM. IL-17+ cells in isotype-treated wt mice are represented by the dotted line. P values were calculated via one-way ANOVA. *p<0.05; **p<0.01. ns – not significant.

To sum up, concomitant blockade of IFNγ and CTLA-4 induced robust break of tolerance in CRP-MBP mice associated with increased numbers of CD4 T cells in spinal cords and increased numbers of IL-17-producing MBP-specific T cells in liver, spleen, and, most strikingly, peripheral blood as compared to isotype-treated CRP-MBP mice.

3.2 Mechanisms of tolerance induction *in vivo* by LSEC-targeting nanoparticles

The tolerogenic properties of the liver can be harnessed to induce tolerance in the periphery as Carambia et al. showed, when they induced tolerance towards EAE by injecting mice with MBP peptide-loaded nanoparticles that were specifically taken up by LSECs [22]. This approach might allow for the treatment of a wide spectrum of autoimmune diseases with well-described autoantigens by harnessing the tolerogenic capacity of the liver. However, the underlying

mechanisms are not fully understood. In the second part of this thesis, it should be investigated whether the identified tolerance mechanisms in CRP-MBP mice might also participate in nanoparticle-induced tolerance.

3.2.1 MBP peptide-loaded LSEC-targeting nanoparticles protect from EAE development

First, it was established that the batch of nanoparticles used in this work protects from induction of autoimmune disease. To this end, mice were immunized to MBP, injected with nanoparticles on the same day, and the EAE score was monitored. Indeed, as shown before [22], mice that were injected with MBP-NP were protected from disease as compared to controls receiving empty NP (Fig. 37).

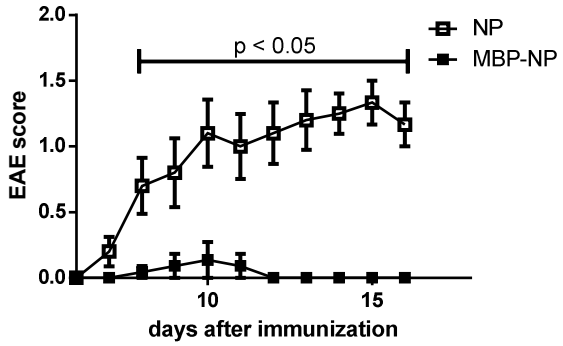

Figure 37. MBP peptide-loaded NP protect from EAE development.
Wt mice were immunized to MBP and injected with empty or MBP peptide-loaded NP on the same day (n = 10-11). EAE score was monitored for 16 days. Data correspond to mean ± SEM. P values were calculated via Mann-Whitney U test.

3.2.2 Nanoparticle-treatment does not cause liver damage

In order to study MBP-specific T cells, one day after immunization and administration of nanoparticles, mice received 5 x 10^6 congenic, MBP-specific T cells by adoptive transfer. At day seven after immunization, livers were analyzed for the presence of infiltrating cells via HE staining. In both, mice treated with empty or MBP peptide-loaded NP, only few infiltrating cells were seen with a tendency towards larger lymphocytic infiltrates in MBP-NP-treated mice (Fig. 38A). ALT measurement, however, could not detect a significant difference concerning

liver damage between NP- and MBP-NP-treated mice, even though ALT levels were slightly elevated in MBP-NP-treated mice (39.8 U/L vs. 25.2 U/L; p = 0.3095) (Fig. 38B).

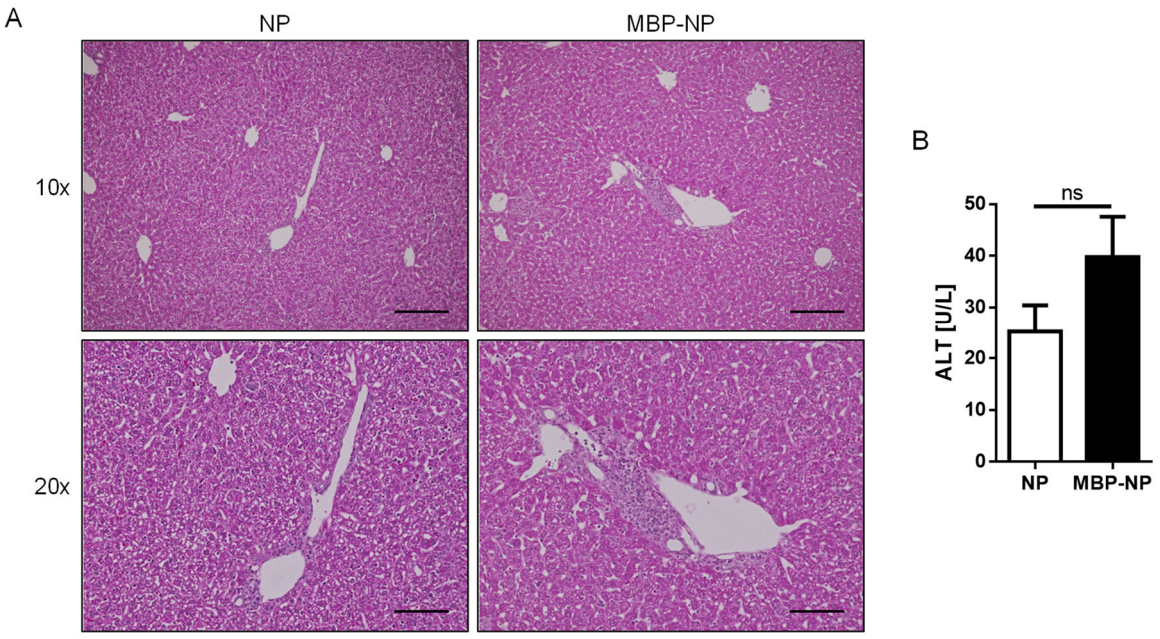

Figure 38. Analysis of liver damage in empty NP- and MBP-NP-treated mice.
Wt mice were immunized to MBP and injected with empty or MBP peptide-loaded NP (n = 5). One day later, mice were replenished with MBP-specific T cells. A. On day 7 after immunization, livers were perfused and stained with HE. Representative images are shown. Scale bar: 200 µm (10x); 100 µm (20x). B. ALT was measured in the serum. Data correspond to mean ± SEM. Data was analyzed via Mann-Whitney U test. ns – not significant.

3.2.3 MBP-specific T cells are present in liver, spleen, and blood of MBP-NP-treated mice

In order to study the presence of MBP-specific T cells in the liver upon MBP-NP treatment, NPCs were isolated and analyzed via flow cytometry. In accordance with the slightly increased lymphocytic infiltrates seen in HE staining, the number of NPCs isolated from the liver was slightly, but not significantly increased in MBP-NP-treated mice compared to mice treated with empty NP (14.36 x 10^6 vs. 9.88 x 10^6; p = 0.2443) (Fig. 39A). The percentage of MBP-specific CD4 T cells from all living cells, however, was increased in MBP-NP-treated mice (7.69% in MBP-NP vs. 1.18% in empty NP; p < 0.0001) (Fig. 39B). Also the total number of transferred, MBP-specific T cells was 10-fold higher in mice treated with MBP peptide-loaded NP as compared to control NP (1.12 x 10^6 vs 0.11 x 10^6 vs.; p < 0.0001) (Fig. 39C).

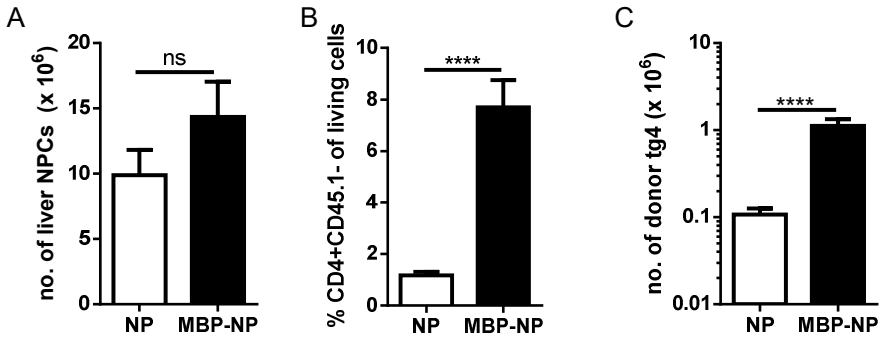

Figure 39. MBP-specific T cells accumulate in livers of MBP-NP-treated mice.
Wt mice were immunized to MBP and injected with empty or MBP peptide-loaded NP. One day later, mice were replenished with MBP-specific T cells. On day 7 after immunization, livers were perfused and A. NPCs were isolated and counted, B. MBP-specific (CD4+CD45.1-) T cells in the liver were analyzed, and C. the absolute number of MBP-specific T cells in the liver was calculated. Pooled data of two independent experiments are shown (n = 10). Data correspond to mean ± SEM. P values were calculated via Mann-Whitney U test. ****p<0.0001. ns – not significant.

In order to study the T cell response in the periphery, splenocytes and whole blood were analyzed for the presence of MBP-specific T cells. Indeed, the number of transferred, MBP-specific T cells was also highly increased in MBP-NP-treated mice in both spleen-derived cells (5.89% vs. 1.01%; $p < 0.0001$) and whole blood cells (4.04% vs. 0.52%; $p < 0.0001$) (Fig. 40).

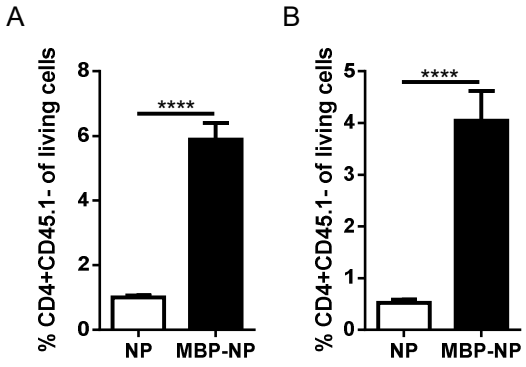

Figure 40. MBP-specific T cells accumulate in spleen and blood of MBP-NP-treated mice.
Wt mice were immunized to MBP and injected with empty or MBP peptide-loaded NP. One day later, mice were replenished with MBP-specific T cells. On day 7 after immunization, the presence of MBP-specific (CD4+CD45.1-) T cells was analyzed in spleen (A) and whole blood (B). Pooled data of two independent experiments are shown (n = 10). Data correspond to mean ± SEM. P values were calculated via Mann-Whitney U test. ****p<0.0001.

3.2.4 MBP-specific Tregs are reduced and endogenous Tregs induced in MBP-NP-treated mice

The tolerogenic properties of nanoparticles are often linked to their Treg-inducing capacity [168]. The nanoparticles used here were also shown to induce Tregs in an LSEC-dependent manner [22]. Interestingly, the number of transferred, MBP-specific cells that express Foxp3 differed between treatment with empty NP and MBP peptide-loaded NP. Surprisingly, treatment with MBP peptide-loaded NP significantly reduced the number of MBP-specific Tregs in the liver (1.0% in MBP-NP vs. 2% in empty NP; p = 0.0001) and in the spleen (1.1% in MBP-NP vs. 2.6% in empty NP; p = 0.0007). In whole blood, there was no significant difference in Foxp3+ MBP-specific T cells (0.8% in MBP-NP vs. 1.3% in empty NP; p = 0.2393) (Fig. 41).

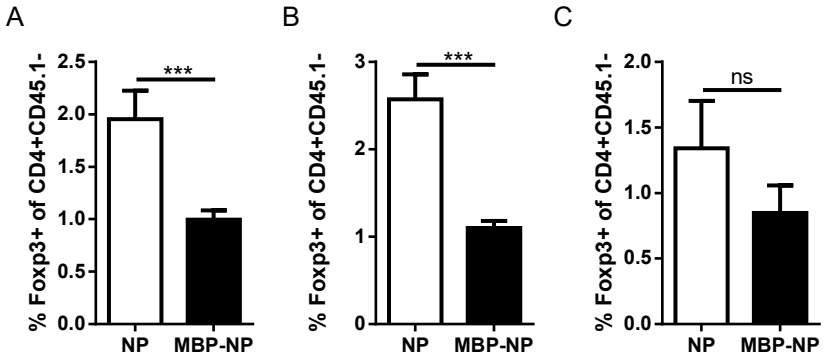

Figure 41. Tregs are reduced in MBP-specific T cells in MBP-NP-treated mice.
Wt mice were immunized to MBP and injected with empty or MBP peptide-loaded NP. One day later, mice were replenished with MBP-specific T cells. On day 7 after immunization, Foxp3+ Tregs were analyzed in MBP-specific cells in liver (A), spleen (B), and blood (C) of empty NP- and MBP-NP-treated mice. Pooled data of two independent experiments are shown (n = 10). Data correspond to mean ± SEM. P values were calculated via Mann-Whitney U test. ***p<0.001. ns – not significant.

The Treg-inducing capacity of MBP peptide-loaded NP was seen when analyzing the compartment of endogenous CD4 T cells in the liver. Treatment with MBP peptide-loaded NP significantly increased hepatic Treg numbers from 6.6% to 7.9% (p = 0.0098) (Fig. 42A). Splenic Treg numbers did not differ between groups (13.6% in empty NP vs. 13.8% in MBP-NP; p = 0.5911) (Fig. 42B). A moderate, but not significant increase in Treg numbers was seen in CD4 T cells from whole blood (11.1% in MBP-NP vs. 9.2% in empty NP; p = 0.3630) (Fig. 42C).

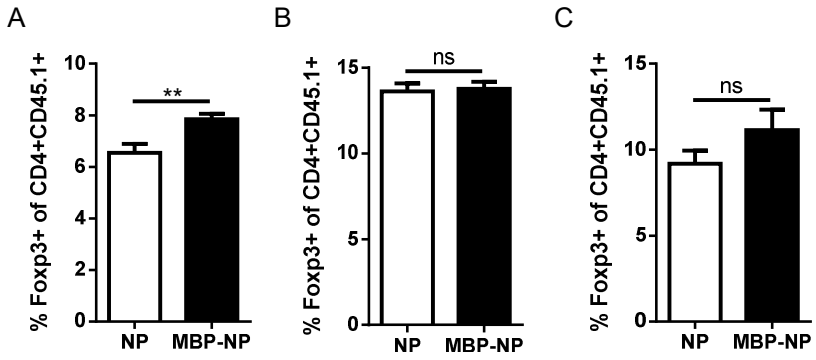

Figure 42. Analysis of Tregs in endogenous CD4 T cells.
Wt mice were immunized to MBP and injected with empty or MBP peptide-loaded NP. One day later, mice were replenished with MBP-specific T cells. On day 7 after immunization, Foxp3+ Tregs were analyzed in non-MBP-specific CD4 T cells in liver (A), spleen (B), and blood (C) of empty NP- and MBP-NP-treated mice. Pooled data of two independent experiments are shown (n = 10). Data correspond to mean ± SEM. P values were calculated via Mann-Whitney U test. **p<0.01. ns – not significant.

The expression of the characteristic surface markers for Tr1 cells, Lag-3 and CD49b, was analyzed on MBP-specific T cells from liver, spleen, and blood. In the liver, there was no significant difference in Lag-3+CD49b+ cells (7.5% in empty NP vs. 9.3% in MBP-NP; p = 0.1883) (Fig. 43A). However, Tr1-like cells were induced in both spleen (15.4% in MBP-NP vs. 8.0% in empty NP; p < 0.0001) and blood (4.6% in MBP-NP vs. 1.6% in empty NP; p = 0.0113) of MBP-NP-treated mice (Fig. 43B+C).

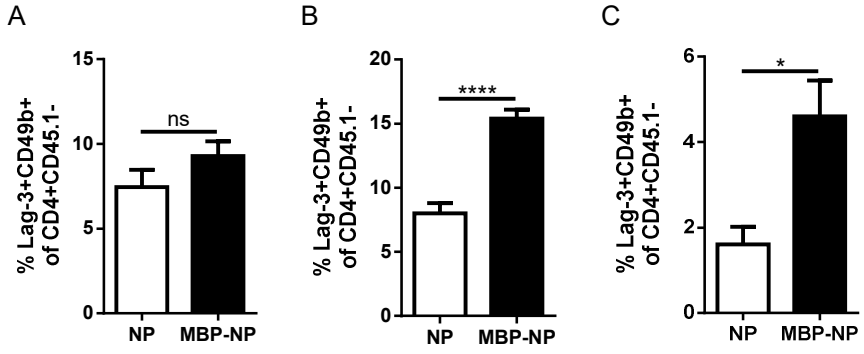

Figure 43. Analysis of Lag-3+CD49b+ MBP-specific T cells.
Wt mice were immunized to MBP and injected with empty or MBP peptide-loaded NP. One day later, mice were replenished with MBP-specific T cells. On day 7 after immunization, Lag-3 and CD49b co-expression was analyzed in MBP-specific CD4 T cells in liver (A), spleen (B), and blood (C) of empty NP- and MBP-NP-treated mice. Pooled data of two independent experiments are shown (n = 10). Data correspond to mean ± SEM. P values were calculated via Mann-Whitney U test. *p<0.05; ****p<0.0001. ns – not significant.

In the endogenous CD4 T cells, few cells co-expressed the Tr1 marker Lag-3 and CD49b and there was no difference between MBP-NP- and empty NP-treated mice (data not shown). In

brief, MBP peptide-loaded NP induced Tregs in the liver in the endogenous CD4 T cells and Lag-3+CD49b+ MBP-specific potential Tr1 cells were increased in spleen and blood of MBP-NP-treated mice.

3.2.5 Analysis of cytokines in MBP-specific T cells following MBP-NP treatment

The cytokine profile of MBP-specific T cells in the livers of CRP-MBP mice was characterized by increased expression of IFNγ (Fig. 13A) and IL-10 (Fig. 20). To draw comparisons, NPCs from the liver, splenocytes, as well as whole blood from nanoparticle-treated mice were stimulated with PMA/ionomycin for 4h and analyzed for their expression of IFNγ, IL-17, TNFα, and IL-10 (Fig. 44). MBP-specific T cells from mice treated with MBP peptide-loaded NP produced more IFNγ in liver (50.6% vs. 28.9%; $p = 0.0011$), spleen (31.5% vs. 17.8%; $p = 0.0011$), and blood (21.9% vs. 7.6%; $p = 0.0317$) compared to MBP-specific T cells from mice treated with empty NP. Furthermore, IL-10 was increased in the hepatic MBP-specific T cells (6.3% in MBP-NP vs. 3.2% in empty NP; $p = 0.0068$) and in MBP-specific T cell derived from the blood (8.6% in MBP-NP vs. 3.6% in empty NP; $p = 0.0159$), but not in the spleen (3.4% in MBP-NP vs. 3.6% in empty NP; $p = 0.5678$). Interestingly, IL-17 production was decreased in MBP-specific T cells in MBP-NP-treated mice compared to empty NP-treated mice in both liver (20.6% vs. 40.3%; $p = 0.0015$) and spleen (6.6% vs. 25.8%; $p = 0.0007$), whereas IL-17 was not differentially expressed by MBP-specific T cells from the blood (21.2% in MBP-NP vs. 22.4% in empty NP; $p = 0.9444$). There was no significant difference in TNFα production in any of the tested organs.

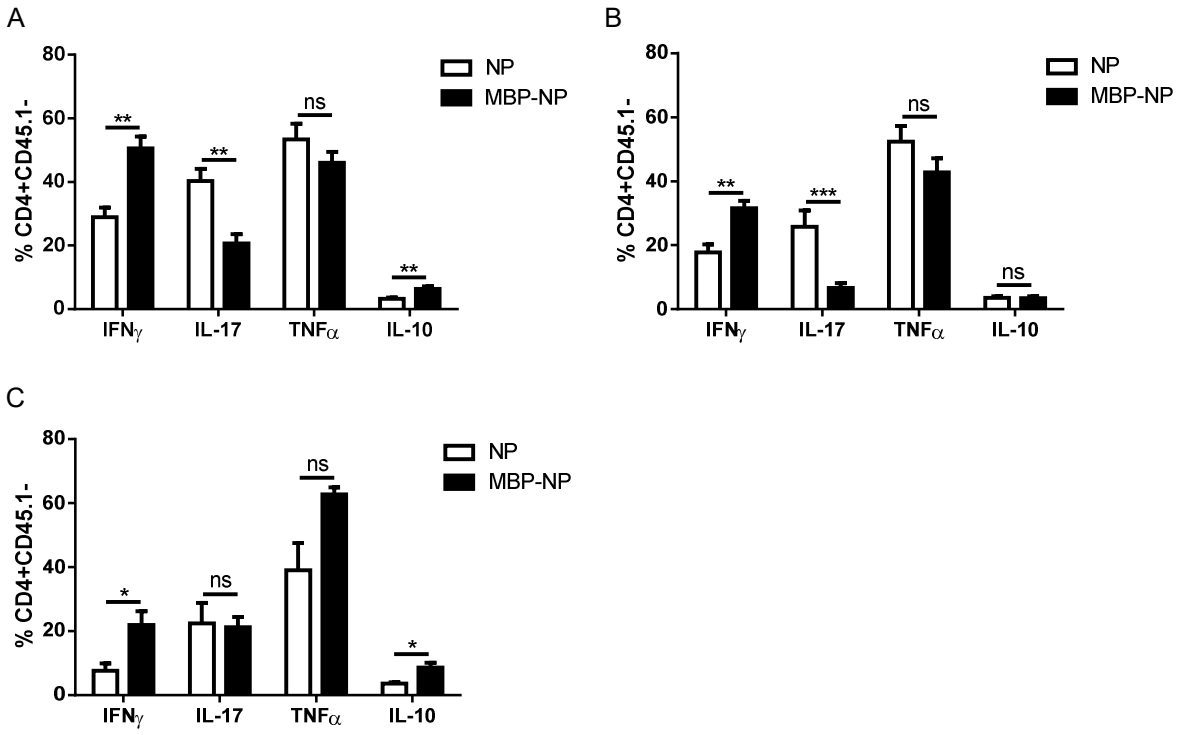

Figure 44. Cytokine profile of MBP-specific T cells.
Wt mice were immunized to MBP and injected with empty or MBP peptide-loaded NP. One day later, mice were replenished with MBP-specific T cells. On day 7 after immunization, production of IFNγ, IL-17, TNFα, and IL-10 was analyzed in MBP-specific T cells isolated from liver (A), spleen (B), and blood (C) of empty NP- and MBP-NP-treated mice after 4h stimulation with PMA/ionomycin (n = 10 for liver and spleen and n = 5 for blood). Data correspond to mean ± SEM. P values were calculated via Mann-Whitney U test. *p<0.05; **p<0.01; ***p<0.001. ns – not significant.

Comparable to the CRP-MBP model, MBP-specific T cells in MBP-NP-treated mice produced more IFNγ and IL-10 compared to MBP-specific T cells in empty NP-treated mice. Notably, IL-17 expression, which was only reduced in the spleen in CRP-MBP mice compared to wt mice, was reduced in both liver and spleen in MBP-NP-treated mice.

Interestingly, as seen before in CRP-MBP mice (Fig. 24), many IL-10-producing MBP-specific CD4 T cells co-expressed IFNγ in liver (79.6% in empty NP vs. 80.6% in MBP-NP; p = 0.9878) and spleen (59.3% in empty NP vs. 69.7% in MBP-NP; p = 0.1220) both, in mice treated with empty or with MBP peptide-loaded NP (Fig. 45).

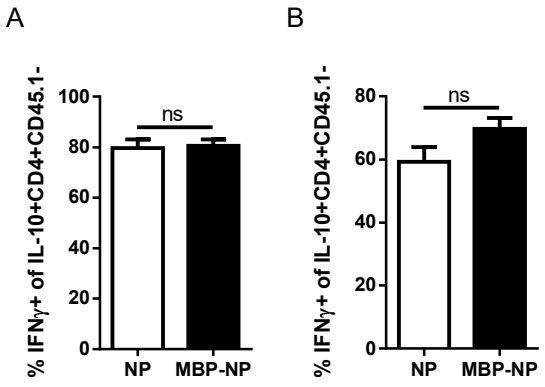

Figure 45. Analysis of IFNγ+ IL-10+ MBP-specific T cells.
Wt mice were immunized to MBP and injected with empty or MBP peptide-loaded NP. One day later, mice were replenished with MBP-specific T cells. On day 7 after immunization, co-production of IFNγ and IL-10 was analyzed in MBP-specific T cells from liver (A) and spleen (B). Pooled data of two independent experiments are shown (n = 10). Data correspond to mean ± SEM. P values were calculated via Mann-Whitney U test. ns – not significant.

3.2.6 The CXCL9-CXCR3 axis is associated with tolerance in MBP-NP-treated mice

As MBP-specific T cells in MBP-NP-treated mice produced more IFNγ compared to empty NP-treated mice, it was assumed that *Cxcl9* and *Cxcr3* expression was also increased in these mice. Gene expression of both genes was analyzed in whole liver tissue and indeed, *Cxcl9* expression was three-fold increased compared to empty NP (p = 0.0079) and *Cxcr3* expression was two times higher (p = 0.0079) (Fig. 46).

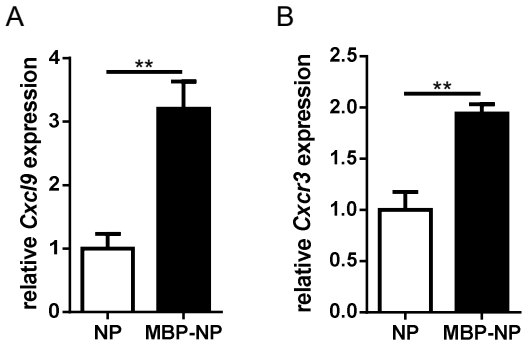

Figure 46. Expression of *Cxcl9* and *Cxcr3* is higher in livers of MBP-NP-treated mice.
Wt mice were immunized to MBP and injected with empty or MBP peptide-loaded NP. One day later, mice were replenished with MBP-specific T cells. Expression of *Cxcl9* (A) and *Cxcr3* (B) was analyzed in whole liver tissue on day 7 after immunization (n = 5). Data correspond to mean ± SEM. P values were calculated via Mann-Whitney U test. **p<0.01.

Analysis of protein expression of CXCR3 on MBP-specific CD4 T cells revealed increased expression in MBP-NP-treated mice in both liver (72.2% vs. 58.4%; p = 0.0159) and spleen (69.3% vs. 48.4%; p = 0.0159) compared to empty NP-treated mice (Fig. 47).

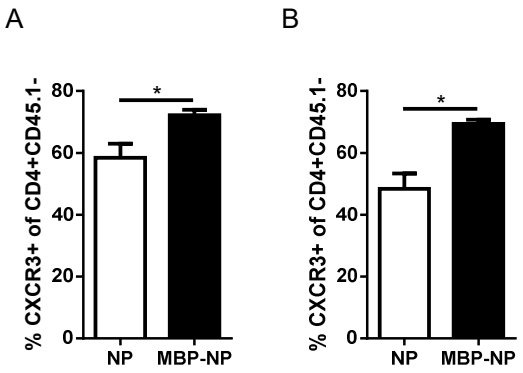

Figure 47. CXCR3 is upregulated on MBP-specific T cells in MBP-NP-treated mice.
Wt mice were immunized to MBP and injected with empty or MBP peptide-loaded NP. One day later, mice were replenished with MBP-specific T cells. On day 7 after immunization, expression of CXCR3 on MBP-specific cells was analyzed in liver (A) and spleen (B) (n = 5). Data correspond to mean ± SEM. P values were calculated via Mann-Whitney U test. *p<0.05.

Thus, induction of the IFNγ-CXCL9-CXCR3 axis was seen in mice treated with MBP peptide-loaded NP. This tolerance mechanism appeared to be shared between tolerance induction via hepatic autoantigen expression in the CRP-MBP model and LSEC-targeting nanoparticle-induced tolerance.

Increased expression of IFNγ induced upregulation of two additional tolerance-associated ISGs in CRP-MBP mice on day seven after immunization: PD-L1 and IDO1 (Fig. 16B+C). Both molecules seemed essential for tolerance in CRP-MBP mice, as blockade of IFNγ and thus reduced expression of both genes (Fig. 32), led to mild symptoms of EAE (Fig. 29A). To establish, whether PD-L1 and IDO1 contribute to tolerance induction via LSEC-targeting NP, expression of both genes was analyzed in whole liver tissue of NP-treated mice and indeed, *Cd274* expression was significantly higher in mice treated with MBP peptide-loaded NP as compared to mice receiving empty NP (1.6-fold expression; p = 0.0079) (Fig. 48A). There was also a trend towards higher *Ido1* expression (2.6-fold expression; p = 0.1032) in MBP-NP-treated mice (Fig. 48B).

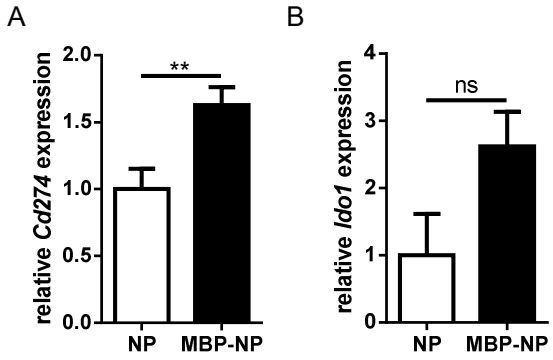

Figure 48. Expression of *Cd274* and *Ido1* is higher in livers of MBP-NP-treated mice.
Wt mice were immunized to MBP and injected with empty or MBP peptide-loaded NP. One day later, mice were replenished with MBP-specific T cells. Expression of *Cd274* (A) and *Ido1* (B) was analyzed in whole liver tissue on day 7 after immunization (n = 4-5). Data correspond to mean ± SEM. P values were calculated via Mann-Whitney U test. **p<0.01. ns – not significant.

3.2.7 Analysis of co-inhibitory receptors on MBP-specific T cells

The first part of this thesis uncovered a population of MBP-specific T cells in the livers of tolerant CRP-MBP mice that was defined by expression of Lag-3, PD-1, TIGIT, Tim-3, and CTLA-4 (Fig. 27A+28). The expression of the aforementioned co-inhibitory receptors was to be analyzed in the tolerant MBP-NP-treated mice on protein level (Fig. 49). Interestingly, expression levels of co-inhibitory receptors on MBP-specific T cells in mice treated with MBP peptide-loaded NP differed substantially from data collected in CRP-MBP mice. CTLA-4 proved to be the predominant co-inhibitory molecule upregulated on MBP-specific T cells in mice treated with MBP peptide-loaded NP compared to empty NP in liver (49.5% vs. 31.3%.; p = 0.0317), spleen (50.2% vs. 32.2%; p = 0.0079), and blood (30.8% vs. 8.0%; p = 0.0079). Lag-3 expression was similar in MBP-specific T cells derived from the liver (16.8% in empty NP vs. 17.5% in MBP-NP; p = 0.6182), but was induced in cells from spleen (18.3% in empty NP vs. 30.6% in MBP-NP; p = 0.0007) and blood (2.6% in empty NP vs. 7.9% in MBP-NP; p = 0.0354) in MBP-NP-treated mice. Surface expression of PD-1 was not differentially regulated in MBP-specific T cells in any of the organs tested. Surprisingly, two co-inhibitory receptors were even reduced on liver- and spleen-derived MBP-specific T cells after treatment with MBP peptide-loaded NP. The number of MBP specific TIGIT+ cells in the liver was 43.5% in control mice and 27.5% in MBP peptide loaded NP-treated mice (p <0.0001) and

additionally, in the spleen, a reduction by 10% was measured (52.1% in empty NP vs. 42.1% in MBP-NP; p = 0.0036). Similar observations were made for expression of Tim-3. In both liver (42.1% vs. 47.7%; p = 0.0041) and spleen (37.9% vs. 43.3%; p = 0.0016), expression was significantly reduced on MBP-specific T cells when mice were treated with MBP peptide-loaded NP compared to empty NP. Tim-3 and TIGIT were not altered on MBP-specific T cells derived from the blood.

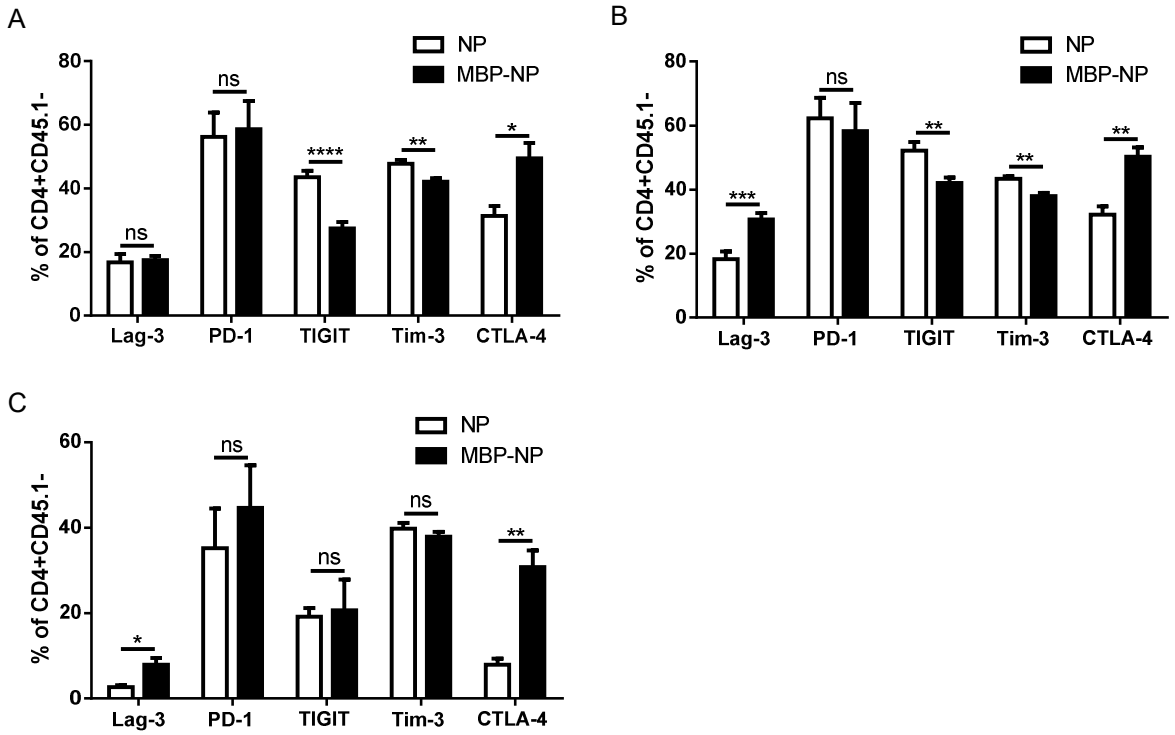

Figure 49. Analysis of co-inhibitory receptors on MBP-specific T cells.
Wt mice were immunized to MBP and injected with empty or MBP peptide-loaded NP. One day later, mice were replenished with MBP-specific T cells. On day 7 after immunization, expression of Lag-3, PD-1, TIGIT, Tim-3, and CTLA-4 was analyzed in MBP-specific T cells in liver (A), spleen (B), and blood (C) (n = 10; CTLA-4, n = 5). Data correspond to mean ± SEM. P values were calculated via Mann-Whitney U test. *p<0.05; **p<0.01; ***p<0.001; ****p<0.0001. ns – not significant.

In brief, on hepatic MBP-specific T cells, CTLA-4 was upregulated and Tim-3 and TIGIT were downregulated upon treatment with MBP peptide-loaded NP. Downregulation of Tim-3 and TIGIT was also observed on spleen-derived cells in MBP-NP-treated mice compared to control mice, whereas they expressed more Lag-3 and CTLA-4. Lag-3 and CTLA-4 were also elevated on MBP-specific T cells derived from the blood in MBP-NP-treated mice. Taken together, whereas in the transgenic CRP-MBP model, all co-inhibitory receptors were induced on MBP-specific T cells retrieved from the livers of CRP-MBP mice and at least three were

upregulated in spleen and blood, only CTLA-4 was upregulated on MBP-specific T cells from MBP-NP-treated mice in all three organs tested. Additionally, Lag-3 was elevated on spleen- and blood-derived MBP-specific T cells.

3.2.8 Blockade of IFNγ breaks MBP-NP-induced tolerance

In the first part of this thesis, IFNγ was identified as a key molecule in establishing immune tolerance. Partial impairment of tolerance in CRP-MBP mice was seen when IFNγ was blocked by a specific antibody. Likewise, IFNγ was blocked in MBP-NP-treated mice during the course of the EAE. Notably, and in contrast to the CRP-MBP model, anti-IFNγ treatment alone completely broke the tolerance in MBP-NP-treated mice and induced neuroinflammation (Fig. 50A). Analysis of the cumulative disease score proved that anti-IFNγ-treated mice receiving MBP-NP had a similar score as control mice treated with empty NP and an isotype-antibody (11.1 in MBP-NP anti-IFNγ vs. 12.4 in empty NP isotype; p = 0.9580) (Fig. 50B). Analysis of the spinal cord of anti-IFNγ-treated MBP-NP-treated mice via HE staining confirmed the presence of infiltrates and was consistent with the EAE score (Fig. 50C). Isotype-treated MBP-NP-treated mice showed no explicit CNS pathology (score of 0.7) and MBP-NP protected from EAE as seen before (Fig. 37). Interestingly, despite being upregulated on MBP-specific T cells in MBP-NP-treated mice, blockade of CTLA-4 alone did not induce strong EAE in MBP-NP-treated mice (score of 2.6), even though, some mice presented with mild symptoms. However, there was no significant difference in cumulative disease score when comparing MBP-NP-treated mice that were treated with isotype antibody to MBP-NP-treated mice that received anti-CTLA-4 antibody (0.7 vs. 2.6; p = 0.9225) (Fig. 50B). Comparable to the transgenic CRP-MBP model, blockade of CTLA-4 signaling alone is not sufficient to impair tolerance.

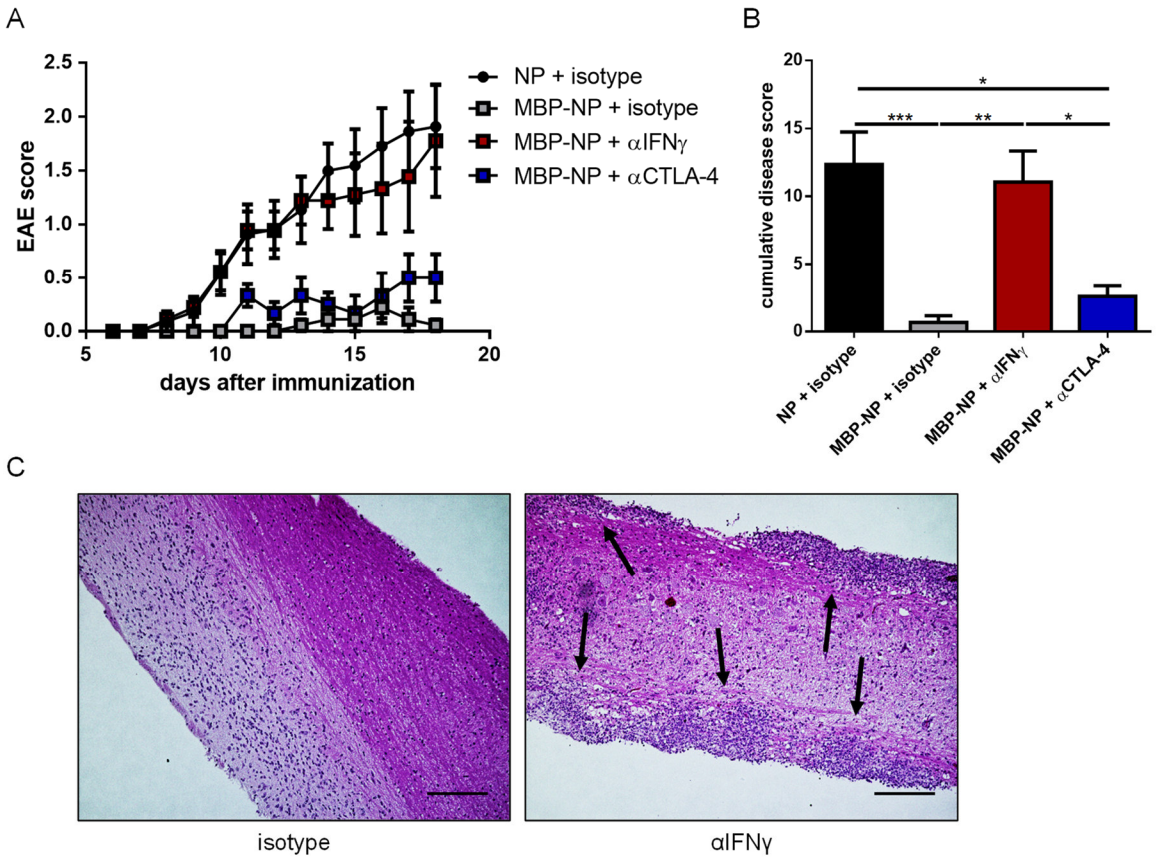

Figure 50. Blockade of IFNγ breaks tolerance in MBP-NP-treated mice.
Wt mice were immunized to MBP and injected with empty or MBP peptide-loaded NP. Mice were injected with 300 µg of anti-IFNγ, anti-CTLA-4, or isotype control 2x/week i.p. The EAE score was followed for 18 days (A) and the cumulative disease score was calculated (B). At peak of disease, spinal cords were isolated and stained with HE. C. Representative images for isotype-treated MBP-NP (left) and anti-IFNγ-treated MBP-NP mice (right) are depicted. The arrows point to lymphocytic infiltrates. Scale bar: 200 µm. Pooled data of two independent experiments are shown (n = 6-11). Data correspond to mean ± SEM. P values were calculated via one-way ANOVA (B). *p<0.05; **p<0.01; ***p<0.001.

Break of tolerance in anti-IFNγ-treated mice in the CRP-MBP model was associated with a decrease in both *Cxcl9* and *Cxcr3* expression in whole liver tissue on day seven after immunization, concomitant reduction in MBP-specific T cell numbers in the liver, mild reduction of co-inhibitory receptor expression on MBP-specific T cells, and generation of a Th17 phenotype. To assess, whether a similar mechanism is responsible for break of MBP peptide-loaded nanoparticle-induced tolerance, wt mice were immunized, injected with MBP peptide-loaded NP, and treated with either anti-IFNγ or isotype antibody. On day seven after immunization, livers were analyzed for the presence of MBP-specific T cells. Indeed, treatment with anti-IFNγ antibody reduced donor tg4 T cells by 61% (0.27×10^6 in anti-IFNγ-treated vs. 0.44×10^6 in isotype-treated mice; $p = 0.0317$). This reduction in hepatic accumulation of

MBP-specific T cells was associated with a decrease in *Cxcl9* expression in whole liver tissue in anti-IFNγ-treated mice (0.98-fold induction in anti-IFNγ- vs. 2.59-fold induction in isotype-treated MBP-NP-treated mice normalized to isotype-treated empty NP mice; p = 0.0079).

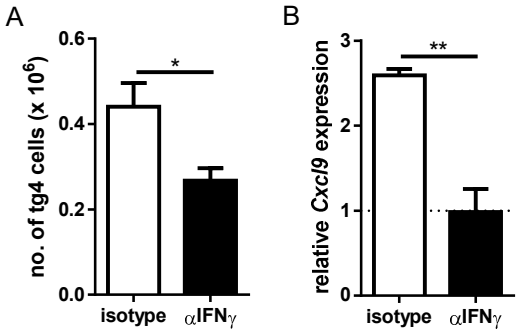

Figure 51. Blockade of IFNγ reduces accumulation of MBP-specific T cells in livers of MBP-NP-treated mice.
Wt mice were immunized to MBP and injected with empty or MBP peptide-loaded NP (n = 5). One day later, mice were replenished with MBP-specific T cells. Mice were injected with 300 µg of anti-IFNγ or isotype control 2x/week i.p. On day 7 after immunization, A. the number of MBP-specific T cells that could be re-isolated from the liver was calculated and B. *Cxcl9* expression in whole liver tissue was normalized to mice treated with empty NP and isotype antibody (dotted line). Data correspond to mean ± SEM. P values were calculated via Mann-Whitney U test. *p<0.05; **p<0.01.

Blockade of IFNγ signaling also reduced the expression of *Cd274* in MBP-NP-treated mice compared to MBP-NP mice treated with isotype control (0.7-fold induction in anti-IFNγ- vs. 1.4-fold induction in isotype-treated MBP-NP-treated mice normalized to isotype-treated empty NP mice; p = 0.0079). *Ido1* expression was completed abrogated by IFNγ blockade compared to low, but detectable expression in isotype-treated MBP-NP-treated mice (0 vs. 4×10^{-5}; p = 0.0476). Notably, IFNγ inhibition was accompanied by a mild reduction of MBP-specific CTLA-4+ T cells in the liver (51.0% in anti-IFNγ-treated MBP-NP vs. 59.5% in isotype-treated MBP-NP; p = 0.0317).

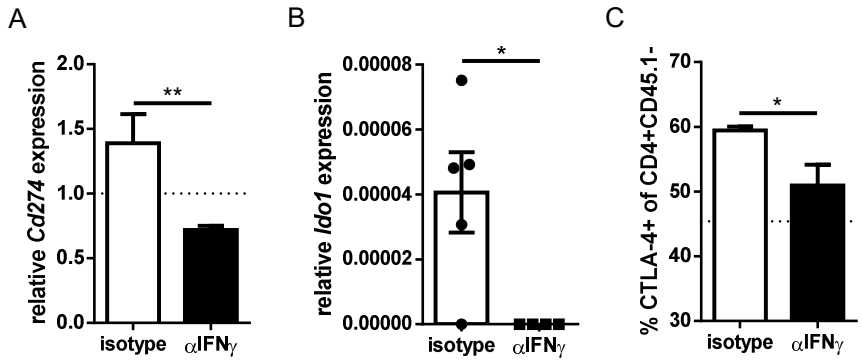

Figure 52. *Cd274*, *Ido1*, and CTLA-4 expression are reduced upon blockade of IFNγ.
Wt mice were immunized to MBP and injected with empty or MBP peptide-loaded NP (n = 5). One day later, mice were replenished with MBP-specific T cells. Mice were injected with 300 µg of anti-IFNγ antibody or isotype control 2x/week i.p. On day 7 after immunization, A. *Cd274* expression was analyzed in whole liver tissue relative to mice treated with empty NP and isotype antibody (dotted line). B. *Ido1* expression was analyzed in whole liver tissue relative to Hprt expression. C. Expression of CTLA-4 was analyzed in MBP-specific T cells from the liver of MBP-NP-treated mice. The dotted line represents expression in wt mice treated with empty NP and isotype antibody. Data correspond to mean ± SEM. P values were calculated via Mann-Whitney U test. *p<0.05; **p<0.01.

Briefly, depletion of IFNγ via monoclonal antibody induced robust disease in mice treated with MBP peptide-loaded NP. This break of tolerance was associated with a reduced accumulation of MBP-specific T cells in the liver and reduced expression of *Cxcl9*, *Cd274*, *Ido1*, and CTLA-4.

4. Discussion

In this study, liver tolerance mechanisms were examined in two mouse models: 1) the transgenic CRP-MBP mouse model, in which hepatic expression of the myelin antigen MBP protects from autoimmune neuroinflammation and 2) the translational model of nanoparticle-induced tolerance, in which MBP peptide-loaded NPs targeting LSECs also prevent EAE development. Two peripheral tolerance mechanisms should be investigated in particular: the suppression by Tr1 cells and inhibition of T cell responses via co-inhibitory receptors. In the course of this work, IFNγ was identified as another key molecule for hepatic tolerance induction.

4.1 Tolerance mechanisms in the CRP-MBP model

Previous work showed an elevation of Tregs in livers and spleens of MBP-expressing mice, which could confer tolerance upon transfer [18, 142]. However, we also found that Tregs were dispensable for tolerance induction [145], indicating additional tolerance mechanisms in this model. In addition to classical Foxp3+ Tregs, Tr1 cells have been described as another suppressive CD4 T cell population that is Foxp3-negative and produces high amounts of IL-10 [82]. Indeed, Tr1 cells seem to equal Foxp3+ Tregs in suppressive capacity [169]. In order to study whether MBP-specific CD4 T cells acquire a suppressive Tr1 phenotype, MBP-specific, congenic CD4 T cells from tg4 mice were transferred into immunized wt and CRP-MBP mice. Of note, a high proportion of MBP-specific T cells in livers and spleens of CRP-MBP, but not of wt mice co-expressed the characteristic surface markers for Tr1 cells, Lag-3 and CD49b [83] (Fig. 19), suggesting a role for Tr1 cells in hepatic tolerance induction. However, upon further characterization of IL-10-producing cells using double IL-10^{eGFP} Foxp3^{mRFP} reporter mice, it became apparent that only 20% of the IL-10+ cells were Tr1 cells (Fig. 22). This confirmed recent data on the necessity of IL-10 staining to characterize Tr1 cells, as the surface markers Lag-3 and CD49b are not exclusive to Tr1 cells [84]. Moreover, t-SNE analysis revealed a high heterogeneity of IL-10+ MBP-specific T cells that clustered into six different populations with differential expression of Lag-3 and CD49b and the co-inhibitory receptors Tim-3, TIGIT, and PD-1 (Fig. 23A). A small, but distinct subpopulation of IL-10+ MBP-specific CD4 T cells expressed multiple co-inhibitory receptors in conjunction with IL-10 and the Tr1 surface markers Lag-3 and CD49b. This supposedly suppressive T cell population was present in higher

frequencies in CRP-MBP mice compared to wt mice (Fig. 23B+C). IL-10 has been mainly described as an anti-inflammatory cytokine suppressing immune responses, which is reflected by spontaneous development of colitis in IL-10 KO mice [170]. However, others also observed high plasticity and heterogeneity among IL-10-producing CD4 T cells, some of which having immunoregulatory and others having inflammatory capacities [171]. Anti-inflammatory function was associated with the expression of co-inhibitory receptors, namely Lag-3, PD-1, TIGIT, and Tim-3 on IL-10-producing CD4 T cells. In patients with inflammatory bowel disease, a reduction in these co-inhibitory receptor-expressing IL-10+ CD4 T cells was observed [171]. In the absence of co-inhibitory receptor signaling, IL-10+ MBP-specific T cells in CRP-MBP mice might thus fail to induce immune tolerance. In order to determine the role of IL-10-producing subpopulations in the CRP-MBP model, a functional analysis of their suppressive capacity in a suppression assay is required. However, as IL-10 signaling proved to be dispensable for hepatic tolerance induction (Fig. 25), this was omitted. Strikingly, many IL-10-producing liver- and spleen-derived MBP-specific T cells co-produced the pro-inflammatory cytokine IFNγ in both wt and CRP-MBP mice (Fig. 24). IL-10 and IFNγ double producers have been identified in both, Th1 and Tr1 populations [172]. However, it was shown that cooperative action of both cytokines could induce tolerogenic IDO expression in DCs and block their immunostimulatory function more effectively as either cytokine alone [172], suggesting a tolerogenic function of IL-10 and IFNγ double producers. Also in human blood, a population of activated IL-10 and IFNγ double-producing CD4 T cells was observed that shows characteristics of both, Th1 and Tr1 cells, and suppresses T cell proliferation [173]. Especially in the context of infection, IL-10 production by Th1 cells was described as a means of limiting an exaggerated immune response directed against the pathogen [174]. In the liver, induction of IL-10 in Th1 cells seemed to depend on stimulation by LSECs: LSECs, which promote tolerance under homeostatic conditions, were shown to induce IL-10 production in Th1 cells *in vitro* and LSEC-stimulated IL-10+ Th1 cells inhibited a Th1-mediated immune response *in vivo* [175]. In CRP-MBP mice, an increase in hepatic and splenic IL-10-producing Tr1 cells was observed (Fig. 21), as well as an increase in IL-10+ cells with high expression of co-inhibitory receptors (Fig. 23) and a population of IL-10 and IFNγ double producers (Fig. 24), – all of which are associated with the generation of tolerogenic immune responses.

However, as mentioned, block of IL-10 signaling by IL-10 receptor antibody did not break tolerance (Fig. 25). In addition, tolerance was maintained in CRP-MBP mice expressing a dominant negative IL-10 receptor in T cells, making them insensitive towards IL-10 signaling [145]. Thus, potentially immunoregulatory IL-10-producing cells seemed to be induced in CRP-MBP mice, but redundant tolerance mechanisms could maintain tolerance in the absence of IL-10 signaling.

Analysis of the cytokine profile of transferred, MBP-specific T cells retrieved from the liver revealed an activated phenotype with high expression of IL-17 and TNFα in both wt and CRP-MBP recipient mice, irrespective of the presence of MBP in the liver (Fig. 13). This phenotype is likely due to the immunization of recipient mice with MBP prior to the transfer of MBP-specific T cells. Notably, IFNγ expression was increased in MBP-specific T cells in livers of CRP-MBP mice compared to wt mice (Fig. 13A). Despite being a classical pro-inflammatory cytokine, IFNγ was assigned a dual role during EAE. Its anti-inflammatory properties were seen when highly susceptible SJL/J mice were treated with IFNγ resulting in reduced morbidity and mortality; less susceptible C57BL/6J mice were treated with a neutralizing antibody against IFNγ causing an increase in both morbidity and mortality [176]. Here, no significant difference concerning the EAE score was observed in wt mice treated with anti-IFNγ compared to wt mice treated with an isotype antibody (Fig. 29A). However, a direct comparison between disease scores was difficult, as anti-IFNγ treatment led to atypical ataxic EAE in most wt mice, compared to classical paralytic EAE in control mice. Scoring of atypical EAE was therefore performed with a modified disease score [158]. Interestingly, symptoms of atypical EAE during IFNγ depletion are associated with an increased Th17 response rather than a Th1 response that induces classical EAE [177]. Besides inhibition of IL-17 production, the anti-inflammatory properties of IFNγ-producing cells in the CNS were described to depend on the induction of Tregs, the induction of T cell apoptosis, and regulation of cytokine production [178]. Interestingly, a disease stage-specific role of IFNγ was seen in EAE: treatment of mice with IFNγ during the initiation phase of disease enhanced disease severity, whereas treatment during the effector phase attenuated disease [158]. The dual role of IFNγ impedes its therapeutical use in treatment of MS patients. In a clinical study, seven out of eighteen relapsing-remitting MS patients that were treated with IFNγ showed a deterioration of disease, while

treatment with anti-IFNγ reduced clinical symptoms in a cohort of secondary progressive MS. However, in progressive MS patients, a high level of serum IFNγ was associated with a better disease outcome and low serum IFNγ was associated with exacerbation of disease (reviewed in [179]). In the spontaneous acceptance of liver allografts, IFNγ was attributed an essential role: transplantation of liver allografts into IFNγ-deficient mice resulted in infiltration, necrosis, and rejection of the transplant and vice versa, liver allografts from IFNγ receptor KO mice were rejected when transplanted into wt hosts [180]. IFNγ is a cytokine with diverse effects and blockade or induction of IFNγ affects many pathways. In the following, different molecules that are influenced by IFNγ were examined. In accordance with higher IFNγ levels, expression of ISGs, such as *Cxcl9*, *Ido1*, and *Cd274* was elevated in CRP-MBP mice (Fig. 14+16). Together with *Cxcl9*, also its receptor *Cxcr3* was induced in whole liver tissue and CXCR3 protein expression was induced on MBP-specific T cells in liver, spleen, and blood of CRP-MBP mice (Fig. 15). Various liver-resident cells have been described to be able to produce CXCL9 upon IFNγ stimulation, including hepatocytes, LSECs [162], and KCs [181]. Here, LSECs were identified as one source of increased CXCL9 expression in CRP-MBP mice (Fig. 15D), but the involvement of other liver-resident cells cannot be precluded. CXCR3 together with its ligands CXCL9, -10, and -11 was shown to regulate differentiation of naïve T cells into Th1 cells and enforces migration of T cells to sites of inflammation [161]. High expression of CXCL9 in the liver and elevated CXCR3 on circulating MBP-specific T cells suggested increased homing of these cells into the liver in CRP-MBP mice. This is further supported by increased expression of different adhesion molecules, such as ICAM-1, MadCAM-1, and VAP-1 in whole liver tissue (Fig. 18A) that were described to play important roles for homing of lymphocytes to the liver and extravasation from the sinusoids [182]. Accordingly, strong accumulation of MBP-specific T cells was seen in livers of CRP-MBP mice, amassing to ten times more intrahepatic cells than in wt mice (Fig. 7D). Interestingly, the IFNγ-CXCL9-CXCR3 axis has been associated with liver-induced systemic tolerance in a mouse model of hepatitis B virus (HBV). Indeed, IFNγ production by anti-viral T cells in the liver induced CXCL9 production in KCs that in turn retained T cells in the liver via CXCR3 ligation [181]. In the liver, these cells were partly eliminated via apoptosis and the periphery was thus depleted from HBV-specific T cells hindering effective viral clearance. A similar role for the liver in maintaining immune tolerance

has been observed in the analysis of recent thymic emigrants (RTEs). A population of RTEs, which produces IL-10 upon activation and is more prone to apoptosis, was identified in the liver suggesting the liver to be an important checkpoint in the periphery to filter and retain autoreactive CD4+ RTEs [183]. Strikingly, the liver has been described as a "graveyard" for CD8 T cells, which is especially important at the end of an immune response when many activated T cells are present. Activated and/or apoptotic CD8+ T cells specifically accumulated in the liver and were eliminated via apoptosis to ensure immune homeostasis [184]. Thus, trapping of (MBP-specific) T cells in the liver and subsequent apoptosis might be a potential mechanism for liver-induced tolerance. However, apoptosis did not seem to be the prevalent response of autoreactive T cells in CRP-MBP mice (Fig. 12). Indeed, MBP-specific T cell numbers in the periphery of CRP-MBP mice were not reduced (Fig. 7C), despite a CXCL9-CXCR3-associated accumulation of antigen-specific T cells in the liver. High T cell numbers in the liver rather seemed to be related to proliferation of MBP-specific T cells in the presence of their cognate antigen, which was confirmed by an increase in Ki-67 expression in these cells (Fig. 11). However, expression of *Ccr7*, which is essential for T cell egress from peripheral tissues [166], was downregulated in NPCs, providing an explanation for the accumulation of MBP-specific T cells in the liver (Fig. 18B). Furthermore, similar to what has been reported for liver-induced systemic tolerance induction towards HBV [181], blockade of IFNγ reduced expression of *Cxcl9* and *Cxcr3* (Fig. 31B+C) and prevented accumulation of MBP-specific T cells in the liver of CRP-MBP mice (Fig. 31A). Consequently, tolerance was compromised in CRP-MBP mice, which developed mild symptoms of EAE (Fig. 29). Taken together, these findings highlight a functional role for the IFNγ-CXCL9-CXCR3 axis for liver-induced antigen-specific tolerance in the CRP-MBP model.

Another tolerance-associated molecule induced by IFNγ is IDO1. *Ido1* expression was induced in livers of CRP-MBP mice (Fig. 16C) and strongly reduced when IFNγ was blocked (Fig. 32B). IDO1 is the rate-limiting enzyme in the degradation of tryptophan, an essential amino acid. An immune-modulating function has been assigned to IDO1, due to its ability to starve T cells for tryptophan and to degrade tryptophan to immune-modulating kynurenines that promote the generation of Tregs (reviewed in [164]). In EAE, IDO1 expression by DCs in lymph nodes is induced by engagement with antigen-specific Tregs and DCs then promote the suppressive

capacity of Tregs to control encephalitogenic T cell clones [185]. While the role of Tregs was shown to be dispensable in the CRP-MBP model, other immune-modulating functions of IDO1 or the tryptophan metabolites might be associated with tolerance. Interestingly, a connection was drawn between IFNγ-induced IDO expression and block of Th17 response in collagen-induced arthritis (CIA) [186]: Whereas C57BL/6 mice are resistant towards CIA, *IFNg* KO mice on C57BL/6 background develop severe arthritis associated with an increase in IL-17-producing cells. *Ex vivo*, Th17-polarized CD4 T cells from *IFNg* KO mice were co-cultured with their respective APCs (which were defined as negatively selected non-CD4 T cells from the same donor) and produced higher IL-17 compared to co-culture of APCs with wt CD4 T cells. Thus, IFNγ seemed to suppress the production of IL-17 in CD4 T cells. CD4 T cells isolated from IDO KO mice produced more IL-17 compared to wt CD4 T cells when cultured in Th17-polarizing conditions leading to the hypothesis that IFNγ inhibits the Th17 response in CIA dependent on IDO [186]. Mechanistically, it was shown that kynurenic acid, an IDO metabolite, modulates the expression of IL-23 and IL-17 in both, DCs and CD4 T cells, by downregulation of cyclic adenosine monophosphate and adenylate cyclase [187]. The trend towards higher MBP-specific Th17 numbers in liver and peripheral blood of CRP-MBP mice when IFNγ signaling was blocked (Fig. 36) might thus be IDO-dependent.

An additional ISG that was higher expressed in livers of CRP-MBP mice compared to wt mice and that was reduced upon blockade of IFNγ was PD-L1 (Fig. 32A). PD-L1 is the ligand for the co-inhibitory receptor PD-1 and is mainly expressed on myeloid cells. In both wt and CRP-MBP mice, it was highly expressed by KCs (Fig. 17A). However, expression of PD-L1 was higher on both liver-derived DCs and LSECs in CRP-MBP mice (Fig. 17B+C). Its striking role for hepatic tolerance induction was demonstrated in a mouse model of liver allograft acceptance. PD-L1 was highly expressed on donor-derived tissue cells and blockade of PD-L1 via antibody or the use of PD-L1 KO mice as donor resulted in allograft rejection [188]. Reduced IFNγ-dependent induction of PD-L1 in liver NPCs likely also contributes to the loss of liver graft acceptance in IFNγ-deficient mice [180]. Thus, signaling of PD-L1 via its receptor PD-1 on MBP-specific T cells, a receptor that was higher expressed on MBP-specific T cells in liver and spleen of tolerant CRP-MBP mice (Fig. 27), might have contributed to hepatic tolerance in the CRP-MBP model. Interestingly, also PD-L1 was shown to be associated with reduced

development of Th17 cells. PD-L1 signaling via an alternative, unidentified receptor blocks Th17 differentiation by interfering with RORγt and IRF-4, which are signature genes for Th17 development [189]. Thus, reduction of PD-L1 might have contributed to the moderately increased Th17 numbers in CRP-MBP mice when IFNγ signaling was blocked.

Another important peripheral tolerance mechanism is the expression of co-inhibitory receptors on T cells. Upregulation of co-inhibitory receptors is associated with an exhausted phenotype especially in CD8 T cells during chronic infections or cancer. Increasing expression of co-inhibitory receptors goes along with decreased proliferative capacity and cytokine production and increased apoptosis [125]. Also on CD4 T cells, co-inhibitory receptors have important functions in immune regulation and loss of e.g. CTLA-4 signaling in CD4 T cells is associated with lymphoproliferation, the generation of autoantibodies, and development of autoimmunity [190]. On day seven after immunization, Lag-3, PD-1, Tim-3, TIGIT, and CTLA-4 were higher expressed on MBP-specific T cells in livers of CRP-MBP mice (Fig. 27A) and in spleen and peripheral blood, three out of five co-inhibitory receptors tested were upregulated (Fig. 27B+C). This is in accordance with clinical data showing that MS patients had reduced levels of Lag-3 and TIGIT in peripheral blood, and that decreased Lag-3 and Tim-3 levels at the time of diagnosis could serve as a prognostic factor for disease development [191]. Co-inhibitory receptor expression thus seemed to correlate with protection from autoimmune neuroinflammation in MS [191] and EAE (Fig. 27). However, despite high expression of co-inhibitory receptors, MBP-specific T cells in CRP-MBP mice did not show reduced production of cytokines (Fig. 13) and had higher proliferative capacity compared to MBP-specific T cells in wt mice (Fig. 11). Of note, Lag-3, Tim-3, and TIGIT are also transiently upregulated on activated CD4 T cells [192]. Expression of these markers on MBP-specific T cells in CRP-MBP mice might thus have reflected their activation status after MBP-specific stimulation in the liver rather than a tolerogenic phenotype. Nonetheless, it was shown that a population of gut-derived intraepithelial lymphocytes that expressed high *Ctla4* and *Lag3* suppressed EAE upon transfer [193]. Interestingly, these suppressive CD4 T cells specifically entered the CNS and exerted their suppressive capacity, which means that the sole presence of CD4 T cells in the CNS is not necessarily associated with neuroinflammation. The importance of Lag-3 in this model became evident, when it was shown that Lag-3 depletion diminished the

protective capacity of gut-derived CD4 T cells [193]. In consideration of the strong increase of Lag-3 expression in hepatic MBP-specific T cells in CRP-MBP mice (Fig. 27), the functional role of Lag-3 was to be analyzed by depleting Lag-3 during EAE. However, in the context of immunization to MBP, blocking Lag-3 was lethal in both wt and CRP-MBP mice (data not shown). Treatment of mice with anti-Lag-3 antibody only early after immunization was not lethal, but did not lead to effective downregulation of Lag-3 on MBP-specific CD4 T cells (data not shown). Thus, it was not possible to determine whether Lag-3 was indispensable for hepatic tolerance. However, CTLA-4 and PD-1 are predicted to be superior to Lag-3, Tim-3, and TIGIT concerning their impact on self-tolerance [192]. PD-1 expression was significantly higher in MBP-specific T cells from liver and spleen of CRP-MBP mice. However, also in wt mice, PD-1 expression was highly upregulated on MBP-specific T cells (Fig. 27). In contrast, expression of CTLA-4 was significantly higher in MBP-specific T cells from liver and peripheral blood in CRP-MBP mice, compared to wt mice (Fig. 27A+C). However, tolerance remained unaffected when CTLA-4 was blocked by a specific antibody in CRP-MBP mice after immunization to MBP (Fig. 34). In the following, the mechanism of induction of the co-inhibitory receptors was to be analyzed. IL-27, in conjunction with Blimp-1 and c-Maf, was assigned a key role in driving the expression of a module of co-inhibitory receptors that includes PD-1, Lag-3, Tim-3, and TIGIT in both CD4 and CD8 T cells in several states of T cell non-responsiveness, such as cancer, viral exhaustion, and tolerance [124]. While *Prdm1*, encoding Blimp-1, was highly upregulated in livers of CRP-MBP mice, IL-27 and c-Maf were not differentially regulated in wt and CRP-MBP mice [145]. Thus, the co-inhibitory receptors do not seem to be regulated collectively as a module. However, CTLA-4 had been shown to be regulated by two other pathways. First, antigen targeting to the mannose receptor expressed on DCs, macrophages, or endothelial cells could induce CTLA-4-dependent T cell tolerance. The mannose receptor directly interacts with CD45 on T cells and inhibits its phosphatase activity, which via reduced Bcl6 expression ultimately leads to induction of CTLA-4 [194]. In the CRP-MBP model, MBP is mainly expressed by hepatocytes, as transcriptional induction of the CRP gene is mostly restricted to hepatocytes [195]. However, a membrane-bound form of CRP was detected on KCs and CRP mRNA was detected within KCs during the acute-phase response in rat liver [196]. Additionally, cross-presentation of MBP by other APCs in the liver cannot be

excluded. Therefore, as LSECs and KCs also carry the mannose receptor [197], antigen presentation by these non-classical APCs could have induced CTLA-4 expression by the aforementioned mechanism. Another mechanism of CTLA-4 induction has been found in melanocytes and melanoma, which linked expression of CTLA-4 to that of IFNγ. IFNγ signaling activated CTLA-4 expression via phosphorylation of STAT1, which subsequently bound a gamma-activated sequence site on the CTLA-4 promoter leading to local chromatin opening and higher *Ctla4* expression [198]. This mechanism could explain why blockade of IFNγ in CRP-MBP mice led to a moderate reduction in CTLA-4 expression by MBP-specific T cells (Fig. 33E).

Strikingly, concomitant blockade of IFNγ and the co-inhibitory receptor CTLA-4 led to both, a robust EAE score (Fig. 34) and a strong increase in MBP-specific IL-17-producing cells in liver, spleen, and, most notably, peripheral blood of CRP-MBP mice (Fig. 36). Blocking the interaction of CTLA-4 and CD80/86 was shown to increase Th17 differentiation and exacerbated disease in a model of experimental autoimmune myocarditis [199]. Interestingly, in a clinical trial with tremelimumab – a human monoclonal antibody against CTLA-4 applied for treatment of melanoma – increased Th17 cells were detected in PBMCs in melanoma patients after treatment [200]. Blockade of CTLA-4 thus seems to be associated with an increase of Th17 cells. Intriguingly, there is a link between CTLA-4 and IDO expression, as binding of CD80/86 on DCs to CTLA-4 derived from CD4 T cells was shown to induce robust IDO expression in DCs [201]. This suggests a role for IDO in the CTLA-4-dependent suppression of Th17 cells in CRP-MBP mice. As a strong Th17 phenotype was only seen when IFNγ and CTLA-4 were blocked in parallel, multiple pathways seem to be involved in regulating MBP-specific Th17 cells in the CRP-MBP model.

In summary, it was established that tolerance in CRP-MBP mice was associated with accumulation of MBP-specific T cells in the liver, upregulation of IL-10, IFNγ, IFNγ-induced genes, notably IDO1 and PD-L1, and induction of co-inhibitory receptor expression on MBP-specific T cells in liver, spleen, and blood. Blockade of IFNγ and CTLA-4 signaling was sufficient to break tolerance and induce neuroinflammation, which was presumably due to an increase in Th17 cells. Findings from the CRP-MBP model thus highlight the remarkable tolerogenic capacity of the liver, as blockade of one single molecule was not sufficient to induce

strong autoimmune disease. Whereas blockade of IL-10 or CTLA-4 could be fully compensated, impairment of IFNγ signaling induced mild symptoms of disease suggesting a central role for IFNγ in liver-induced tolerance. Thus, IFNγ might safeguard hepatic immune tolerance via the IFNγ-CXCL9-CXCR3 axis that facilitates retention of antigen-specific T cells in the liver, via induction of tolerogenic IDO1 and PD-L1 in the liver, and inhibition of Th17 cell development.

4.2 Mechanisms of tolerance induction *in vivo* by LSEC-targeting nanoparticles

The different peripheral tolerance mechanisms that were analyzed in the transgenic CRP-MBP model were also studied in the model of antigen-specific tolerance induction by LSEC-targeting nanoparticles. Besides defined antigen presentation by LSECs, this model allows the translation of hepatic tolerance mechanisms to a therapeutical setting with potential translation into the clinics.

The tolerogenic potential of antigen peptide-loaded nanoparticles has been usually assigned to their capacity to facilitate the generation of antigen-specific Tregs *in vivo* [22, 168]. Especially LSECs, the cellular target of the nanoparticles used here, are known for their capacity to induce Tregs that is superior compared to DCs and KCs [18]. In order to study the generation of MBP-specific Tregs, wt mice were treated with empty or MBP peptide-loaded NP on the day of immunization to MBP and received MBP-specific CD4 T cells by adoptive transfer on the following day. On day seven after immunization, the presence of Foxp3+ Tregs was studied in endogenous and transferred MBP-specific CD4 T cells. A significant increase in Tregs was observed in the endogenous CD4 T cells in the liver when mice were treated with MBP peptide-loaded NP (Fig. 42A). However, MBP-specific Tregs in liver, spleen, and blood were low in numbers in mice treated with empty or MBP peptide-loaded NP (Fig. 41). Notably, Foxp3+ MBP-specific CD4 T cell numbers were even significantly reduced in liver and spleen of protected MBP-NP-treated mice (Fig. 41A+B). Thus, transferred, MBP-specific T cells were not converted into Tregs in MBP-NP-treated mice. The presence of Tr1 cells was only determined by analysis of surface expression of Lag-3 and CD49b on MBP-specific T cells, but not in IL-10 reporter mice. In both spleen and blood, Lag-3+CD49b+ MBP-specific Tr1-like

cells were induced via treatment with MBP peptide-loaded NP (Fig. 43B+C). However, as shown before, additional IL-10 staining in the Lag-3+CD49b+ cells is necessary to categorize these cells as bona fide Tr1 cells [84]. Although IL-10-producing MBP-specific T cells were higher in numbers in MBP-NP-treated mice in liver and blood (Fig. 44A+C), expression of IL-10, Lag-3, and CD49b on the same cells was not analyzed. These data suggest an induction of Tr1-like cells in mice treated with MBP peptide-loaded NP. However, to draw a final conclusion, a more thorough analysis is required. Besides conversion of T cells into Tregs, LSECs have other possibilities to induce immune tolerance. LSECtin on the surface of LSECs binds to the co-inhibitory receptor Lag-3 on T cells and thus downregulates T cell responses [108]. However, expression of Lag-3 on MBP-specific T cells was only upregulated in spleen and peripheral blood in MBP-NP-treated mice (Fig. 49B+C). In the liver, where T cells encounter LSECs, MBP peptide-loaded NP did not induce elevated expression of Lag-3 (Fig. 49A). Furthermore, expression of *Clec4g*, which encodes LSECtin, was also not elevated in the livers of MBP-NP-treated mice (data not shown). Therefore, T cell tolerance via ligation of LSECtin on LSECs to Lag-3 on MBP-specific T cells seems unlikely to mediate tolerance in this model. Regarding CD8 T cell tolerance, binding of PD-L1 on LSECs to PD-1 on CD8 T cells during antigen-cross-presentation is an important mechanism to shutdown T cell responses [23]. Notably, the PD-1-PD-L1 axis is also important to downregulate CD4 T cell responses [20]. DC-induced IFNγ production by CD4 T cells *in vitro* was greatly diminished when LSECs were added to the culture. The use of PD-1 KO CD4 T cells, however, abrogated this LSEC-induced inhibition. Conversely, LSECs derived from IL-10 KO mice, which showed reduced PD-L1 expression and increased MHC II, failed to downregulate DC-induced IFNγ by CD4 T cells [20]. Thus, both PD-1 expression on CD4 T cells and PD-L1 expression on LSECs appear to be important for generation of CD4 T cell tolerance by LSECs. While PD-1 expression was not different in mice treated with empty or MBP peptide-loaded NP (Fig. 49), *Cd274* gene expression was slightly but significantly increased in livers of MBP-NP-treated mice (Fig. 48A). This suggests that upon antigen-presentation, LSECs deliver an inhibitory signal to CD4 T cells via PD-1-PD-L1 ligation.

Regarding co-inhibitory receptor expression, there are striking differences between the two tolerance models. In the transgenic CRP-MBP mouse model, tolerance was associated with

upregulation of Lag-3, PD-1, TIGIT, Tim-3, and CTLA-4 on CD4 T cells in the liver and upregulation of at least three co-inhibitory receptors in spleen and peripheral blood (Fig. 27). In MBP-NP-treated mice, CTLA-4 was the only co-inhibitory receptor that was higher expressed on MBP-specific T cells retrieved from liver, spleen, and blood. Furthermore, Lag-3 was upregulated on MBP-specific T cells from spleen and blood in MBP-NP-treated mice compared to control mice. All other co-inhibitory receptors were either not different between both groups or in the case of TIGIT and Tim-3 even significantly downregulated on MBP-specific T cells in MBP-NP-treated mice in liver and spleen (Fig. 49). Considering the redundant role of these co-inhibitory receptors, one can speculate that inhibition via CTLA-4 is sufficient to downregulate the antigen-specific T cell response. In this model of tolerance induction via LSEC-targeting nanoparticles, potential antigen targeting towards the mannose receptor, a C-type lectin that is also expressed by LSECs, and subsequent induction of CTLA-4 [194] might favor a tolerogenic immune response. However, blockade of CTLA-4 did not break tolerance in mice treated with MBP peptide-loaded NP (Fig. 50A+B). Similar to the transgenic CRP-MBP model, loss of CTLA-4 signaling alone did not abrogate tolerance.

In the transgenic CRP-MBP model, IFNγ proved to be an important mediator of immune tolerance as block of IFNγ induced mild disease associated with decreased accumulation of MBP-specific T cells in the liver and reduced gene expression of different tolerance-associated ISGs (Fig. 29+31+32). The role of IFNγ for MBP-NP-induced immune tolerance appeared to be similar to that in the CRP-MBP transgenic mouse model, as there were more IFNγ+ MBP-specific T cells in liver, spleen, and blood of MBP-NP-treated mice compared to control mice (Fig. 44), and IFNγ production was associated with upregulation of *Cxcl9, Cxcr3*, and *Cd274* expression in the liver (Fig. 46+48). Low liver transaminases indicated the absence of liver damage and hepatitis (Fig. 38B), which is a highly relevant finding with respect to the use of nanoparticles in patients. Nonetheless, flow cytometric analysis revealed accumulation of MBP-specific T cells in the livers of mice treated with MBP peptide-loaded NP (Fig. 39). As *Cxcl9* was elevated in the liver (Fig. 46A) and MBP-specific T cells upregulated CXCR3 (Fig. 47), a role for the IFNγ-CXCL9-CXCR3 axis can thus also be assumed in MBP-NP-induced tolerance. Accordingly, block of IFNγ signaling inhibited the induction of hepatic *Cxcl9* and reduced MBP-specific T cell numbers in the liver in MBP-NP-treated mice

(Fig. 51). In contrast to CRP-MBP mice, in which IFNγ blockade only induced mild EAE symptoms, blockade of IFNγ in MBP-NP-treated mice induced robust disease comparable to control mice. Thus, MBP-NP-induced immune tolerance was IFNγ-dependent (Fig. 50). Break of MBP-NP-induced tolerance was associated with a slight, but significant reduction in hepatic CTLA-4+ MBP-specific T cells highlighting again the role of CTLA-4 in MBP-NP-induced tolerance (Fig. 52C). Of note, expression of *Cd274* and *Ido1* was also reduced upon IFNγ impairment (Fig. 52A+B). As described above, IFNγ can block the Th17 response dependent on IDO1 and PD-L1 [186, 189] and in the CRP-MBP model, concomitant blockade of IFNγ and CTLA-4 induced a strong Th17 response associated with break of tolerance (Fig. 34+36). Thus, it can be assumed that an increased Th17 response during IFNγ depletion also contributes to break of MBP-NP-induced tolerance. The Th17 response seems of particular importance for this model, as in mice treated with MBP peptide-loaded NP, a strong decrease in IL-17-producing MBP-specific T cells was observed in liver and spleen on day seven after immunization compared to control mice (Fig. 44A+B). However, the importance of increased Th17 cells for break of MBP-NP-induced tolerance is yet to be proven.

Identification of mechanisms underlying tolerance induction by autoantigen peptide delivery to LSECs via nanoparticles is of particular interest, as this approach is already employed in first clinical studies assessing safety and efficacy in human autoimmune disease. Most data generated here focus on processes that take place in the liver, as hepatic tolerance mechanisms were studied. However, there is no access to liver tissue samples from patients, and therefore, mainly peripheral blood will be studied. Thus, it will be of interest to determine whether the differences between MBP-NP-treated and control mice observed in peripheral blood are transferable from mouse to human. After adoptive cell transfer, MBP-specific T cells could be readily detected in peripheral blood in high numbers and there were profound differences between mice treated with empty or MBP peptide-loaded NP. The number of IFNγ+ and IL-10+ MBP-specific T cells was elevated in mice treated with MBP peptide-loaded NP (Fig. 44C). Furthermore, expression of the co-inhibitory receptors Lag-3 and CTLA-4 was elevated on MBP-specific T cells in peripheral blood (Fig. 49C). Analysis of these molecules in patients might serve as biomarkers or prognostic factors for functionality of treatment with autoantigen-loaded nanoparticles and disease outcome.

In summary, tolerance induction by LSEC-targeting autoantigen peptide-loaded nanoparticles was associated with increased endogenous Treg numbers in the liver, upregulation of IL-10, IFNγ, IFNγ-induced genes, and CTLA-4, and reduced IL-17 in liver and spleen. Blockade of IFNγ was sufficient to compromise tolerance and induce EAE, which was associated with reduced accumulation of MBP-specific T cells in the liver, reduction of IFNγ-induced genes, and slightly decreased CTLA-4+ MBP-specific T cells in the liver. Taken together, the central role of IFNγ and IFNγ-induced genes was identified in both models of hepatic tolerance. In addition, CTLA-4 might play a role in liver-induced tolerance, even though blockade of CTLA-4 alone was not sufficient to impair tolerance in neither model.

IFNγ was assigned a key role in MBP-NP-induced immune tolerance. In the future, it will be of particular interest to determine the mechanisms underlying this tolerance. It might be mediated by inhibition of Th17 differentiation, as could be concluded from the CRP-MBP model. Alternatively, tolerance might be based on induction of PD-L1 on LSECs and subsequent ligation of PD-L1 to PD-1 on antigen-specific T cells, or on the induction of tolerogenic IDO1. Additionally, the importance of Tr1 cells for tolerance in this model should be studied, as Lag-3+CD49b+ MBP-specific T cells were elevated in MBP-NP-treated mice, and MBP-specific T cells produced more IL-10 suggesting involvement of Tr1 cells. However, correlation between Lag-3, CD49b, and IL-10 is necessary to characterize Tr1 cells and determine their role in MBP-NP-induced immune tolerance. Finally, it will be of major interest to translate the findings from the mouse model to patients.

5. Summary/Zusammenfassung

5.1 Summary

The liver has a remarkable capacity to induce immune tolerance. Indeed, it has been previously shown that the expression of a myelin antigen, such as myelin basic protein (MBP) in the liver provides resistance to CD4 T cell-mediated autoimmune neuroinflammation. This finding indicated that the stimulation of autoreactive T cells in the liver could prevent autoimmune inflammation of distant organs, such as the CNS. The aim of this study was to identify hepatic tolerance mechanisms that prevent pathogenicity of autoreactive T cells. Two mouse models of liver tolerance were employed in which hepatic expression of MBP protects mice from autoimmune neuroinflammation that was induced by immunization with MBP: the tolerant CRP-MBP transgenic mouse and tolerance induced by selective delivery of MBP peptides to liver sinusoidal endothelial cells (LSECs) by using LSEC-targeting nanoparticles.

In CRP-MBP mice, MBP-specific T cells accumulated in the liver, produced high levels of IFNγ, and upregulated the expression of various co-inhibitory receptors. Accumulation of T cells in the liver was dependent on CXCL9 secretion by LSECs and expression of CXCR3 on MBP-specific T cells. Despite induction of Tr1 and other IL-10-producing cells, IL-10 signaling was shown to be dispensable for hepatic tolerance. Blockade of IFNγ, however, induced mild EAE and was associated with decreased accumulation of MBP-specific T cells in the liver and reduced co-inhibitory receptor expression. Strikingly, a robust break of tolerance was observed when IFNγ and CTLA-4 were blocked concomitantly. Inhibition of IFNγ and CTLA-4 induced Th17 cells, a T cell subtype that plays a crucial role in the pathogenesis of autoimmune diseases. The increase of Th17 cells was most likely dependent on a reduction of the IFNγ-induced tolerogenic molecules PD-L1 and IDO1. In conclusion, IFNγ-dependent hepatic accumulation of autoreactive T cells that upregulated the co-inhibitory receptor CTLA-4 was identified as a major mechanism of tolerance induction in the liver. In the second model in which tolerance was induced by MBP peptide-loaded LSEC-targeting nanoparticles, the essential role of IFNγ and IFNγ-associated genes in hepatic tolerance was confirmed. MBP-specific T cells accumulated in livers of tolerant mice and showed increased expression of IFNγ and IL-10, reduced IL-17 secretion, and upregulation of CTLA-4. Inhibition of IFNγ abrogated hepatic

tolerance and was associated with decreased hepatic MBP-specific T cell numbers, reduced expression of *Cxcl9*, *Cd274,* and *Ido1*, and a moderate reduction of CTLA-4 expression on MBP-specific T cells. Tolerance-associated factors identified in MBP-loaded nanoparticle-induced tolerance represent potential biomarkers to prove targeted delivery and efficacy of peptide-loaded nanoparticles in patients, which is of major interest as LSEC-targeting nanoparticles are already employed in first clinical studies in patients.

Taken together, the results emphasize the exceptional capacity of the liver to tolerize autoreactive CD4 T cell responses. Moreover, IFNγ and CTLA-4 could be identified as key molecules for hepatic induction of antigen-specific T cell tolerance and the protection from autoimmunity at extrahepatic sites.

5.2 Zusammenfassung

Die Leber ist gekennzeichnet durch ihre besondere Fähigkeit, Immuntoleranz zu induzieren. Dies wurde in einem Modell deutlich, in dem die Expression eines Myelin-Antigens in der Leber, dem Myelin basischen Protein (MBP), vor CD4-T-Zell-vermittelter experimenteller autoimmuner Enzephalomyelitis (EAE) schützt. Dies zeigt, dass die Stimulation autoreaktiver T-Zellen in der Leber vor autoimmunen Entzündungen auch in entfernten Organen, wie dem ZNS, schützt. Ziel dieser Arbeit war es, Leber-spezifische Toleranzmechanismen zu identifizieren, die pathogene CD4-T-Zell-Antworten verhindern können. Dazu wurden zwei Mausmodelle verwendet, in denen die Expression von MBP in der Leber vor EAE, ausgelöst durch Immunisierung mit MBP, schützt: das transgene CRP-MBP-Modell und die Toleranzinduktion mittels MBP-beladener Nanopartikel, die spezifisch von Leberendothelzellen (LSECs) aufgenommen werden.

In CRP-MBP-Mäusen fand sich eine Anreicherung MBP-spezifischer T-Zellen in der Leber, die IFNγ produzierten und die Expression verschiedener ko-inhibitorischer Moleküle hochregulierten. Die Anreicherung der T-Zellen war abhängig von einer CXCL9-Sekretion durch LSECs und der Expression von CXCR3 auf der Oberfläche MBP-spezifischer T-Zellen. Trotz der Induktion von Tr1-Zellen sowie anderen IL-10-produzierenden MBP-spezifischen

T-Zellen in der Leber stellte sich heraus, dass IL-10 entbehrlich für die Lebertoleranz ist. Dagegen führte eine Inhibition des IFNγ-Signals zu einer Durchbrechung der Lebertoleranz und einer EAE mit gering ausgeprägter Symptomatik. Dies ging einher mit einer reduzierten Anzahl MBP-spezifischer T-Zellen in der Leber, sowie einer Reduktion der Expression ko-inhibitorischer Moleküle. Wurden sowohl IFNγ als auch CTLA-4 zusätzlich blockiert, entwickelten die Mäuse eine starke EAE. Die Durchbrechung der Toleranz war mit einer erhöhten pathogenen Th17-Immunantwort assoziiert, der wahrscheinlich eine Reduktion der tolerogenen IFNγ-induzierten Moleküle PD-L1 und IDO1 zugrunde lag. Zusammenfassend wurde gezeigt, dass die IFNγ-abhängige Akkumulation von Antigen-spezifischen T-Zellen, die den ko-inhibitorischen Rezeptor CTLA-4 exprimieren, ein wichtiger Toleranzmechanismus in der Leber ist. In dem zweiten Toleranzmodell wurde bewiesen, dass IFNγ und IFNγ-assoziierte Gene auch für die Nanopartikel-induzierte Toleranz wichtig sind. Auch in den Lebern von Mäusen, die mit MBP-beladenen Nanopartikeln behandelt wurden, fand sich eine Anreicherung MBP-spezifischer T-Zellen. Im Vergleich zu Mäusen, die mit leeren Nanopartikeln behandelt wurden, waren diese Zellen charakterisiert durch eine höhere Expression von IFNγ, IL-10 und CTLA-4, sowie eine reduzierte Sekretion von IL-17. IFNγ-Inhibition führte zu einer Durchbrechung der Lebertoleranz, was einherging mit einer reduzierten Anzahl an MBP-spezifischen T-Zellen in der Leber, reduzierter Expression von *Cxcl9*, *Cd274* und *Ido1* und einer leichten Runterregulierung von CTLA-4 auf den MBP-spezifischen T-Zellen. Faktoren, die bei der Toleranzinduktion durch Autoantigen-beladene Nanopartikel eine Rolle spielen, könnten sich als wertvolle Biomarker herausstellen, um die Wirkung der Nanopartikel auch in Patienten zu verifizieren. Dies ist besonders wichtig, da Autoantigen-beladene Nanopartikel bereits in ersten klinischen Studien an Patienten getestet werden und Marker benötigt werden, um ihre Wirksamkeit nachzuweisen.

Insgesamt betonen die Ergebnisse dieser Arbeit die besondere tolerogene Fähigkeit der Leber, die autoreaktive CD4-T-Zell-Antworten inhibieren kann. Die Inhibition Antigen-spezifischer T-Zell-Antworten war abhängig von der Expression von IFNγ und CTLA-4, die als Schlüsselmoleküle für die hepatische Immuntoleranz und den Schutz vor Autoimmunerkrankungen identifiziert wurden.

6. References

1. Bajaj, J.S., O'Leary, J.G., Wong, F., Reddy, K.R., and Kamath, P.S., Bacterial infections in end-stage liver disease: current challenges and future directions. Gut, 2012. 61(8): p. 1219-25.
2. Vollmar, B. and Menger, M.D., The hepatic microcirculation: mechanistic contributions and therapeutic targets in liver injury and repair. Physiol Rev, 2009. 89(4): p. 1269-339.
3. Bogdanos, D.P., Gao, B., and Gershwin, M.E., Liver immunology. Compr Physiol, 2013. 3(2): p. 567-98.
4. Yao, Z., Mates, J.M., Cheplowitz, A.M., Hammer, L.P., Maiseyeu, A., Phillips, G.S., Wewers, M.D., Rajaram, M.V., Robinson, J.M., Anderson, C.L., and Ganesan, L.P., Blood-Borne Lipopolysaccharide Is Rapidly Eliminated by Liver Sinusoidal Endothelial Cells via High-Density Lipoprotein. J Immunol, 2016. 197(6): p. 2390-9.
5. Vinas, O., Bataller, R., Sancho-Bru, P., Gines, P., Berenguer, C., Enrich, C., Nicolas, J.M., Ercilla, G., Gallart, T., Vives, J., Arroyo, V., and Rodes, J., Human hepatic stellate cells show features of antigen-presenting cells and stimulate lymphocyte proliferation. Hepatology, 2003. 38(4): p. 919-929.
6. Friedman, S.L., Hepatic stellate cells: protean, multifunctional, and enigmatic cells of the liver. Physiol Rev, 2008. 88(1): p. 125-72.
7. Bilzer, M., Roggel, F., and Gerbes, A.L., Role of Kupffer cells in host defense and liver disease. Liver Int, 2006. 26(10): p. 1175-86.
8. You, Q., Cheng, L., Kedl, R.M., and Ju, C., Mechanism of T cell tolerance induction by murine hepatic Kupffer cells. Hepatology, 2008. 48(3): p. 978-90.
9. Knolle, P., Schlaak, J., Uhrig, A., Kempf, P., Meyer zum Buschenfelde, K.H., and Gerken, G., Human Kupffer cells secrete IL-10 in response to lipopolysaccharide (LPS) challenge. J Hepatol, 1995. 22(2): p. 226-9.
10. Heymann, F., Peusquens, J., Ludwig-Portugall, I., Kohlhepp, M., Ergen, C., Niemietz, P., Martin, C., van Rooijen, N., Ochando, J.C., Randolph, G.J., Luedde, T., Ginhoux, F., Kurts, C., Trautwein, C., and Tacke, F., Liver inflammation abrogates immunological tolerance induced by Kupffer cells. Hepatology, 2015. 62(1): p. 279-91.
11. Pillarisetty, V.G., Shah, A.B., Miller, G., Bleier, J.I., and DeMatteo, R.P., Liver Dendritic Cells Are Less Immunogenic Than Spleen Dendritic Cells because of Differences in Subtype Composition. The Journal of Immunology, 2004. 172(2): p. 1009-1017.
12. Thomson, A.W. and Knolle, P.A., Antigen-presenting cell function in the tolerogenic liver environment. Nat Rev Immunol, 2010. 10(11): p. 753-66.

13. Bamboat, Z.M., Stableford, J.A., Plitas, G., Burt, B.M., Nguyen, H.M., Welles, A.P., Gonen, M., Young, J.W., and DeMatteo, R.P., Human liver dendritic cells promote T cell hyporesponsiveness. J Immunol, 2009. 182(4): p. 1901-11.

14. Matta, B.M., Castellaneta, A., and Thomson, A.W., Tolerogenic plasmacytoid DC. Eur J Immunol, 2010. 40(10): p. 2667-76.

15. Knolle, P.A. and Gerken, G., Local control of the immune response in the liver. Immunological Reviews, 2000. 174: p. 21-34.

16. Sørensen, K.K., McCourt, P., Berg, T., Crossley, C., Couteur, D.L., Wake, K., and Smedsrød, B., The scavenger endothelial cell: a new player in homeostasis and immunity. American Journal of Physiology-Regulatory, Integrative and Comparative Physiology, 2012. 303(12): p. R1217-R1230.

17. Huang, S., Zou, S., Chen, M., Gao, X., Chen, L., Yang, X., Yu, Q., Zhao, X., Du, Y., Yang, X., Lin, Y., Wang, B., Lu, Y., Liu, J., Zheng, X., Gong, F., Lu, M., Yang, D., and Wu, J., Local Stimulation of Liver Sinusoidal Endothelial Cells with a NOD1 Agonist Activates T Cells and Suppresses Hepatitis B Virus Replication in Mice. J Immunol, 2018. 200(9): p. 3170-3179.

18. Carambia, A., Freund, B., Schwinge, D., Heine, M., Laschtowitz, A., Huber, S., Wraith, D.C., Korn, T., Schramm, C., Lohse, A.W., Heeren, J., and Herkel, J., TGF-beta-dependent induction of CD4(+)CD25(+)Foxp3(+) Tregs by liver sinusoidal endothelial cells. J Hepatol, 2014. 61(3): p. 594-9.

19. Kruse, N., Neumann, K., Schrage, A., Derkow, K., Schott, E., Erben, U., Kuhl, A., Loddenkemper, C., Zeitz, M., Hamann, A., and Klugewitz, K., Priming of CD4+ T cells by liver sinusoidal endothelial cells induces CD25low forkhead box protein 3-regulatory T cells suppressing autoimmune hepatitis. Hepatology, 2009. 50(6): p. 1904-13.

20. Carambia, A., Frenzel, C., Bruns, O.T., Schwinge, D., Reimer, R., Hohenberg, H., Huber, S., Tiegs, G., Schramm, C., Lohse, A.W., and Herkel, J., Inhibition of inflammatory CD4 T cell activity by murine liver sinusoidal endothelial cells. J Hepatol, 2013. 58(1): p. 112-8.

21. Tang, L., Yang, J., Liu, W., Tang, X., Chen, J., Zhao, D., Wang, M., Xu, F., Lu, Y., Liu, B., Sun, Q., Zhang, L., and He, F., Liver sinusoidal endothelial cell lectin, LSECtin, negatively regulates hepatic T-cell immune response. Gastroenterology, 2009. 137(4): p. 1498-508 e1-5.

22. Carambia, A., Freund, B., Schwinge, D., Bruns, O.T., Salmen, S.C., Ittrich, H., Reimer, R., Heine, M., Huber, S., Waurisch, C., Eychmuller, A., Wraith, D.C., Korn, T., Nielsen, P., Weller, H., Schramm, C., Luth, S., Lohse, A.W., Heeren, J., and Herkel, J., Nanoparticle-based autoantigen delivery to Treg-inducing liver sinusoidal endothelial cells enables control of autoimmunity in mice. J Hepatol, 2015. 62(6): p. 1349-56.

23. Schurich, A., Berg, M., Stabenow, D., Bottcher, J., Kern, M., Schild, H.J., Kurts, C., Schuette, V., Burgdorf, S., Diehl, L., Limmer, A., and Knolle, P.A., Dynamic regulation of CD8 T cell tolerance induction by liver sinusoidal endothelial cells. J Immunol, 2010. 184(8): p. 4107-14.

24. Franco, A., Barnaba, V., Natali, P., Balsano, C., Musca, A., and Balsano, F., Expression of class I and class II major histocompatibility complex antigens on human hepatocytes. Hepatology, 1988. 8(3): p. 449-54.

25. Burghardt, S., Erhardt, A., Claass, B., Huber, S., Adler, G., Jacobs, T., Chalaris, A., Schmidt-Arras, D., Rose-John, S., Karimi, K., and Tiegs, G., Hepatocytes contribute to immune regulation in the liver by activation of the Notch signaling pathway in T cells. J Immunol, 2013. 191(11): p. 5574-82.

26. Burghardt, S., Claass, B., Erhardt, A., Karimi, K., and Tiegs, G., Hepatocytes induce Foxp3(+) regulatory T cells by Notch signaling. J Leukoc Biol, 2014. 96(4): p. 571-7.

27. Lombard, C.A., Sana, G., LeMaoult, J., Najar, M., Ravau, J., Andre, F., Bouhtit, F., Daouya, M., Loustau, M., Najimi, M., Lagneaux, L., Carosella, E.D., and Sokal, E.M., Human Hepatocytes and Differentiated Adult-Derived Human Liver Stem/Progenitor Cells Display In Vitro Immunosuppressive Properties Mediated, at Least in Part, through the Nonclassical HLA Class I Molecule HLA-G. J Immunol Res, 2019. 2019: p. 8250584.

28. Winau, F., Hegasy, G., Weiskirchen, R., Weber, S., Cassan, C., Sieling, P.A., Modlin, R.L., Liblau, R.S., Gressner, A.M., and Kaufmann, S.H., Ito cells are liver-resident antigen-presenting cells for activating T cell responses. Immunity, 2007. 26(1): p. 117-29.

29. Dunham, R.M., Thapa, M., Velazquez, V.M., Elrod, E.J., Denning, T.L., Pulendran, B., and Grakoui, A., Hepatic stellate cells preferentially induce Foxp3+ regulatory T cells by production of retinoic acid. J Immunol, 2013. 190(5): p. 2009-16.

30. Ichikawa, S., Mucida, D., Tyznik, A.J., Kronenberg, M., and Cheroutre, H., Hepatic stellate cells function as regulatory bystanders. J Immunol, 2011. 186(10): p. 5549-55.

31. Cooper, G.S., Bynum, M.L., and Somers, E.C., Recent insights in the epidemiology of autoimmune diseases: improved prevalence estimates and understanding of clustering of diseases. J Autoimmun, 2009. 33(3-4): p. 197-207.

32. Cruz-Tapias, P., Pérez-Fernández, O.M., Rojas-Villarraga, A., Rodríguez-Rodríguez, A., Arango, M.-T., and Anaya, J.-M., Shared HLA Class II in Six Autoimmune Diseases in Latin America: A Meta-Analysis. Autoimmune Diseases, 2012. 2012: p. 1-10.

33. Vang, T., Congia, M., Macis, M.D., Musumeci, L., Orru, V., Zavattari, P., Nika, K., Tautz, L., Tasken, K., Cucca, F., Mustelin, T., and Bottini, N., Autoimmune-associated lymphoid tyrosine phosphatase is a gain-of-function variant. Nat Genet, 2005. 37(12): p. 1317-9.

34. International Multiple Sclerosis Genetics, C., Hafler, D.A., Compston, A., Sawcer, S., Lander, E.S., Daly, M.J., De Jager, P.L., de Bakker, P.I., Gabriel, S.B., Mirel, D.B., Ivinson, A.J., Pericak-Vance, M.A., Gregory, S.G., Rioux, J.D., McCauley, J.L., Haines, J.L., Barcellos, L.F., Cree, B., Oksenberg, J.R., and Hauser, S.L., Risk alleles for multiple sclerosis identified by a genomewide study. N Engl J Med, 2007. 357(9): p. 851-62.

35. Vella, A., Cooper, J.D., Lowe, C.E., Walker, N., Nutland, S., Widmer, B., Jones, R., Ring, S.M., McArdle, W., Pembrey, M.E., Strachan, D.P., Dunger, D.B., Twells, R.C.J., Clayton, D.G., and Todd, J.A., Localization of a type 1 diabetes locus in the IL2RA/CD25 region by use of tag single-nucleotide polymorphisms. American Journal of Human Genetics, 2005. 76(5): p. 773-779.

36. Brand, O.J., Lowe, C.E., Heward, J.M., Franklyn, J.A., Cooper, J.D., Todd, J.A., and Gough, S.C., Association of the interleukin-2 receptor alpha (IL-2Ralpha)/CD25 gene region with Graves' disease using a multilocus test and tag SNPs. Clin Endocrinol (Oxf), 2007. 66(4): p. 508-12.

37. Brucklacher-Waldert, V., Stuerner, K., Kolster, M., Wolthausen, J., and Tolosa, E., Phenotypical and functional characterization of T helper 17 cells in multiple sclerosis. Brain, 2009. 132(Pt 12): p. 3329-41.

38. Klarenbeek, P.L., de Hair, M.J., Doorenspleet, M.E., van Schaik, B.D., Esveldt, R.E., van de Sande, M.G., Cantaert, T., Gerlag, D.M., Baeten, D., van Kampen, A.H., Baas, F., Tak, P.P., and de Vries, N., Inflamed target tissue provides a specific niche for highly expanded T-cell clones in early human autoimmune disease. Ann Rheum Dis, 2012. 71(6): p. 1088-93.

39. Mueller, D.L., Jenkins, M.K., and Schwartz, R.H., Clonal expansion versus functional clonal inactivation: a costimulatory signalling pathway determines the outcome of T cell antigen receptor occupancy. Annu Rev Immunol, 1989. 7: p. 445-80.

40. Mosmann, T.R., Cherwinski, H., Bond, M.W., Giedlin, M.A., and Coffman, R.L., Two types of murine helper T cell clone. I. Definition according to profiles of lymphokine activities and secreted proteins. J Immunol, 1986. 136(7): p. 2348-57.

41. Mosmann, T.R. and Coffman, R.L., Two types of mouse helper T-cell clone Implications for immune regulation. Immunol Today, 1987. 8(7-8): p. 223-7.

42. Cher, D.J. and Mosmann, T.R., Two types of murine helper T cell clone. II. Delayed-type hypersensitivity is mediated by TH1 clones. J Immunol, 1987. 138(11): p. 3688-94.

43. Sakaguchi, S., Sakaguchi, N., Asano, M., Itoh, M., and Toda, M., Pillars article: immunologic self-tolerance maintained by activated T cells expressing IL-2 receptor alpha-chains (CD25). Breakdown of a single mechanism of self-tolerance causes various autoimmune diseases. J. Immunol. 1995. J Immunol, 2011. 186(7): p. 3808-21.

44. Fontenot, J.D., Gavin, M.A., and Rudensky, A.Y., Foxp3 programs the development and function of CD4+CD25+ regulatory T cells. Nat Immunol, 2003. 4(4): p. 330-6.

45. Hori, S., Nomura, T., and Sakaguchi, S., Control of regulatory T cell development by the transcription factor Foxp3. Science, 2003. 299(5609): p. 1057-1061.

46. Khattri, R., Cox, T., Yasayko, S.A., and Ramsdell, F., An essential role for Scurfin in CD4+CD25+ T regulatory cells. Nat Immunol, 2003. 4(4): p. 337-42.

47. Langrish, C.L., Chen, Y., Blumenschein, W.M., Mattson, J., Basham, B., Sedgwick, J.D., McClanahan, T., Kastelein, R.A., and Cua, D.J., IL-23 drives a pathogenic T cell population that induces autoimmune inflammation. J Exp Med, 2005. 201(2): p. 233-40.

48. Dardalhon, V., Awasthi, A., Kwon, H., Galileos, G., Gao, W., Sobel, R.A., Mitsdoerffer, M., Strom, T.B., Elyaman, W., Ho, I.C., Khoury, S., Oukka, M., and Kuchroo, V.K., IL-4 inhibits TGF-beta-induced Foxp3+ T cells and, together with TGF-beta, generates IL-9+ IL-10+ Foxp3(-) effector T cells. Nat Immunol, 2008. 9(12): p. 1347-55.

49. Veldhoen, M., Uyttenhove, C., van Snick, J., Helmby, H., Westendorf, A., Buer, J., Martin, B., Wilhelm, C., and Stockinger, B., Transforming growth factor-beta 'reprograms' the differentiation of T helper 2 cells and promotes an interleukin 9-producing subset. Nat Immunol, 2008. 9(12): p. 1341-6.

50. Chang, H.C., Sehra, S., Goswami, R., Yao, W., Yu, Q., Stritesky, G.L., Jabeen, R., McKinley, C., Ahyi, A.N., Han, L., Nguyen, E.T., Robertson, M.J., Perumal, N.B., Tepper, R.S., Nutt, S.L., and Kaplan, M.H., The transcription factor PU.1 is required for the development of IL-9-producing T cells and allergic inflammation. Nat Immunol, 2010. 11(6): p. 527-34.

51. Staudt, V., Bothur, E., Klein, M., Lingnau, K., Reuter, S., Grebe, N., Gerlitzki, B., Hoffmann, M., Ulges, A., Taube, C., Dehzad, N., Becker, M., Stassen, M., Steinborn, A., Lohoff, M., Schild, H., Schmitt, E., and Bopp, T., Interferon-regulatory factor 4 is essential for the developmental program of T helper 9 cells. Immunity, 2010. 33(2): p. 192-202.

52. Plank, M.W., Kaiko, G.E., Maltby, S., Weaver, J., Tay, H.L., Shen, W., Wilson, M.S., Durum, S.K., and Foster, P.S., Th22 Cells Form a Distinct Th Lineage from Th17 Cells In Vitro with Unique Transcriptional Properties and Tbet-Dependent Th1 Plasticity. J Immunol, 2017. 198(5): p. 2182-2190.

53. Schaerli, P., Willimann, K., Lang, A.B., Lipp, M., Loetscher, P., and Moser, B., CXC chemokine receptor 5 expression defines follicular homing T cells with B cell helper function. J Exp Med, 2000. 192(11): p. 1553-62.

54. Breitfeld, D., Ohl, L., Kremmer, E., Ellwart, J., Sallusto, F., Lipp, M., and Forster, R., Follicular B helper T cells express CXC chemokine receptor 5, localize to B cell follicles, and support immunoglobulin production. J Exp Med, 2000. 192(11): p. 1545-52.

55. Mackay, C.R., Follicular homing T helper (Th) cells and the Th1/Th2 paradigm. J Exp Med, 2000. 192(11): p. F31-4.

56. Danke, N.A., Koelle, D.M., Yee, C., Beheray, S., and Kwok, W.W., Autoreactive T cells in healthy individuals. J Immunol, 2004. 172(10): p. 5967-72.

57. Cao, Y., Goods, B.A., Raddassi, K., Nepom, G.T., Kwok, W.W., Love, J.C., and Hafler, D.A., Functional inflammatory profiles distinguish myelin-reactive T cells from patients with multiple sclerosis. Sci Transl Med, 2015. 7(287): p. 287ra74.

58. Charlton, B. and Lafferty, K.J., The Th1/Th2 balance in autoimmunity. Curr Opin Immunol, 1995. 7(6): p. 793-8.

59. Rostami, A. and Ciric, B., Role of Th17 cells in the pathogenesis of CNS inflammatory demyelination. J Neurol Sci, 2013. 333(1-2): p. 76-87.

60. Hirota, K., Duarte, J.H., Veldhoen, M., Hornsby, E., Li, Y., Cua, D.J., Ahlfors, H., Wilhelm, C., Tolaini, M., Menzel, U., Garefalaki, A., Potocnik, A.J., and Stockinger, B., Fate mapping of IL-17-producing T cells in inflammatory responses. Nat Immunol, 2011. 12(3): p. 255-63.

61. Roeleveld, D.M. and Koenders, M.I., The role of the Th17 cytokines IL-17 and IL-22 in Rheumatoid Arthritis pathogenesis and developments in cytokine immunotherapy. Cytokine, 2015. 74(1): p. 101-7.

62. Emamaullee, J.A., Davis, J., Merani, S., Toso, C., Elliott, J.F., Thiesen, A., and Shapiro, A.M., Inhibition of Th17 cells regulates autoimmune diabetes in NOD mice. Diabetes, 2009. 58(6): p. 1302-11.

63. Mease, P.J., Inhibition of interleukin-17, interleukin-23 and the TH17 cell pathway in the treatment of psoriatic arthritis and psoriasis. Curr Opin Rheumatol, 2015. 27(2): p. 127-33.

64. Solt, L.A., Kumar, N., Nuhant, P., Wang, Y., Lauer, J.L., Liu, J., Istrate, M.A., Kamenecka, T.M., Roush, W.R., Vidovic, D., Schurer, S.C., Xu, J., Wagoner, G., Drew, P.D., Griffin, P.R., and Burris, T.P., Suppression of TH17 differentiation and autoimmunity by a synthetic ROR ligand. Nature, 2011. 472(7344): p. 491-4.

65. Ouyang, H., Shi, Y., Liu, Z., Feng, S., Li, L., Su, N., Lu, Y., and Kong, S., Increased interleukin9 and CD4+IL-9+ T cells in patients with systemic lupus erythematosus. Mol Med Rep, 2013. 7(3): p. 1031-7.

66. Ciccia, F., Guggino, G., Ferrante, A., Cipriani, P., Giacomelli, R., and Triolo, G., Interleukin-9 and T helper type 9 cells in rheumatic diseases. Clinical & Experimental Immunology, 2016. 185(2): p. 125-132.

67. Li, H., Nourbakhsh, B., Cullimore, M., Zhang, G.X., and Rostami, A., IL-9 is important for T-cell activation and differentiation in autoimmune inflammation of the central nervous system. Eur J Immunol, 2011. 41(8): p. 2197-206.

68. Jager, A., Dardalhon, V., Sobel, R.A., Bettelli, E., and Kuchroo, V.K., Th1, Th17, and Th9 effector cells induce experimental autoimmune encephalomyelitis with different pathological phenotypes. J Immunol, 2009. 183(11): p. 7169-77.

69. Zhao, L., Jiang, Z., Jiang, Y., Ma, N., Zhang, Y., Feng, L., and Wang, K., IL-22+ CD4+ T cells in patients with rheumatoid arthritis. Int J Rheum Dis, 2013. 16(5): p. 518-26.

70. Dolff, S., Scharpenberg, C., Specker, C., Kribben, A., Witzke, O., and Wilde, B., IL-22 production of effector CD4(+) T-cells is altered in SLE patients. Eur J Med Res, 2019. 24(1): p. 24.

71. Gensous, N., Charrier, M., Duluc, D., Contin-Bordes, C., Truchetet, M.E., Lazaro, E., Duffau, P., Blanco, P., and Richez, C., T Follicular Helper Cells in Autoimmune Disorders. Front Immunol, 2018. 9: p. 1637.

72. Bacchetta, R., Barzaghi, F., and Roncarolo, M.G., From IPEX syndrome to FOXP3 mutation: a lesson on immune dysregulation. Ann N Y Acad Sci, 2018. 1417(1): p. 5-22.

73. Ramsdell, F. and Ziegler, S.F., Disruption of a new forkhead/winged-helix protein, scurfin, results in the fatal lymphoproliferative disorder of the scurfy mouse. nature genetics, 2001. 27.

74. Viglietta, V., Baecher-Allan, C., Weiner, H.L., and Hafler, D.A., Loss of functional suppression by CD4+CD25+ regulatory T cells in patients with multiple sclerosis. J Exp Med, 2004. 199(7): p. 971-9.

75. Lindley, S., Dayan, C.M., Bishop, A., Roep, B.O., Peakman, M., and Tree, T.I., Defective suppressor function in CD4(+)CD25(+) T-cells from patients with type 1 diabetes. Diabetes, 2005. 54(1): p. 92-9.

76. Roth, D.B., V(D)J Recombination: Mechanism, Errors, and Fidelity. Microbiol Spectr, 2014. 2(6).

77. Laydon, D.J., Bangham, C.R., and Asquith, B., Estimating T-cell repertoire diversity: limitations of classical estimators and a new approach. Philos Trans R Soc Lond B Biol Sci, 2015. 370(1675).

78. Hogquist, K.A., Baldwin, T.A., and Jameson, S.C., Central tolerance: learning self-control in the thymus. Nat Rev Immunol, 2005. 5(10): p. 772-82.

79. Zhou, R., Horai, R., Silver, P.B., Mattapallil, M.J., Zarate-Blades, C.R., Chong, W.P., Chen, J., Rigden, R.C., Villasmil, R., and Caspi, R.R., The living eye "disarms" uncommitted autoreactive T cells by converting them to Foxp3(+) regulatory cells following local antigen recognition. J Immunol, 2012. 188(4): p. 1742-50.

80. Kuklina, E.M., Molecular mechanisms of T-cell anergy. Biochemistry (Mosc), 2013. 78(2): p. 144-56.

81. Fu, S., Zhang, N., Yopp, A.C., Chen, D., Mao, M., Chen, D., Zhang, H., Ding, Y., and Bromberg, J.S., TGF-beta induces Foxp3 + T-regulatory cells from CD4 + CD25 - precursors. Am J Transplant, 2004. 4(10): p. 1614-27.

82. Groux, H., OGarra, A., Bigler, M., Rouleau, M., Antonenko, S., deVries, J.E., and Roncarolo, M.G., A CD4(+) T-cell subset inhibits antigen-specific T-cell responses and prevents colitis. Nature, 1997. 389(6652): p. 737-742.

83. Gagliani, N., Magnani, C.F., Huber, S., Gianolini, M.E., Pala, M., Licona-Limon, P., Guo, B., Herbert, D.R., Bulfone, A., Trentini, F., Di Serio, C., Bacchetta, R., Andreani, M., Brockmann, L., Gregori, S., Flavell, R.A., and Roncarolo, M.G., Coexpression of CD49b and LAG-3 identifies human and mouse T regulatory type 1 cells. Nat Med, 2013. 19(6): p. 739-46.

84. Brockmann, L., Gagliani, N., Steglich, B., Giannou, A.D., Kempski, J., Pelczar, P., Geffken, M., Mfarrej, B., Huber, F., Herkel, J., Wan, Y.Y., Esplugues, E., Battaglia, M., Krebs, C.F., Flavell, R.A., and Huber, S., IL-10 Receptor Signaling Is Essential for TR1 Cell Function In Vivo. J Immunol, 2016.

85. Singh, B., Summers, K.L., and Kerfoot, S.M., Novel regulatory Th17 cells and regulatory B cells in modulating autoimmune diseases. Cell Immunol, 2019. 339: p. 29-32.

86. Kluger, M.A., Meyer, M.C., Nosko, A., Goerke, B., Luig, M., Wegscheid, C., Tiegs, G., Stahl, R.A., Panzer, U., and Steinmetz, O.M., RORgammat(+)Foxp3(+) Cells are an Independent Bifunctional Regulatory T Cell Lineage and Mediate Crescentic GN. J Am Soc Nephrol, 2016. 27(2): p. 454-65.

87. Inobe, J., Slavin, A.J., Komagata, Y., Chen, Y.H., Liu, L.M., and Weiner, H.L., IL-4 is a differentiation factor for transforming growth factor-beta secreting Th3 cells and oral administration of IL-4 enhances oral tolerance in experimental allergic encephalomyelitis. European Journal of Immunology, 1998. 28(9): p. 2780-2790.

88. Peterson, R.A., Regulatory T-cells: diverse phenotypes integral to immune homeostasis and suppression. Toxicol Pathol, 2012. 40(2): p. 186-204.

89. Yamaguchi, T., Wing, J.B., and Sakaguchi, S., Two modes of immune suppression by Foxp3(+) regulatory T cells under inflammatory or non-inflammatory conditions. Semin Immunol, 2011. 23(6): p. 424-30.

90. Mezrich, J.D., Fechner, J.H., Zhang, X., Johnson, B.P., Burlingham, W.J., and Bradfield, C.A., An interaction between kynurenine and the aryl hydrocarbon receptor can generate regulatory T cells. J Immunol, 2010. 185(6): p. 3190-8.

91. Holt, M.P., Punkosdy, G.A., Glass, D.D., and Shevach, E.M., TCR Signaling and CD28/CTLA-4 Signaling Cooperatively Modulate T Regulatory Cell Homeostasis. J Immunol, 2017. 198(4): p. 1503-1511.

92. Georgiev, P., Charbonnier, L.M., and Chatila, T.A., Regulatory T Cells: the Many Faces of Foxp3. J Clin Immunol, 2019.

93. Kelly, E., Won, A., Refaeli, Y., and Van Parijs, L., IL-2 and related cytokines can promote T cell survival by activating AKT. J Immunol, 2002. 168(2): p. 597-603.

94. McNally, A., Hill, G.R., Sparwasser, T., Thomas, R., and Steptoe, R.J., CD4+CD25+ regulatory T cells control CD8+ T-cell effector differentiation by modulating IL-2 homeostasis. Proc Natl Acad Sci U S A, 2011. 108(18): p. 7529-34.

95. Romano, M., Fanelli, G., Albany, C.J., Giganti, G., and Lombardi, G., Past, Present, and Future of Regulatory T Cell Therapy in Transplantation and Autoimmunity. Front Immunol, 2019. 10: p. 43.

96. Linsley, P.S. and Ledbetter, J.A., The role of the CD28 receptor during T cell responses to antigen. Annu Rev Immunol, 1993. 11: p. 191-212.

97. van Berkel, M.E. and Oosterwegel, M.A., CD28 and ICOS: similar or separate costimulators of T cells? Immunol Lett, 2006. 105(2): p. 115-22.

98. Leach, D.R., Krummel, M.F., and Allison, J.P., Enhancement of antitumor immunity by CTLA-4 blockade. Science, 1996. 271(5256): p. 1734-1736.

99. Dejean, A.S., Beisner, D.R., Ch'en, I.L., Kerdiles, Y.M., Babour, A., Arden, K.C., Castrillon, D.H., DePinho, R.A., and Hedrick, S.M., Transcription factor Foxo3 controls the magnitude of T cell immune responses by modulating the function of dendritic cells. Nat Immunol, 2009. 10(5): p. 504-13.

100. Valk, E., Rudd, C.E., and Schneider, H., CTLA-4 trafficking and surface expression. Trends Immunol, 2008. 29(6): p. 272-9.

101. Yamazaki, T., Akiba, H., Iwai, H., Matsuda, H., Aoki, M., Tanno, Y., Shin, T., Tsuchiya, H., Pardoll, D.M., Okumura, K., Azuma, M., and Yagita, H., Expression of programmed death 1 ligands by murine T cells and APC. J Immunol, 2002. 169(10): p. 5538-45.

102. Nishimura, H., Nose, M., Hiai, H., Minato, N., and Honjo, T., Development of lupus-like autoimmune diseases by disruption of the PD-1 gene encoding an ITIM motif-carrying immunoreceptor. Immunity, 1999. 11(2): p. 141-51.

103. Monney, L., Sabatos, C.A., Gaglia, J.L., Ryu, A., Waldner, H., Chernova, T., Manning, S., Greenfield, E.A., Coyle, A.J., Sobel, R.A., Freeman, G.J., and Kuchroo, V.K., Th1-specific cell surface protein Tim-3 regulates macrophage activation and severity of an autoimmune disease. Nature, 2002. 415(6871): p. 536-41.

104. Dardalhon, V., Anderson, A.C., Karman, J., Apetoh, L., Chandwaskar, R., Lee, D.H., Cornejo, M., Nishi, N., Yamauchi, A., Quintana, F.J., Sobel, R.A., Hirashima, M., and Kuchroo, V.K., Tim-3/galectin-9 pathway: regulation of Th1 immunity through promotion of CD11b+Ly-6G+ myeloid cells. J Immunol, 2010. 185(3): p. 1383-92.

105. Huang, Y.H., Zhu, C., Kondo, Y., Anderson, A.C., Gandhi, A., Russell, A., Dougan, S.K., Petersen, B.S., Melum, E., Pertel, T., Clayton, K.L., Raab, M., Chen, Q., Beauchemin, N., Yazaki, P.J., Pyzik, M., Ostrowski, M.A., Glickman, J.N., Rudd, C.E., Ploegh, H.L., Franke, A., Petsko, G.A., Kuchroo, V.K., and Blumberg, R.S., CEACAM1 regulates TIM-3-mediated tolerance and exhaustion. Nature, 2015. 517(7534): p. 386-90.

106. Gautron, A.S., Dominguez-Villar, M., de Marcken, M., and Hafler, D.A., Enhanced suppressor function of TIM-3+ FoxP3+ regulatory T cells. Eur J Immunol, 2014. 44(9): p. 2703-2711.

107. Huard, B., Prigent, P., Tournier, M., Bruniquel, D., and Triebel, F., CD4/major histocompatibility complex class II interaction analyzed with CD4- and lymphocyte activation gene-3 (LAG-3)-Ig fusion proteins. Eur J Immunol, 1995. 25(9): p. 2718-21.

108. Xu, F., Liu, J., Liu, D., Liu, B., Wang, M., Hu, Z., Du, X., Tang, L., and He, F., LSECtin expressed on melanoma cells promotes tumor progression by inhibiting antitumor T-cell responses. Cancer Res, 2014. 74(13): p. 3418-28.

109. Kouo, T., Huang, L., Pucsek, A.B., Cao, M., Solt, S., Armstrong, T., and Jaffee, E., Galectin-3 Shapes Antitumor Immune Responses by Suppressing CD8+ T Cells via LAG-3 and Inhibiting Expansion of Plasmacytoid Dendritic Cells. Cancer Immunol Res, 2015. 3(4): p. 412-23.

110. Hannier, S., Tournier, M., Bismuth, G., and Triebel, F., CD3/TCR complex-associated lymphocyte activation gene-3 molecules inhibit CD3/TCR signaling. J Immunol, 1998. 161(8): p. 4058-65.

111. Huang, C.T., Workman, C.J., Flies, D., Pan, X., Marson, A.L., Zhou, G., Hipkiss, E.L., Ravi, S., Kowalski, J., Levitsky, H.I., Powell, J.D., Pardoll, D.M., Drake, C.G., and Vignali, D.A., Role of LAG-3 in regulatory T cells. Immunity, 2004. 21(4): p. 503-13.

112. Liang, B., Workman, C., Lee, J., Chew, C., Dale, B.M., Colonna, L., Flores, M., Li, N., Schweighoffer, E., Greenberg, S., Tybulewicz, V., Vignali, D., and Clynes, R., Regulatory T cells inhibit dendritic cells by lymphocyte activation gene-3 engagement of MHC class II. J Immunol, 2008. 180(9): p. 5916-26.

113. Levin, S.D., Taft, D.W., Brandt, C.S., Bucher, C., Howard, E.D., Chadwick, E.M., Johnston, J., Hammond, A., Bontadelli, K., Ardourel, D., Hebb, L., Wolf, A., Bukowski, T.R., Rixon, M.W., Kuijper, J.L., Ostrander, C.D., West, J.W., Bilsborough, J., Fox, B., Gao, Z., Xu, W., Ramsdell, F., Blazar, B.R., and Lewis, K.E., Vstm3 is a member of the CD28 family and an important modulator of T-cell function. Eur J Immunol, 2011. 41(4): p. 902-15.

114. Bottino, C., Castriconi, R., Pende, D., Rivera, P., Nanni, M., Carnemolla, B., Cantoni, C., Grassi, J., Marcenaro, S., Reymond, N., Vitale, M., Moretta, L., Lopez, M., and Moretta, A., Identification of PVR (CD155) and Nectin-2 (CD112) as cell surface ligands for the human DNAM-1 (CD226) activating molecule. J Exp Med, 2003. 198(4): p. 557-67.

115. Johnston, R.J., Comps-Agrar, L., Hackney, J., Yu, X., Huseni, M., Yang, Y., Park, S., Javinal, V., Chiu, H., Irving, B., Eaton, D.L., and Grogan, J.L., The immunoreceptor TIGIT regulates antitumor and antiviral CD8(+) T cell effector function. Cancer Cell, 2014. 26(6): p. 923-937.

116. Boles, K.S., Vermi, W., Facchetti, F., Fuchs, A., Wilson, T.J., Diacovo, T.G., Cella, M., and Colonna, M., A novel molecular interaction for the adhesion of follicular CD4 T cells to follicular DC. Eur J Immunol, 2009. 39(3): p. 695-703.

117. Joller, N., Hafler, J.P., Brynedal, B., Kassam, N., Spoerl, S., Levin, S.D., Sharpe, A.H., and Kuchroo, V.K., Cutting edge: TIGIT has T cell-intrinsic inhibitory functions. J Immunol, 2011. 186(3): p. 1338-42.

118. Fuhrman, C.A., Yeh, W.I., Seay, H.R., Saikumar Lakshmi, P., Chopra, G., Zhang, L., Perry, D.J., McClymont, S.A., Yadav, M., Lopez, M.C., Baker, H.V., Zhang, Y., Li, Y., Whitley, M., von Schack, D., Atkinson, M.A., Bluestone, J.A., and Brusko, T.M., Divergent Phenotypes of Human Regulatory T Cells Expressing the Receptors TIGIT and CD226. J Immunol, 2015. 195(1): p. 145-55.

119. Joller, N., Lozano, E., Burkett, P.R., Patel, B., Xiao, S., Zhu, C., Xia, J., Tan, T.G., Sefik, E., Yajnik, V., Sharpe, A.H., Quintana, F.J., Mathis, D., Benoist, C., Hafler, D.A., and Kuchroo, V.K., Treg cells expressing the coinhibitory molecule TIGIT selectively inhibit proinflammatory Th1 and Th17 cell responses. Immunity, 2014. 40(4): p. 569-81.

120. Paulos, C.M. and June, C.H., Putting the brakes on BTLA in T cell-mediated cancer immunotherapy. J Clin Invest, 2010. 120(1): p. 76-80.

121. Wang, L., Rubinstein, R., Lines, J.L., Wasiuk, A., Ahonen, C., Guo, Y., Lu, L.F., Gondek, D., Wang, Y., Fava, R.A., Fiser, A., Almo, S., and Noelle, R.J., VISTA, a novel mouse Ig superfamily ligand that negatively regulates T cell responses. J Exp Med, 2011. 208(3): p. 577-92.

122. Wang, C., Lin, G.H., McPherson, A.J., and Watts, T.H., Immune regulation by 4-1BB and 4-1BBL: complexities and challenges. Immunol Rev, 2009. 229(1): p. 192-215.

123. Tinoco, R., Otero, D.C., Takahashi, A.A., and Bradley, L.M., PSGL-1: A New Player in the Immune Checkpoint Landscape. Trends Immunol, 2017. 38(5): p. 323-335.

124. Chihara, N., Madi, A., Kondo, T., Zhang, H., Acharya, N., Singer, M., Nyman, J., Marjanovic, N.D., Kowalczyk, M.S., Wang, C., Kurtulus, S., Law, T., Etminan, Y., Nevin, J., Buckley, C.D., Burkett, P.R., Buenrostro, J.D., Rozenblatt-Rosen, O., Anderson, A.C., Regev, A., and Kuchroo, V.K., Induction and transcriptional regulation of the co-inhibitory gene module in T cells. Nature, 2018.

125. Wherry, E.J., T cell exhaustion. Nature Immunology, 2011. 12(6): p. 492-499.

126. Tivol, E.A., Borriello, F., Schweitzer, A.N., Lynch, W.P., Bluestone, J.A., and Sharpe, A.H., Loss of CTLA-4 leads to massive lymphoproliferation and fatal multiorgan tissue destruction, revealing a critical negative regulatory role of CTLA-4. Immunity, 1995. 3(5): p. 541-7.

127. Nishimura, H., Okazaki, T., Tanaka, Y., Nakatani, K., Hara, M., Matsumori, A., Sasayama, S., Mizoguchi, A., Hiai, H., Minato, N., and Honjo, T., Autoimmune dilated cardiomyopathy in PD-1 receptor-deficient mice. Science, 2001. 291(5502): p. 319-322.

128. Bettini, M., Szymczak-Workman, A.L., Forbes, K., Castellaw, A.H., Selby, M., Pan, X., Drake, C.G., Korman, A.J., and Vignali, D.A., Cutting edge: accelerated autoimmune diabetes in the absence of LAG-3. J Immunol, 2011. 187(7): p. 3493-8.

129. Kuehn, H.S., Ouyang, W., Lo, B., Deenick, E.K., Niemela, J.E., Avery, D.T., Schickel, J.N., Tran, D.Q., Stoddard, J., Zhang, Y., Frucht, D.M., Dumitriu, B., Scheinberg, P., Folio, L.R., Frein, C.A., Price, S., Koh, C., Heller, T., Seroogy, C.M., Huttenlocher, A., Rao, V.K., Su, H.C., Kleiner, D., Notarangelo, L.D., Rampertaap, Y., Olivier, K.N., McElwee, J., Hughes, J., Pittaluga, S., Oliveira, J.B., Meffre, E., Fleisher, T.A., Holland, S.M., Lenardo, M.J., Tangye, S.G., and Uzel, G., Immune dysregulation in human subjects with heterozygous germline mutations in CTLA4. Science, 2014. 345(6204): p. 1623-1627.

130. Kroner, A., Mehling, M., Hemmer, B., Rieckmann, P., Toyka, K.V., Maurer, M., and Wiendl, H., A PD-1 polymorphism is associated with disease progression in multiple sclerosis. Ann Neurol, 2005. 58(1): p. 50-7.

131. Pawlak-Adamska, E., Nowak, O., Karabon, L., Pokryszko-Dragan, A., Partyka, A., Tomkiewicz, A., Ptaszkowski, J., Frydecka, I., Podemski, R., Dybko, J., and Bilinska, M., PD-1 gene polymorphic variation is linked with first symptom of disease and severity of relapsing-remitting form of MS. J Neuroimmunol, 2017. 305: p. 115-127.

132. Lee, Y.H., Woo, J.H., Choi, S.J., Ji, J.D., and Song, G.G., Association of programmed cell death 1 polymorphisms and systemic lupus erythematosus: a meta-analysis. Lupus, 2009. 18(1): p. 9-15.

133. Tseng, C.C., Lin, Y.Z., Lin, C.H., Li, R.N., Tsai, W.C., Ou, T.T., Wu, C.C., Sung, W.Y., and Yen, J.H., Genetic and Epigenetic Alteration of the Programmed Cell Death 1 (PDCD1) in Rheumatoid Arthritis. Eur J Clin Invest, 2019: p. e13094.

134. Pouladian, M., Ganjalikhani-Hakemi, M., Alsahebfosul, F., Homayouni, V., Khosravi, S., Etemadifar, M., Mazrouei, F., and Salehi, R., The +4259A>C polymorphism of TIM-3 but not -1637C>T polymorphism of TIM-1 is associated with Multiple sclerosis in Isfahan population. Mult Scler Relat Disord, 2017. 18: p. 152-156.

135. Razi, B., Reykandeh, S.E., Alizadeh, S., Amirzargar, A., Saghazadeh, A., and Rezaei, N., TIM family gene polymorphism and susceptibility to rheumatoid arthritis: Systematic review and meta-analysis. PLoS One, 2019. 14(2): p. e0211146.

136. Tsai, H.F. and Hsu, P.N., Cancer immunotherapy by targeting immune checkpoints: mechanism of T cell dysfunction in cancer immunity and new therapeutic targets. J Biomed Sci, 2017. 24(1): p. 35.

137. Myers, G., Immune-related adverse events of immune checkpoint inhibitors: a brief review. Curr Oncol, 2018. 25(5): p. 342-347.

138. Paluch, C., Santos, A.M., Anzilotti, C., Cornall, R.J., and Davis, S.J., Immune Checkpoints as Therapeutic Targets in Autoimmunity. Frontiers in Immunology, 2018. 9.

139. Blair, H.A. and Deeks, E.D., Abatacept: A Review in Rheumatoid Arthritis. Drugs, 2017. 77(11): p. 1221-1233.

140. Lee, S., Moon, J.S., Lee, C.R., Kim, H.E., Baek, S.M., Hwang, S., Kang, G.H., Seo, J.K., Shin, C.H., Kang, H.J., Ko, J.S., Park, S.G., and Choi, M., Abatacept alleviates severe autoimmune symptoms in a patient carrying a de novo variant in CTLA-4. J Allergy Clin Immunol, 2016. 137(1): p. 327-330.

141. Group, A.T., Treatment of lupus nephritis with abatacept: the Abatacept and Cyclophosphamide Combination Efficacy and Safety Study. Arthritis Rheumatol, 2014. 66(11): p. 3096-104.

142. Luth, S., Huber, S., Schramm, C., Buch, T., Zander, S., Stadelmann, C., Bruck, W., Wraith, D.C., Herkel, J., and Lohse, A.W., Ectopic expression of neural autoantigen in mouse liver suppresses experimental autoimmune neuroinflammation by inducing antigen-specific Tregs. J Clin Invest, 2008. 118(10): p. 3403-10.

143. Fairchild, P.J., Wildgoose, R., Atherton, E., Webb, S., and Wraith, D.C., An Autoantigenic T-Cell Epitope Forms Unstable Complexes with Class-Ii Mhc - a Novel Route for Escape from Tolerance Induction. International Immunology, 1993. 5(9): p. 1151-1158.

144. Liu, G.Y., Fairchild, P.J., Smith, R.M., Prowle, J.R., Kioussis, D., and Wraith, D.C., Low avidity recognition of self-antigen by T cells permits escape from central tolerance. Immunity, 1995. 3(4): p. 407-15.

145. Leypoldt, L.B., Untersuchung von Mechanismen der hepatischen Immuntoleranz im Tiermodell der Experimentellen Autoimmunen Enzephalomyelitis, in Department of Medicine I, UKE Hamburg. 2019, University of Hamburg.

146. Laschtowitz, A., Mechanismen zur Auslösung von Autoimmunität in der Leber, in Department of Mecidine I, UKE Hamburg. 2018, University of Hamburg.

147. Kishimoto, T.K. and Maldonado, R.A., Nanoparticles for the Induction of Antigen-Specific Immunological Tolerance. Front Immunol, 2018. 9: p. 230.

148. Liu, Q., Wang, X., Liu, X., Kumar, S., Gochman, G., Ji, Y., Liao, Y.-P., Chang, C.H., Situ, W., Lu, J., Jiang, J., Mei, K.-C., Meng, H., Xia, T., and Nel, A.E., Use of Polymeric Nanoparticle Platform Targeting the Liver To Induce Treg-Mediated Antigen-Specific Immune Tolerance in a Pulmonary Allergen Sensitization Model. ACS Nano, 2019.

149. Linsley, P.S., Bradshaw, J., Greene, J., Peach, R., Bennett, K.L., and Mittler, R.S., Intracellular trafficking of CTLA-4 and focal localization towards sites of TCR engagement. Immunity, 1996. 4(6): p. 535-543.

150. Kamanaka, M., Kim, S.T., Wan, Y.Y., Sutterwala, F.S., Lara-Tejero, M., Galan, J.E., Harhaj, E., and Flavell, R.A., Expression of interleukin-10 in intestinal lymphocytes detected by an interleukin-10 reporter knockin tiger mouse. Immunity, 2006. 25(6): p. 941-52.

151. Wan, Y.S.Y. and Flavell, R.A., Identifying Foxp3-expressing suppressor T cells with a bicistronic reporter. Proceedings of the National Academy of Sciences of the United States of America, 2005. 102(14): p. 5126-5131.

152. Kilkenny, C., Browne, W.J., Cuthill, I.C., Emerson, M., and Altman, D.G., Improving bioscience research reporting: the ARRIVE guidelines for reporting animal research. PLoS Biol, 2010. 8(6): p. e1000412.

153. McKinnon, K.M., Flow Cytometry: An Overview. Curr Protoc Immunol, 2018. 120: p. 5 1 1-5 1 11.

154. Niedel, J.E., Kuhn, L.J., and Vandenbark, G.R., Phorbol diester receptor copurifies with protein kinase C. Proc Natl Acad Sci U S A, 1983. 80(1): p. 36-40.

155. Chatila, T., Silverman, L., Miller, R., and Geha, R., Mechanisms of T cell activation by the calcium ionophore ionomycin. J Immunol, 1989. 143(4): p. 1283-9.

156. Andree, H.A., Reutelingsperger, C.P., Hauptmann, R., Hemker, H.C., Hermens, W.T., and Willems, G.M., Binding of vascular anticoagulant alpha (VAC alpha) to planar phospholipid bilayers. J Biol Chem, 1990. 265(9): p. 4923-8.

157. Van der Maaten, L. and Hinton, G., Visualizing Data using t-SNE. Journal of Machine Learning Research, 2008. 9: p. 2579-2605.

158. Naves, R., Singh, S.P., Cashman, K.S., Rowse, A.L., Axtell, R.C., Steinman, L., Mountz, J.D., Steele, C., De Sarno, P., and Raman, C., The interdependent, overlapping, and differential roles of type I and II IFNs in the pathogenesis of experimental autoimmune encephalomyelitis. J Immunol, 2013. 191(6): p. 2967-77.

159. Scholzen, T. and Gerdes, J., The Ki-67 protein: from the known and the unknown. J Cell Physiol, 2000. 182(3): p. 311-22.

160. Schneider, W.M., Chevillotte, M.D., and Rice, C.M., Interferon-stimulated genes: a complex web of host defenses. Annu Rev Immunol, 2014. 32: p. 513-45.

161. Tokunaga, R., Zhang, W., Naseem, M., Puccini, A., Berger, M.D., Soni, S., McSkane, M., Baba, H., and Lenz, H.J., CXCL9, CXCL10, CXCL11/CXCR3 axis for immune activation - A target for novel cancer therapy. Cancer Treat Rev, 2018. 63: p. 40-47.

162. Erhardt, A., Wegscheid, C., Claass, B., Carambia, A., Herkel, J., Mittrucker, H.W., Panzer, U., and Tiegs, G., CXCR3 deficiency exacerbates liver disease and abrogates tolerance in a mouse model of immune-mediated hepatitis. J Immunol, 2011. 186(9): p. 5284-93.

163. Kythreotou, A., Siddique, A., Mauri, F.A., Bower, M., and Pinato, D.J., Pd-L1. J Clin Pathol, 2018. 71(3): p. 189-194.

164. Mbongue, J.C., Nicholas, D.A., Torrez, T.W., Kim, N.S., Firek, A.F., and Langridge, W.H., The Role of Indoleamine 2, 3-Dioxygenase in Immune Suppression and Autoimmunity. Vaccines (Basel), 2015. 3(3): p. 703-29.

165. Crispe, I.N., Migration of lymphocytes into hepatic sinusoids. J Hepatol, 2012. 57(1): p. 218-20.

166. Debes, G.F., Arnold, C.N., Young, A.J., Krautwald, S., Lipp, M., Hay, J.B., and Butcher, E.C., Chemokine receptor CCR7 required for T lymphocyte exit from peripheral tissues. Nat Immunol, 2005. 6(9): p. 889-94.

167. Mackay, L.K., Braun, A., Macleod, B.L., Collins, N., Tebartz, C., Bedoui, S., Carbone, F.R., and Gebhardt, T., Cutting edge: CD69 interference with sphingosine-1-phosphate receptor function regulates peripheral T cell retention. J Immunol, 2015. 194(5): p. 2059-63.

168. LaMothe, R.A., Kolte, P.N., Vo, T., Ferrari, J.D., Gelsinger, T.C., Wong, J., Chan, V.T., Ahmed, S., Srinivasan, A., Deitemeyer, P., Maldonado, R.A., and Kishimoto, T.K., Tolerogenic Nanoparticles Induce Antigen-Specific Regulatory T Cells and Provide Therapeutic Efficacy and Transferrable Tolerance against Experimental Autoimmune Encephalomyelitis. Front Immunol, 2018. 9: p. 281.

169. Vieira, P.L., Christensen, J.R., Minaee, S., O'Neill, E.J., Barrat, F.J., Boonstra, A., Barthlott, T., Stockinger, B., Wraith, D.C., and O'Garra, A., IL-10-Secreting Regulatory T Cells Do Not Express Foxp3 but Have Comparable Regulatory Function to Naturally Occurring CD4+CD25+ Regulatory T Cells. The Journal of Immunology, 2004. 172(10): p. 5986-5993.

170. Kuhn, R., Lohler, J., Rennick, D., Rajewsky, K., and Muller, W., Interleukin-10-Deficient Mice Develop Chronic Enterocolitis. Cell, 1993. 75(2): p. 263-274.

171. Brockmann, L., Soukou, S., Steglich, B., Czarnewski, P., Zhao, L., Wende, S., Bedke, T., Ergen, C., Manthey, C., Agalioti, T., Geffken, M., Seiz, O., Parigi, S.M., Sorini, C., Geginat, J., Fujio, K., Jacobs, T., Roesch, T., Izbicki, J.R., Lohse, A.W., Flavell, R.A., Krebs, C., Gustafsson, J.A., Antonson, P., Roncarolo, M.G., Villablanca, E.J., Gagliani, N., and Huber, S., Molecular and functional heterogeneity of IL-10-producing CD4(+) T cells. Nat Commun, 2018. 9(1): p. 5457.

172. Yanagawa, Y., Iwabuchi, K., and Onoe, K., Co-operative action of interleukin-10 and interferon-gamma to regulate dendritic cell functions. Immunology, 2009. 127(3): p. 345-53.

173. Haringer, B., Lozza, L., Steckel, B., and Geginat, J., Identification and characterization of IL-10/IFN-gamma-producing effector-like T cells with regulatory function in human blood. J Exp Med, 2009. 206(5): p. 1009-17.

174. Trinchieri, G., Interleukin-10 production by effector T cells: Th1 cells show self control. J Exp Med, 2007. 204(2): p. 239-43.

175. Neumann, K., Rudolph, C., Neumann, C., Janke, M., Amsen, D., and Scheffold, A., Liver sinusoidal endothelial cells induce immunosuppressive IL-10-producing Th1 cells via the Notch pathway. European Journal of Immunology, 2015. 45(7): p. 2008-2016.

176. Billiau, A., Heremans, H., Vandekerckhove, F., Dijkmans, R., Sobis, H., Meulepas, E., and Carton, H., Enhancement of experimental allergic encephalomyelitis in mice by antibodies against IFN-gamma. J Immunol, 1988. 140(5): p. 1506-10.

177. Domingues, H.S., Mues, M., Lassmann, H., Wekerle, H., and Krishnamoorthy, G., Functional and pathogenic differences of Th1 and Th17 cells in experimental autoimmune encephalomyelitis. PLoS One, 2010. 5(11): p. e15531.

178. Miller, N.M., Wang, J., Tan, Y., and Dittel, B.N., Anti-inflammatory mechanisms of IFN-gamma studied in experimental autoimmune encephalomyelitis reveal neutrophils as a potential target in multiple sclerosis. Front Neurosci, 2015. 9: p. 287.

179. Arellano, G., Ottum, P.A., Reyes, L.I., Burgos, P.I., and Naves, R., Stage-Specific Role of Interferon-Gamma in Experimental Autoimmune Encephalomyelitis and Multiple Sclerosis. Front Immunol, 2015. 6: p. 492.

180. Mele, T.S., Kneteman, N.M., Zhu, L.F., Ramassar, V., Urmson, J., Halloran, B., Churchill, T.A., Jewell, L., Kane, K., and Halloran, P.F., IFN-gamma is an absolute requirement for spontaneous acceptance of liver allografts. American Journal of Transplantation, 2003. 3(8): p. 942-951.

181. Zeng, Z., Li, L., Chen, Y., Wei, H., Sun, R., and Tian, Z., Interferon-gamma facilitates hepatic antiviral T cell retention for the maintenance of liver-induced systemic tolerance. J Exp Med, 2016. 213(6): p. 1079-93.

182. Borchers, A.T., Shimoda, S., Bowlus, C., Keen, C.L., and Gershwin, M.E., Lymphocyte recruitment and homing to the liver in primary biliary cirrhosis and primary sclerosing cholangitis. Semin Immunopathol, 2009. 31(3): p. 309-22.

183. Xu, X., Zhang, S., Jin, R., Wang, K., Li, P., Lin, L., Dong, J., Hao, J., Zhang, Y., Sun, X., Pang, X., Qian, X., Zhang, J., Wu, H., Zhang, Y., and Ge, Q., Retention and tolerance of autoreactive CD4(+) recent thymic emigrants in the liver. J Autoimmun, 2015. 56: p. 87-97.

184. Crispe, I.N., Dao, T., Klugewitz, K., Mehal, W.Z., and Metz, D.P., The liver as a site of T-cell apoptosis: graveyard, or krilling field? Immunological Reviews, 2000. 174: p. 47-62.

185. Lippens, C., Duraes, F.V., Dubrot, J., Brighouse, D., Lacroix, M., Irla, M., Aubry-Lachainaye, J.P., Reith, W., Mandl, J.N., and Hugues, S., IDO-orchestrated crosstalk between pDCs and Tregs inhibits autoimmunity. J Autoimmun, 2016. 75: p. 39-49.

186. Lee, J., Lee, J., Park, M.K., Lim, M.A., Park, E.M., Kim, E.K., Yang, E.J., Lee, S.Y., Jhun, J.Y., Park, S.H., Kim, H.Y., and Cho, M.L., Interferon gamma suppresses collagen-induced arthritis by regulation of Th17 through the induction of indoleamine-2,3-deoxygenase. PLoS One, 2013. 8(4): p. e60900.

187. Salimi Elizei, S., Poormasjedi-Meibod, M.S., Wang, X., Kheirandish, M., and Ghahary, A., Kynurenic acid downregulates IL-17/1L-23 axis in vitro. Mol Cell Biochem, 2017. 431(1-2): p. 55-65.

188. Morita, M., Fujino, M., Jiang, G., Kitazawa, Y., Xie, L., Azuma, M., Yagita, H., Nagao, S., Sugioka, A., Kurosawa, Y., Takahara, S., Fung, J., Qian, S., Lu, L., and Li, X.K., PD-1/B7-H1 interaction contribute to the spontaneous acceptance of mouse liver allograft. Am J Transplant, 2010. 10(1): p. 40-6.

189. Herold, M., Posevitz, V., Chudyka, D., Hucke, S., Gross, C., Kurth, F., Leder, C., Loser, K., Kurts, C., Knolle, P., Klotz, L., and Wiendl, H., B7-H1 Selectively Controls TH17 Differentiation and Central Nervous System Autoimmunity via a Novel Non-PD-1-Mediated Pathway. J Immunol, 2015. 195(8): p. 3584-95.

190. Klocke, K., Sakaguchi, S., Holmdahl, R., and Wing, K., Induction of autoimmune disease by deletion of CTLA-4 in mice in adulthood. Proc Natl Acad Sci U S A, 2016. 113(17): p. E2383-92.

191. Lavon, I., Heli, C., Brill, L., Charbit, H., and Vaknin-Dembinsky, A., Blood Levels of Co-inhibitory-Receptors: A Biomarker of Disease Prognosis in Multiple Sclerosis. Front Immunol, 2019. 10: p. 835.

192. Anderson, A.C., Joller, N., and Kuchroo, V.K., Lag-3, Tim-3, and TIGIT: Co-inhibitory Receptors with Specialized Functions in Immune Regulation. Immunity, 2016. 44(5): p. 989-1004.

193. Kadowaki, A., Miyake, S., Saga, R., Chiba, A., Mochizuki, H., and Yamamura, T., Gut environment-induced intraepithelial autoreactive CD4(+) T cells suppress central nervous system autoimmunity via LAG-3. Nat Commun, 2016. 7: p. 11639.

194. Schuette, V., Embgenbroich, M., Ulas, T., Welz, M., Schulte-Schrepping, J., Draffehn, A.M., Quast, T., Koch, K., Nehring, M., Konig, J., Zweynert, A., Harms, F.L., Steiner, N., Limmer, A., Forster, I., Berberich-Siebelt, F., Knolle, P.A., Wohlleber, D., Kolanus, W., Beyer, M., Schultze, J.L., and Burgdorf, S., Mannose receptor induces T-cell tolerance via inhibition of CD45 and up-regulation of CTLA-4. Proc Natl Acad Sci U S A, 2016. 113(38): p. 10649-54.

195. Ciliberto, G., Arcone, R., Wagner, E.F., and Ruther, U., Inducible and tissue-specific expression of human C-reactive protein in transgenic mice. EMBO J, 1987. 6(13): p. 4017-22.

196. Egenhofer, C., Alsdorff, K., Fehsel, K., and Kolbbachofen, V., Membrane-Associated C-Reactive Protein on Rat-Liver Macrophages Is Synthesized within the Macrophages, Expressed as Neo-C-Reactive Protein and Bound through a C-Reactive Protein-Specific Membrane-Receptor. Hepatology, 1993. 18(5): p. 1216-1223.

197. Malovic, I., Sorensen, K.K., Elvevold, K.H., Nedredal, G.I., Paulsen, S., Erofeev, A.V., Smedsrod, B.H., and McCourt, P.A., The mannose receptor on murine liver sinusoidal endothelial cells is the main denatured collagen clearance receptor. Hepatology, 2007. 45(6): p. 1454-61.

198. Mo, X., Zhang, H., Preston, S., Martin, K., Zhou, B., Vadalia, N., Gamero, A.M., Soboloff, J., Tempera, I., and Zaidi, M.R., Interferon-gamma Signaling in Melanocytes and Melanoma Cells Regulates Expression of CTLA-4. Cancer Res, 2018. 78(2): p. 436-450.

199. Ying, H., Yang, L., Qiao, G., Li, Z., Zhang, L., Yin, F., Xie, D., and Zhang, J., Cutting edge: CTLA-4--B7 interaction suppresses Th17 cell differentiation. J Immunol, 2010. 185(3): p. 1375-8.

200. von Euw, E., Chodon, T., Attar, N., Jalil, J., Koya, R.C., Comin-Anduix, B., and Ribas, A., CTLA4 blockade increases Th17 cells in patients with metastatic melanoma. J Transl Med, 2009. 7: p. 35.

201. Munn, D.H., Sharma, M.D., and Mellor, A.L., Ligation of B7-1/B7-2 by human CD4+ T cells triggers indoleamine 2,3-dioxygenase activity in dendritic cells. J Immunol, 2004. 172(7): p. 4100-10.

Congress contributions

46th Annual Meeting of the German Society for Immunology, Hamburg, 2016

Redundant mechanisms maintain hepatic tolerance in case of Treg impairment

Daria Krzikalla, Lisa Leypoldt, Alena Laschtowitz, Dorothee Schwinge, Christoph Schramm, Ansgar W. Lohse, Johannes Herkel, Antonella Carambia

12th ENII EFIS Summer School on Advanced Immunology, Porto Cervo, 2017

Hepatic tolerance operates through redundant mechanisms to prevent autoimmune disease

Daria Krzikalla, Lisa Leypoldt, Alena Laschtowitz, Dorothee Schwinge, Christoph Schramm, Ansgar W. Lohse, Antonella Carambia, Johannes Herkel

II Joint Meeting of the German Society for Immunology (DGfI) and the Italian Society of Immunology, Clinical Immunology and Allergology (SIICA), Munich, 2019

Restimulation of activated, circulating myelin-specific CD4 T cells in the liver prevents autoimmune neuroinflammation

Daria Krzikalla, Lisa Leypoldt, Alena Laschtowitz, Dorothee Schwinge, Christoph Schramm, Ansgar W. Lohse, Antonella Carambia*, Johannes Herkel*

* joint last author

Danksagung

Zunächst möchte ich mich bei Professor Ansgar W. Lohse für die Möglichkeit bedanken, meine Doktorarbeit in seiner Klinik anzufertigen. Außerdem danke ich Professor Jörg Ganzhorn, der als Zweitgutachter dieser Arbeit fungiert hat.

Mein besonderer Dank gilt Professor Johannes Herkel und Dr. Antonella Carambia für die außerordentlich gute Betreuung, die lebhaften Diskussionen, viele neue Anregungen und das immer konstruktive Feedback.

Ich danke außerdem Angelika Schmidt, Jennifer Wigger, Marko Hilken, Martina Fahl, Nina Verse und Sabrina Kreß für ihre technische Unterstützung in jeglichen Labordingen, sei es Genotypisierungen, Färbungen, qPCRs, Arbeit mit Mäusen und noch so vielem mehr. Dazu danke ich auch allen Mitgliedern der „AG Lohse“, die immer ein offenes Ohr hatten, sei es für Hilfestellungen bei Laborfragen oder einen netten Plausch in der Küche / im Büro.

Ganz besonders bedanke ich mich bei Anja Koop, Annika Volmari, Jenny Wigger, Sabrina Kreß und Steffi Stein für die entstandene Freundschaft, die gemeinsamen Dänemark-Urlaube und die Trash-TV-Sessions.

Bedanken möchte ich mich außerdem bei meiner Schwester Clara, die als Nicht-Biologin eine Korrektur dieser Arbeit auf sich genommen hat, sowie bei Donna Winston, die mir Feedback und Tipps zur sprachlichen Korrektheit im amerikanischen Englisch gegeben hat. Ein besonderer Dank gilt auch Jan Hertel für jegliche Unterstützung außerhalb des Labor-Kosmos.

Schließlich möchte ich mich bei meinen Eltern bedanken, die mich immer vorbehaltlos unterstützt und in meinen Entscheidungen bestärkt haben.

Eidesstattliche Erklärung

Hiermit erkläre ich an Eides statt, dass ich die vorliegende Dissertationsschrift selbst verfasst und keine anderen als die angegebenen Quellen und Hilfsmittel benutzt habe.

Ort, Datum

Unterschrift